



# Prifysgol Abertawe Swansea University

## **Green synthesis of lipophilic capping agents and functionalised gold nanoparticles for potential biomedical applications**

Author: Pranav Pazhamukku Premdas

Submitted to Swansea University in fulfilment of the requirements for  
the Degree of MSc in Nanotechnology by Research

Principal supervisor: Dr Yon Ju-Nam

Second supervisor: Dr Jesus Ojeda Ledo

Swansea University, UK

2023

Copyright: The Author, Pranav Pazhamukku Premdas, 2023.

Distributed under the terms of a Creative Commons Attribution Non Commercial 4.0  
License (CC BY-NC 4.0).

## Abstract

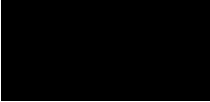
This thesis focuses on the development of green synthetic methods and strategies for the production of cationic lipophilic gold nanoparticles (AuNPs) and hydrophobic organic compound such as hydroxypropyltripheylphosphonium bromide. For the green synthesis of the latter, a novel approach for method development was successfully employed, which consisted of the use of Aspen Plus simulation software to model the reaction between triphenylphosphine and bromopropanol in 100% water, prior planning experimental work in the laboratory.

Operating parameters generated from the simulation work (100% water, temperature 85<sup>0</sup>C, reaction time 5 hours, atmospheric pressure) were replicated in the laboratory, and hydroxypropyltripheylphosphonium bromide crystals were obtained. The infrared spectrum of this compound indicated the presence of the most characteristic functional groups from the chemical structure (-OH, P-C, C=C and C-H). The initial Aspen simulation work helped to reduce excessive use of reactants and reagents, and chemical wastage in the laboratory.

Following the theme of this thesis, green chemistry principles were employed to improve the synthesis of cationic lipophilic AuNPs. Two green methods were developed for the functionalisation of AuNPs both using different ratios of dimethylformamide: water (1:2 and 1:5) and reaction temperatures of 80 and 100<sup>0</sup>C, following different orders in which the reactants were mixed. TEM analyses showed that the mixing order of the reactants, temperature and concentration of reducing agent were the main factors affecting the particle sizes in the gold colloidal samples (3.13 – 8.01 nm). Cationic lipophilic AuNPs prepared following a greener method showed good stability over a period of 6 months.

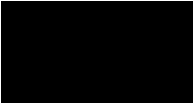
## Declarations and Statements

This work has not previously been accepted in substance for any degree and is not being concurrently submitted in candidature for any degree.

Signed: 

Date: 09/06/2023

This thesis is the result of my own investigations, except where otherwise stated. Other sources are acknowledged by footnotes giving explicit references. A bibliography is appended.

Signed: 

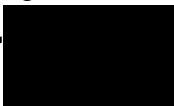
Date: 09/06/2023

I hereby give consent for my thesis, if accepted, to be available for electronic sharing after expiry of a bar on access approved by the Swansea University.

Signed: 

Date: 09/06/2023

The University's ethical procedures have been followed and, where appropriate, ethical approval has been granted.

Signed: 

Date: 09/06/2023

# Contents

Chapter 1 .....	12
Introduction and the literature review.....	12
1.1 Introduction.....	12
1.2 Gold nanoparticles (AuNPs) .....	14
1.2.1 Properties of the AuNPs .....	16
1.3 Methods for the synthesis of AuNPs.....	17
1.3.1 Physical method (Top-down approach) .....	17
1.3.2 Chemical methods (Bottom-up approach).....	18
1.3.3 Stabilisation of AuNPs .....	20
1.3.4 Functionalisation of AuNPs.....	22
1.4 Green synthesis of the AuNPs .....	22
1.4.1 Biosynthesis of the AuNPs from the plant extracts.....	23
1.4.2 Using microorganisms .....	24
1.4.3 Fungi and algae .....	24
1.5 Biomedical application of the AuNPs.....	25
1.5.1 Drug delivery .....	25
1.5.2 Imaging .....	26
1.5.3 Biosensors .....	27
1.6 Overall objective and specific aims of the thesis .....	28
Chapter 2 .....	29
Characterisation techniques.....	29
2.1 Introduction.....	29
2.2 Analytical techniques.....	29
2.2.1 ATR-FTIR spectroscopy .....	29
2.2.2 Melting point .....	30
2.2.3 Rotary Evaporator .....	31
2.2.4 Thin layer chromatography TLC.....	32
2.2.5 Transmission Electron Microscope (TEM) .....	33
2.2.6 UV-Visible spectroscopy.....	35
2.2.7 X-ray photoelectron spectroscopy (XPS).....	37
Chapter 3 .....	38

<b>Green synthesis of phosphonioalkylthiosulfate ligand - Aspen modelling to experimental trials</b> .....	<b>38</b>
<b>3.1 Introduction</b> .....	<b>38</b>
<b>3.2 Materials and methodology</b> .....	<b>40</b>
<b>3.2.1 Chemicals</b> .....	<b>40</b>
<b>3.2.2 Synthesis of triphenylphosphoniopropylthiosulfate zwitterion (Ligand) using the Conventional Route</b> .....	<b>40</b>
<b>3.2.2.1 Synthesis of hydroxypropylphosphonium salt (Intermediate #1)</b> .....	<b>40</b>
<b>3.2.2.2 Synthesis of <math>\omega</math>-bromopropyltriphenylphosphoniumbromide (Intermediate #2)</b> .....	<b>42</b>
<b>3.2.2.3 Synthesis of triphenylphosphoniopropylthiosulfate zwitterion (Ligand)</b> .....	<b>43</b>
<b>3.2.3 Aspen Plus simulation of Reaction #1</b> .....	<b>45</b>
<b>3.2.3.1 Joback method</b> .....	<b>46</b>
<b>3.2.3.1.1 Critical properties required for Reaction #1 simulation</b> .....	<b>51</b>
<b>3.2.3.2 Continuous mode simulation</b> .....	<b>51</b>
<b>3.2.3.3 Batch mode simulation</b> .....	<b>52</b>
<b>3.2.3.4 Simulation of Reaction #1 using the CSTR and the Batch reactors (Conventional Route)</b> .....	<b>52</b>
<b>3.2.3.5 Simulation of Reaction #1 using CSTR reactor (Green Route)</b> .....	<b>53</b>
<b>3.2.4 Synthesis of Intermediate #1 in the laboratory using 100% water (Green Route):</b> .....	<b>53</b>
<b>3.3 Results and Discussions</b> .....	<b>54</b>
<b>3.3.1 Characterisation of the Intermediate #1, Intermediate #2 and Ligand obtained following Conventional Route</b> .....	<b>54</b>
<b>3.3.1.1 ATR-FTIR spectroscopy analyses of Intermediates #1 and #2 and Ligand</b> .....	<b>55</b>
<b>3.3.2 Aspen simulation of Reaction #1: estimated properties for TPP and Intermediate #1 (Conventional Route) using Joback method</b> .....	<b>57</b>
<b>3.3.3 Specific heat capacity of TPP and Intermediate #1</b> .....	<b>58</b>
<b>3.3.4 Aspen simulation of Reaction #1 using CSTR reactor (Conventional- Route)</b> .....	<b>60</b>
<b>3.3.5 Aspen simulation of Reaction #1 using Batch reactor (Conventional-Route)</b> .....	<b>61</b>
<b>3.3.6 Comparison of simulations carried out in continuous and batch modes (Conventional Route)</b> .....	<b>62</b>
<b>3.3.7 Aspen simulation of Reaction #1 using CSTR reactor (Green Route)</b> .....	<b>62</b>
<b>3.3.8 Green synthesis of Reaction #1 using Aspen simulation outputs</b> .....	<b>64</b>
<b>Chapter 4</b> .....	<b>66</b>
<b>Green synthesis of the cationic lipophilic AuNPs</b> .....	<b>66</b>
<b>4.1 Introduction</b> .....	<b>66</b>
<b>4.2 Materials and Methods</b> .....	<b>67</b>
<b>4.2.1 Chemicals</b> .....	<b>67</b>

4.2.2 Synthesis of cationic lipophilic AuNPs .....	67
4.2.2.1 Conventional Method .....	67
4.2.2.2 Green Methods .....	68
4.3 Results and Discussions .....	70
4.3.1 UV-Visible spectroscopy analysis .....	70
4.3.1.1 UV-Vis spectroscopy analysis of cationic lipophilic AuNP solutions obtained using the Conventional Method .....	71
4.3.1.2 UV-Vis spectroscopy analysis of cationic lipophilic AuNP solutions obtained using the Green Methods .....	73
4.3.2 TEM analysis of cationic lipophilic AuNPs synthesised following Green Methods .....	77
4.3.2.1 TEM analysis of the cationic lipophilic AuNPs synthesised using Conventional Method .....	77
4.3.2.2 TEM analysis of the cationic lipophilic AuNPs synthesised via Green Methods .....	78
4.3.3 XPS analysis of the cationic lipophilic AuNPs produced following Green Method #1 .....	85
Chapter 5 .....	89
Conclusions and Recommendations .....	89
Appendices .....	92
Glossary .....	97
Bibliography .....	98

## **Acknowledgements**

I would like to express my hearty thanks to a lot of people who gave their time and effort for the completion of my project work. Firstly, I acknowledge my Project Supervisor, Dr Yon Ju-Nam who has always been a source of inspiration, motivation, and guidance throughout my project work. Without her support, this project would never have been possible. I owe you for your tremendous effort, brilliant supervision, and encouragement throughout my work. Her dynamic vision and sincerity gave me total positivity in doing this work. I am also greatly indebted to my second supervisor Dr. Jesus Ojeda Ledo for his valuable suggestions and direction to accomplish the study. I would take this opportunity to thank all the technical laboratory staff of Chemical Engineering, Swansea University for being a constant source of motivation and for their constant support. I would also take this opportunity to thank Uchechakwu Unwukwe of Brunel University for their tireless support for the TEM analysis.

Finally, I would record my sincere thanks for the help rendered by my parents, without their blessings, love, and prayer I would never accomplish anything. Above all, I'm thankful to almighty GOD. I humbly dedicate this thesis to my parents and teachers.

## List of tables

<b>Table 3.1.</b> Estimated properties for TPP using the Joback method (CheCalc.com).....	57
<b>Table 3.2.</b> Estimated properties for Intermediate #1 using the Joback method (CheCalc.com) .....	58
<b>Table 3.3.</b> Regression coefficients for TPP from Knovel library.....	59
<b>Table 3.4.</b> Specific heat capacity obtained for TPP, temperature range: 150 - 500 K. ....	59
<b>Table 3.5.</b> Stream results of Reaction #1 using CSTR reactor .....	60
<b>Table 3.6.</b> Comparison of Reaction #1 using batch reactor at different stop times (ST), 1-5hrs. ....	61
<b>Table 3.7.</b> Reaction #1 using CSTR reactor with different concentrations of Water and Acetonitrile (ACN) .....	63
<b>Table 4.1.</b> Temperatures and DMF:DI water ratio used for all six samples of AuNPs.....	70
<b>Table 4.2.</b> Average particle size of AuNPs synthesised at different temperatures and various concentrations of DMF. ....	84



## List of figures

<b>Figure 1.1.</b> Size comparisons between several human-made nanodevices and biological Species (Yadav et al., 2021). .....	13
<b>Figure 1.2.</b> Structural based classifications of AuNPs (De Freitas et al., 2018). .....	14
<b>Figure 1.3.</b> Representation of Turkevich method (Imbraguglio, et al., 2013).....	19
<b>Figure 1.4.</b> Representation of the Brust-Schiffrin method (Yafout et al., 2021).....	19
<b>Figure 1.5.</b> Representation of the seed-mediated growth method (Xia et al., 2017).....	20
<b>Figure 2.1.</b> PerkinElmer UATR Two was used for the analysis of Intermediate #1, Intermediate #2 and the Ligands.....	30
<b>Figure 2.2.</b> Melting point apparatus .....	31
<b>Figure 2.3.</b> Instrumentation of the rotary evaporator .....	32
<b>Figure 2.4.</b> Schematic representation of TLC (Sathya, 2017).....	33
<b>Figure 2.5.</b> Schematic representation of TEM (PeakD, n.d.).....	34
<b>Figure 2.6.</b> Perkin-Elmer 25 UV-Vis spectrophotometer was used for the analysis of the colloidal gold nanoparticles .....	36
<b>Figure 2.7.</b> X-ray Photoelectron Spectroscopic technique (West Campus Materials Characterisation Core, n.d.) .....	37
<b>Figure 3.1.</b> Conventional Route (three-stage process) to produce Intermediate #1, Intermediate #2 and Ligand (triphenylphosphoniopropylthiosulfate zwitterion). .....	39
<b>Figure 3.2.</b> Reaction #1 for the synthesis of Intermediate #1 (Ju-Nam et al., 2016).....	41
<b>Figure 3.3.</b> Flowchart representation for the synthesis of Intermediate #1. ....	41
<b>Figure 3.4.</b> Reaction #2 for the synthesis of Intermediate #2 (Ju-Nam et al., 2016).....	42
<b>Figure 3.5.</b> Flowchart representation for the synthesis of Intermediate #2 .....	43
<b>Figure 3.6.</b> Reaction #3 for the synthesis of Ligand (Ju-Nam et al., 2016) .....	44
<b>Figure 3.7.</b> Flowchart representation for the synthesis of Ligand.....	44
<b>Figure 3.8.</b> Representation of the CSTR reactor .....	51
<b>Figure 3.9.</b> Representation of the Batch reactor.....	52
<b>Figure 3.10.</b> Crystals of (a) Intermediate #1, (b) Intermediate #2, (c) Ligand obtained using the Conventional Route of synthesis.....	54
<b>Figure 3.11.</b> Infrared spectra of (a) Intermediate #1, (b) Intermediate #2, (c) Ligand obtained using ATR-FTIR technique. ....	56
<b>Figure 3.12.</b> Crystals obtained for the Intermediate #1 using the Green Route. ....	64
<b>Figure 3.13.</b> FTIR spectrum of the synthesised Intermediate #1 with 100 % water .....	65
<b>Figure 4.1.</b> Synthesis of cationic lipophilic AuNPs using the conventional method (Ju-Nam et al., 2006). .....	68
<b>Figure 4.2.</b> Cationic lipophilic AuNP solution prepared following the Conventional Method using NaBH <sub>4</sub> as the reducing agent.....	71
<b>Figure 4.3.</b> Absorption spectra of the functionalised AuNPs via Conventional Method. ....	72

<b>Figure 4.4.</b> UV-visible spectra of functionalised AuNPs with after 1, 2, 3, and 4 months (solutions made using same dilution).....	73
<b>Figure 4.5.</b> UV-Vis Spectra of Sample 1 (100 <sup>0</sup> C, 1:2 DMF:DI water), Sample 2 (100 <sup>0</sup> C, 1:5 DMF:DI water), Sample 3 (80 <sup>0</sup> C 1:2 DMF:DI water), Sample 4 (80 <sup>0</sup> C, 1:5 DMF: DI water) and Sample 5 (80 <sup>0</sup> C, 1:2 DMF:DI water), Sample 6 (100 <sup>0</sup> C, 1:2 DMF:DI water).....	74
<b>Figure 4.6.</b> Comparison of the absorption spectra corresponding to different synthesis temperatures Sample #1 100 <sup>0</sup> C and Sample #3 80 <sup>0</sup> C.....	75
<b>Figure 4.7.</b> UV-visible spectra of functionalised AuNPs (Sample 1) produced following Green Method #1 (red line – time 0, blue line – time 6 months).....	76
<b>Figure 4.8.</b> (a) TEM image of cationic lipophilic AuNPs (image scale: 10 nm), (b) particle size distribution of the functionalised AuNPs via Conventional Method.....	78
<b>Figure 4.9.</b> (a), (b) TEM micrographs (images scale: 20 nm) of Sample #1 (100 <sup>0</sup> C, 33%DMF), and (c) particle size histograms of AuNPs synthesised by Green Method #1. Mean particle size $3.13 \pm 0.5\text{nm}$ , in each histogram 200 nanoparticles were counted.....	79
<b>Figure 4.10.</b> (a), (b) TEM micrographs (image (a) scale: 20 nm, image (b) scale: 50 nm) of Sample #2 (100 <sup>0</sup> C, 16% DMF), and (c) particle size histograms of AuNPs synthesised by Green Method #1. Mean particle size $3.74 \pm 0.6\text{nm}$ , in each histogram 200 nanoparticles were counted. ....	80
<b>Figure 4.11.</b> (a), (b) TEM micrographs (image (a) scale: 50 nm, image (b) scale: 20 nm) of Sample #3 (80 <sup>0</sup> C 33% DMF), and (c) particle size histograms of AuNPs synthesised by Green Method #1. Mean particle size $3.45 \pm 0.5\text{nm}$ , in each histogram 200 nanoparticles were counted. ....	81
<b>Figure 4.12.</b> (a), (b) TEM micrographs (images scale: 25 nm) of Sample #4 (80 <sup>0</sup> C, 16% DMF), and (c) particle size histograms of AuNPs synthesised by Green Method #1. Mean particle size $7.52 \pm 0.97\text{nm}$ , in each histogram 200 nanoparticles were counted.....	82
<b>Figure 4.13.</b> (a), (b) TEM micrographs (image (a) scale: 15 nm, and image (b) scale: 20nm) of Sample #5 (80 <sup>0</sup> C, 33% DMF) and (c) particle size histograms of AuNPs synthesised by Green Method #2. Mean particle size $8.01 \pm 1.1\text{nm}$ , in each histogram 200 nanoparticles were counted. ....	83
<b>Figure 4.14.</b> XPS survey spectrum of the cationic lipophilic AuNPs (from Sample 1).....	85
<b>Figure 4.15.</b> XPS high resolution spectrum for Au <sub>4f</sub> of the AuNPs, with corresponding peak deconvolution to assess the local chemical environment of this element. ....	86
<b>Figure 4.16.</b> XPS high resolution spectrum for S <sub>2p</sub> of the AuNPs, with corresponding peak deconvolution to assess the local chemical environment of this element.....	87

## Abbreviations

<b>AuNPS</b>	Gold nanoparticles
<b>DMF</b>	Dimethylformamide
<b>DCM</b>	Dichloromethane
<b>DI water</b>	Deionised water
<b>TPP</b>	Triphenylphosphine
<b>ACN</b>	Acetonitrile
<b>LSPR</b>	Localised surface plasmon resonance
<b>SPR</b>	Surface plasmon resonance
<b>TEM</b>	Transmission electron microscopy
<b>XPS</b>	X-ray photoelectron spectroscopy
<b>UV-Vis</b>	Ultraviolet-Visible
<b>INTR #1</b>	Intermediate #1
<b>ATR-FTIR</b>	Attenuated total reflection- Fourier-transform infrared spectroscopy

# Chapter 1

## Introduction and the literature review

### 1.1 Introduction

Nanotechnology is an interdisciplinary field that involves the study, modification, and design of materials at the nanoscale (typically between 1 and 100 nanometers). It links various scientific and engineering disciplines, including physics, chemistry, biotechnology, and medicine (Bayda et al., 2019). The ability to manufacture materials at the nanoscale level is one of the distinguishing features of nanotechnology, which creates new possibilities for the design and development of novel materials and products. A wide variety of materials, including metals, metal oxides, semiconductors, polymers, magnetic compounds, liposomes, carbon, and silica-based materials, can be used to create nanomaterials. Researchers from all around the world have shown a great deal of interest in and investment in the field of nanotechnology. The potential of nanotechnology is being investigated in areas including electronics, textiles, cosmetics, medicines, and environmental remediation (Shah et al., 2022) in order to create new goods and technologies with enhanced functionality.

In recent years, nanotechnology has emerged as a promising field of research, particularly in the area of noble metal nanoparticles. These nanoparticles possess unique mechanical, chemical, electrochemical, and optical properties that make them suitable for a range of applications in both industrial and biological domains. According to Doria and coworkers 2012 and Khlebtsov and Dykman 2010, noble metal nanoparticles are widely used in optics, drug delivery, diagnosis, and therapy. Among the coinage family of metals, copper, platinum, gold, silver, and palladium are commonly used for the synthesis of metal nanoparticles (Narayanan, 2010). The widespread application of noble metal nanoparticles can be attributed to their distinct physical and chemical properties, such as high surface area to volume ratio, surface morphology, and electronic properties (Mansoori et al., 2007). These properties make them ideal for use in various applications, including drug delivery, diagnostic imaging, and cancer therapy (Doria et al., 2012). Shown in Figure 1.1. the size comparison of different physical and biological samples. The field of nanotechnology has contributed significantly to the development of advanced techniques, which have led to the production of new materials and chemicals that offer enhanced performance while reducing

material and energy consumption and minimising ecological damage (Lee et al., 2010). As a result, noble metal nanoparticles have attracted considerable attention from researchers and industrialists (Khlebtsov and Dykman, 2010).

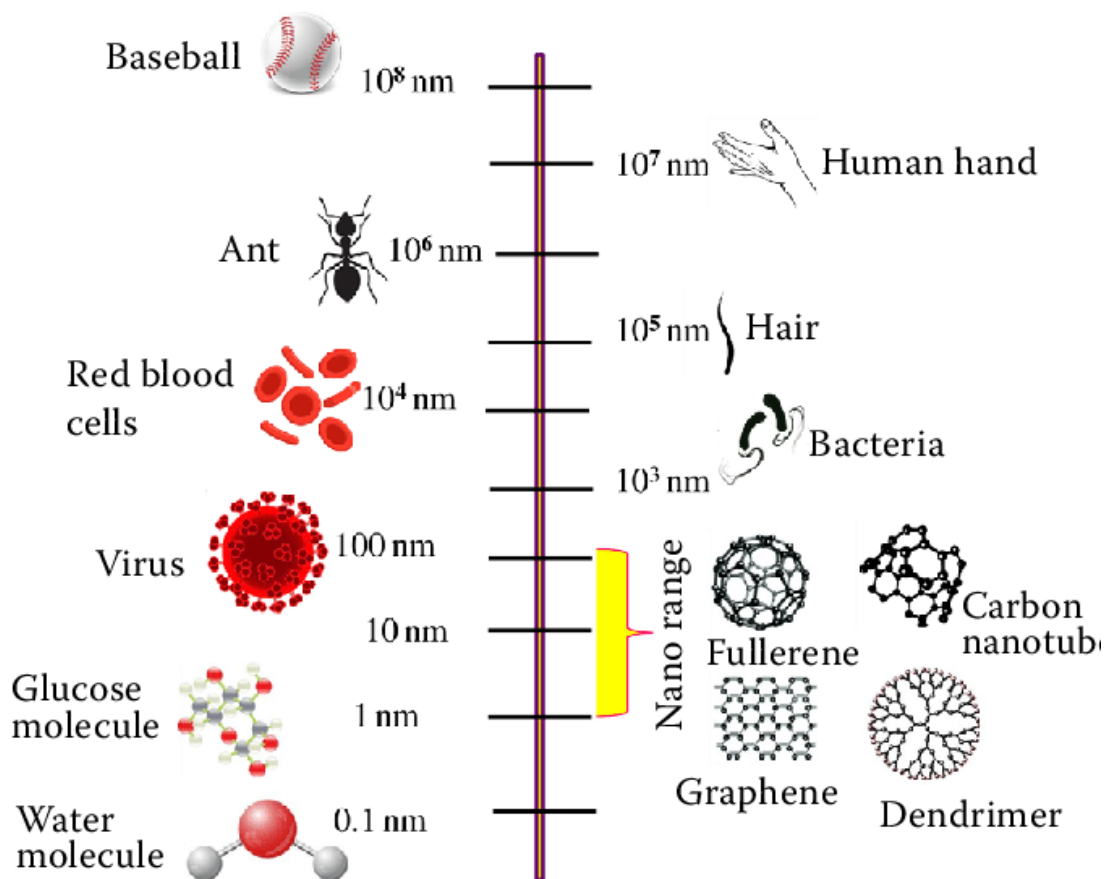


**Figure 1. 1.** Size comparisons between several human-made nanodevices and biological Species (Yadav et al., 2021).

Nanoparticles with various physicochemical properties (Farjadian et al. 2019) can be obtained using different materials and methods (chemical and physical).

## 1.2 Gold nanoparticles (AuNPs)

AuNPs are a group of particles with a gold core and a surface coating. The fundamental characteristics of AuNPs are defined by the core and the protective coating of the core can be modified for stabilising them and to improve the interaction with the environment (Chen et al., 2014). AuNPs are highly popular due to their unique surface plasmon resonance (SPR) properties, which make them suitable for use in various applications, including optoelectronic devices, biomedical and environmental applications (Zhao et al., 2013). However, colloidal AuNPs have a high surface energy, making them susceptible to aggregation in the absence of a stabilising agent. To address this issue, several techniques have been developed for the benign synthesis of AuNPs, including chemical, physical, and electrochemical techniques (Zhao et al., 2013). Figure 1.2. shows the different possible structures of the AuNPs.

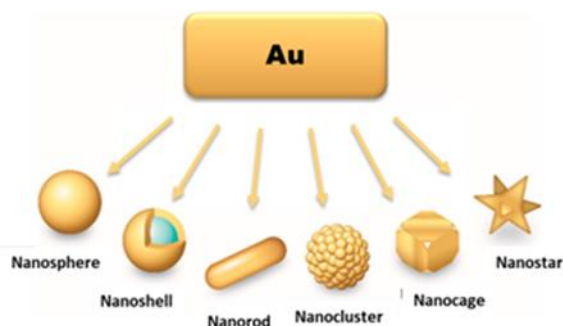


**Figure 1.2.** Structural based classifications of AuNPs (De Freitas et al., 2018).

Gold has captured the attention of humanity since its discovery (Vajtai, 2013), being recognised as the noblest of metals due to its resistance to corrosion and enduring lustre over time (Zhao et al., 2013). The realisation that gold can be highly active as a catalyst when reduced to the nanoscale has boosted significant scientific discoveries (Haruta, 2005). Michael Faraday's pioneering work on the interactions between light and metal particles paved the way for contemporary colloidal chemistry, providing a basis for the combination of nanoscience with nanotechnology. Faraday's investigations and analyses of metal particles laid the foundation for the study of colloidal systems, which is essential to the development of nanotechnology (Chari et al., 2022). Faraday demonstrated that Au-chloride could be reduced upon heat treatment, due to the side reactions with numerous reagents, including phosphorus and organic compounds (Faraday, 1857). Particles of varied sizes would display colours different from their original colour when they are smaller than

the wavelength of light (Faraday, 1857). Zsigmondy's method for the production of gold nanoparticles involved the reduction of gold chloride ( $\text{AuCl}_3$ ) using a reducing agent (Slepička et al., 2019; Zsigmondy, 1909). He prepared a gold chloride solution and added a suitable reducing agent, such as sodium citrate or sodium borohydride. The solution was gently heated and stirred to promote the reduction reaction, resulting in the formation of small gold nanoparticles. To prevent aggregation and maintain stability, a stabilising agent, such as citric acid or polyvinylpyrrolidone (PVP), was often added (Slepička et al., 2019; Zsigmondy, 1909). He observed that when gold metal is reduced to extremely small particle sizes, it exhibits unique optical properties, giving rise to intense colours. He explained the reason for changes in colours might be due to the coagulated particles in different sizes, and the action of protective agents could inhibit coagulation (Slepička et al., 2019; Zsigmondy, 1909). Ostwald has made a significant contribution to the synthesis of Au sols using a variety of theoretical and practical techniques. Ostwald made an effort to concentrate on the significance of particle size for dispersion and provides numerous examples to describe the phenomenon of Au sols and other colloids (Bastús et al., 2011; Ostwald, 1904). AuNPs are highly attractive due to their apparent non-toxicity, inertness, biocompatibility, ease of synthesis, and tunable optical characteristics. Their unique optical properties make them highly useful in biomedical imaging, drug delivery, and cancer therapy, among other applications (Chen et al., 2019).

Due to their simplicity in manufacture, stability, biocompatibility, and presumed biological inertness, AuNPs have emerged as one of the most extensively researched and well-characterised nanomaterials to date. AuNPs are extremely useful for a variety of applications in industries including healthcare and electronics due to their distinctive optical and electrical features, such as SPR and are being investigated for their potential as diagnostic and therapeutic agents in biomedicine. To facilitate targeted administration and imaging, they can be functionalised with biomolecules like antibodies or nucleic acids (Tripathi and Driskell, 2018). Depending on their appearance, dimensions, and physical characteristics nanomaterials can be classified into different forms such as nanospheres, nanorods, nanocages, nanoshells, nanoclusters, and nanostars (Landvik et al., 2018). AuNPs have been extensively investigated for their potential applications in biomedicine, due to their unique optical and physical properties, as well as their biocompatibility. One such application is in cancer therapy, where AuNPs can be used for targeted drug delivery and photothermal therapy (PTT) (Hu et al., 2020).

### **1.2.1 Properties of the AuNPs**

Spherical AuNPs have excellent properties such as size and shape-related optoelectronic properties (Yeh, 2012) a high surface-to-volume ratio, good biocompatibility, and low toxicity (Khlebtsov, 2011). Due to these properties, AuNPs are considered to be an important tool for bionanotechnology. Surface plasmon resonance (SPR) and the ability to quench fluorescence are two important physical properties of AuNPs.

SPR is a phenomenon that occurs when light is reflected off a metallic surface (Nordlander et al., 2004). When the light of a certain wavelength is incident upon a metallic surface, it can cause the electrons in the metal to oscillate collectively in a phenomenon called surface plasmon. This oscillation of electrons creates a resonant absorption peak in the reflectance spectrum of the metal, which is known as surface plasmon resonance. One of the key properties of surface plasmons is that they can be highly confined to the surface of the metal, and as a result, they can interact with materials that are close to the surface (Nordlander et al., 2004). This makes surface plasmons an attractive tool for chemical and biological sensing, as they can be used to detect the presence of specific molecules in a sample by measuring the changes in the resonance frequency of the surface plasmon. Spherical AuNPs in an aqueous solution show a variety of colours such as (brown, orange, red, and purple) it is due to the increase in the core size from 1 to 100 nm, which leads to the shift in the absorption peak from 500 to 550 nm (Eustis and El-Sayed, 2006). This absorption band is called a surface plasmon band. This band is seen for both small nanoparticles ( $d < 2\text{nm}$ ) and bulk material. This phenomenon is influenced not just by size, but also by shape, solvent, surface ligand, core charge, temperature, and proximity to other nanoparticles (Yeh, 2012). Due to the interparticle plasmon coupling, nanoparticle aggregation leads to a significant red-shifting of SPR frequency, broadening of the surface plasmon band, and a change in solution colour from red to blue (Khlebtsov, 2011). The excellent quenching ability of AuNPs to proximal fluorophores is due to the great overlap between the emission spectrum of excited fluorophores and the AuNPs surface plasmon band (Bigioni, 2000). This fluorescence resonance energy transfer (FRET) phenomenon is observed even in the presence of 1nm AuNPs as the nanoparticles affect both the radiative and nonradiative decay rates of fluorescent molecules (Bigioni, 2000). AuNPs can however act as electron acceptors to quench fluorophores in the photoinduced electron transfer (PET) process (Sengupta et al., 2018). This PET process is modulated by charging and discharging the gold core, which can be used to fabricate sensors (Sengupta et al., 2018).



AuNPs have wide applications for surface-enhanced Raman scattering (SERS), to detect various components in living cells (Altunbek et al., 2016). Two major amplifications lead to the mechanism of the SERS. Electromagnetic enhancement and short-range chemical enhancement both these leads to an increase in the cross-section of Raman scattering (Altunbek et al., 2016). In electromagnetic enhancement, the local electric field at the surface of the nanoparticle is amplified by the resonance of the applied light field and the collective oscillations of the electrons of nanostructures. Short-range chemical enhancement is caused by the change in the polarisability of molecules as a result of their charge-transfer interaction with nanoparticle surfaces (Huang et al., 2007). AuNPs are effective instruments for electrochemical sensing (Kumar et al., 2011) and electrical devices (Lee et al., 2008) due to their oxidation-reduction processes. Surface-enhanced Raman scattering makes them useful for imaging (Thuy et al., 2010) and sensing (Zavaleta et al., 2009) (SERS). SPR studies have demonstrated that AuNPs may be utilised for colorimetric sensing (Li et al., 2010) and laser ablation (Huang et al., 2010) while their fluorescence quenching capabilities make them suitable for usage in the fields of material engineering and sensor development (Dubertret et al., 2001). As the size of the particles changes, so does the melting point of AuNPs. It is also observed that AuNPs have a lower melting point than bulk materials. The weakening of the attractive force of the core results in the reduction of the number of nearby atoms that decreases the melting point. This reduces the interaction between inner and surface atoms and increases the surface energy of surface atoms (Amina and Guo, 2020) the melting points therefore drop. Electrical properties of AuNPs are different from those of bulk material (Buffat and Borel, 1976). However, different materials may be used in combination to optimise their electrical and optical characteristics. As the particle size decreases, the surface area increases which then reduces electrical conductivity (Zawrah et al., 2016).

### **1.3 Methods for the synthesis of AuNPs**

The synthesis of nanoparticles can be accomplished using various techniques, with physical and chemical methods being the two most commonly employed approaches. This thesis is focused on the chemical method for the synthesis of functionalised AuNPs.

#### **1.3.1 Physical method (Top-down approach)**

The top-down approach for synthesising AuNPs involves starting with a larger piece of material and breaking it down into smaller nanoparticles through physical methods such as grinding or

milling (Nagarajan, 2008) This approach is often used to produce nanoparticles with a wide range of sizes, but it is more difficult to achieve precise control over the size and shape of the resulting particles (Nagarajan, 2008). One common method for synthesising AuNPs using a top-down approach is electrochemical synthesis, in which a gold precursor is reduced to gold metal at a cathode using an electric current (Hassan et al., 2022). This method allows for the production of large quantities of AuNPs in a short period of time, but it is difficult to achieve precise control over the size and shape of the resulting particles (Hassan et al., 2022). Another method for synthesising AuNPs using a top-down approach is photochemical synthesis, in which light is used to initiate the formation of AuNPs from a gold precursor (Jara et al., 2021). This method allows for the production of highly monodisperse nanoparticle populations, but it requires the use of specialised equipment and is a time-consuming method (Jara et al., 2021).

### **1.3.2 Chemical methods (Bottom-up approach)**

The Turkevich method is one of the most commonly used methods for the synthesis of AuNPs (Dong et al., 2020). This method was first reported by John Turkevich and colleagues in 1951, the method involves the reduction of gold ions using citrate as a reducing agent (Turkevich et al., 1951). Citrate ion, which is a trivalent anion, has a strong affinity for gold ions due to its negatively charged surface. It is able to reduce  $\text{AuCl}_4^-$  to Au(0) through the donation of electrons, resulting in the formation of AuNPs (Ali et al., 2018). In the Turkevich method, the reduction reaction takes place in an aqueous solution containing gold ions and citrate. The reaction is typically carried out at a temperature of around  $100^\circ\text{C}$  and a pH of 7. Figure 1.3. shows the Turkevich method (Imbraguglio, et al., 2013). The size of the resulting nanoparticles can be controlled by varying the concentration of the gold precursor and the sodium citrate-reducing agent, Citrate ions have negatively charged functional groups that adsorb onto the gold surface, resulting in a negatively charged layer represented by a red negative symbol. The blue positive symbol indicates the +1 oxidation state of sodium counterion. (Kumar et al., 2019).

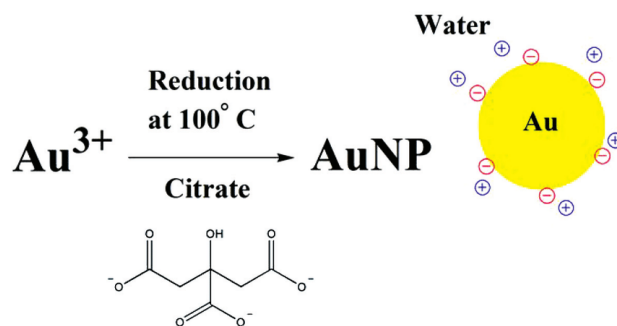


**Figure 1.3.** Representation of Turkevich method (Imbraguglio, et al., 2013)

The Brust-Schiffrin method is another commonly used method for the synthesis of AuNPs. This method involves the use of thiol compounds such as alkanethiols to reduce gold ions and stabilises the nanoparticles (Dreaden et al., 2012). The reduction reaction takes place in a two-phase system consisting of an aqueous phase and an organic phase. In the first step of the reaction, the thiol compound is added to an aqueous solution of gold ions to form a monolayer on the surface of the AuNPs. The organic phase, which contains a reducing agent such as sodium borohydride, is then added to the mixture, resulting in the reduction of the gold ions and the formation of stable AuNPs (Frens, 1973). Figure 1.4. gives the schematic representation of the Brust-Schiffrin method (Yafout et al., 2021). The size and shape of the nanoparticles can be controlled by adjusting the ratio of the thiol compound to gold ions and the amount of reducing agent used (Amina and Guo, 2020)

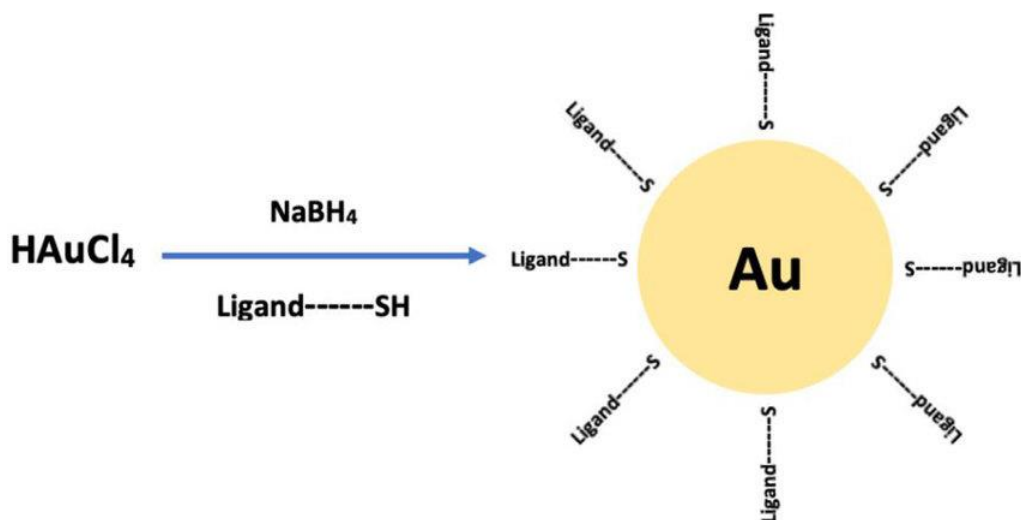


**Figure 1.4.** Representation of the Brust-Schiffrin method (Yafout et al., 2021)

Seed-mediated growth is a method commonly used for the synthesis of AuNPs with controlled size and shape. This method involves the use of small, pre-formed AuNPs as seeds for the growth of larger nanoparticles (Jana et al., 2001b). In the first step of the reaction, gold seeds are synthesised using a reducing agent such as sodium borohydride. These seeds are then added to a solution containing a gold precursor and a reducing agent, such as ascorbic acid. The gold precursor is reduced in the presence of the gold seeds, resulting in the growth of larger nanoparticles (Nikoobakht and El-Sayed, 2003). Figure 1.5. shows the seed-mediated growth method (Xia et al., 2017). The size and shape of the resulting nanoparticles can be controlled by adjusting the size and concentration of the seeds, as well as the reaction conditions (Jana et al., 2001a).

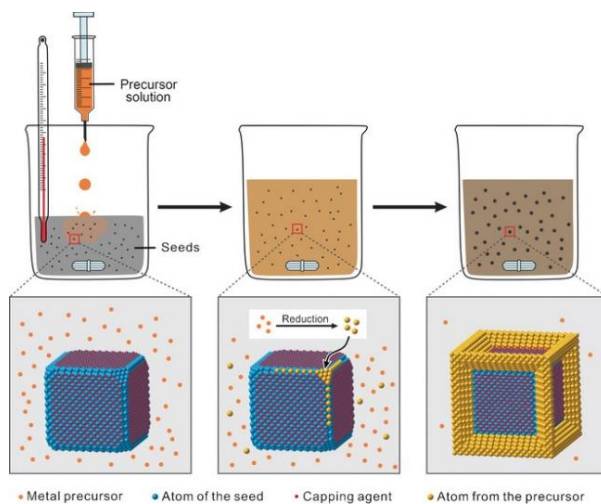


**Figure 1.5.** Representation of the seed-mediated growth method (Xia et al., 2017)

### 1.3.3 Stabilisation of AuNPs

One common method for stabilising AuNPs is through the use of capping agents. Capping agents are molecules that adsorb onto the surface of the AuNPs and prevent aggregation (Javed et al., 2020). The main function of the capping agent is to restrict the over-growth of nanoparticle clusters. Capping agents are added separately for the physical and chemical synthesis of the nanoparticles, in most cases, they are added during the synthesis (Javed et al., 2016; Latha et al., 2017). Some well-known capping agents for the synthesis of the nanoparticles are Polyethylene glycol (PEG), polyvinylpyrrolidone (PVP), polyvinyl alcohol (PVA), bovine serum albumin

(BSA), ethylenediaminetetraacetic acid (EDTA), and chitosan (Javed et al., 2020). All of the above-mentioned capping agents have the potential to alter the physicochemical properties of nanoparticles, making them suitable for applications in nanomedicine (Ajitha et al., 2016). To provide nanoparticles with appropriate physicochemical and functional qualities, capping agents are required. Their functional groups and surface charges distinguish them from one another. While choosing capping agents the intended size and shape of nanoparticles, in addition to their potential applications, must be taken into consideration (Latha et al., 2017). The type of functional groups, their hydrophobic or hydrophilic nature, their charge on capping agents, the length of the carbon chain or linker, and other factors are also taken into account. A minor modification in any particular parameter can have a significant impact on the overall properties of the nanoparticle (Niu and Li, 2013). Electrostatic stabilisation and steric stabilisation are also methods used to stabilise AuNPs (Mohrhusen and Osmić, 2017). Electrostatic stabilisation involves the adsorption of charged molecules onto the surface of the particles. This creates a repulsive force between the particles, which prevents aggregation and maintains the stability of the nanoparticles (Mohrhusen and Osmić, 2017). The charged molecules that are commonly used for electrostatic stabilisation include surfactants and polymers, such as polyvinyl alcohol and polyethylene glycol (Cortés et al., 2021). These molecules adsorb onto the surface of the nanoparticles and create a protective layer that prevents the particles from interacting with each other. This layer of charged molecules also helps to maintain the size and shape of the nanoparticles, ensuring their stability over time (Petersen et al., 2022). Steric stabilisation is another common method used to stabilise AuNPs by adsorbing polymers or surfactants onto their surface, creating a steric barrier that prevents aggregation (Yang et al., 2020). Examples of steric stabilisers include polyvinylpyrrolidone (PVP) and polystyrene sulfonate (PSS). The polymer chains or surfactant molecules on the surface of the nanoparticles provide steric hindrance, which prevents the particles from coming into close contact with each other. This maintains the stability of the nanoparticles over time and prevents them from aggregating (Yang et al., 2020). pH control is another way for stabilising AuNPs by manipulating the electrostatic interactions between the nanoparticles and surrounding molecules. The surface charge of the nanoparticles and the pH of the solution can influence the stability of the nanoparticles, as changes in pH can cause changes in surface charge and thus, stability (Ghosh et al., 2015). For instance, negatively charged AuNPs tend to aggregate at low pH values but can be stabilised by raising the pH of the solution (Ghosh et al., 2015). On the other hand, positively

charged AuNPs tend to aggregate at high pH values but can be stabilised by lowering the pH of the solution. Therefore, pH control can be used to adjust the surface charge of the nanoparticles, and thus stabilise them against aggregation (Ghosh et al., 2015).

### **1.3.4 Functionalisation of AuNPs**

There are several ways that AuNPs may be functionalised, allowing a wide range of design options for different drug delivery systems (DDS). No particular bond cleavage is necessary to carry out efficient drug release when non-covalent interactions are exploited to load drugs on nanoparticles. Instead, changes in natural physical forces are only required (Park et al., 2009). For instance, altering the local hydrophobicity can be used to release hydrophobic drugs. Similar to this, the drug may be covalently bound to AuNPs through cleavable bonds to produce a prodrug that can be delivered to the cell while the drug is still bound to AuNPs using either internal or external interaction (Han et al., 2006; Hong et al., 2006). Regardless of the drug delivery technique, the extracellular or intracellular discharge mechanisms depend heavily on the alteration monolayer of the AuNPs (Amina and Guo, 2020). To strengthen their bonding with biological molecules and to make AuNPs with functional moieties better drug-carriers with increased selectivity, different methods for their synthesis are being developed (Amina and Guo, 2020). The use of one or more of the functional groups, such as oligo or polyethylene glycol (PEG), bovine serum albumin (BSA), amino acids and polypeptides, oligonucleotides, antibodies, receptors, and several other comparable particles, is being used to functionalise AuNPs (Amina and Guo, 2020). The numerous functional groups, their ligand moieties, and distinguishing characteristics that make them good candidates for biological applications.

### **1.4 Green synthesis of the AuNPs**

AuNPs can be synthesised using bioreduction methods, which involve the use of biological materials such as enzymes, microorganisms, or plant extracts to reduce a gold salt and produce AuNPs (Alsaiani et al., 2023). This method has several advantages over chemical reduction methods, including being environmentally friendly and producing AuNPs with a narrow size distribution and a high degree of monodispersity (Leng et al., 2015). One example of a bioreduction method for synthesising AuNPs is the use of bacteria or fungi to reduce a gold salt and produce AuNPs (Kitching et al., 2015). This method has been used to synthesise AuNPs with a wide range of sizes and shapes, and it has the advantage of being fast and easy to scale up

(Kitching et al., 2015). Another example of a bioreduction method is the use of plant extracts to reduce a gold salt and produce AuNPs (Aljabali et al., 2018). This method has the advantage of being environmentally friendly and produces AuNPs with a narrow size distribution and a high degree of monodispersity (Aljabali et al., 2018). Bioreduction methods are a promising approach for synthesising AuNPs and have many potential applications in fields such as medicine, electronics, and catalysis (Singh et al., 2018).

For green synthesis processes, water is regarded as the best and most appropriate solvent system. Water has been used as a solvent for the synthesis of numerous nanoparticles ever since the development of nanoscience and nanotechnology. A laser ablation method in an aqueous solution was used to generate AuNPs. The O<sub>2</sub> in the H<sub>2</sub>O causes the generated AuNPs to partially oxidise, which ultimately increased their chemical reactivity and had a significant influence on their development (Tran et al., 2016a). Alcohol ionic liquids serve as both a stabiliser and a reducing agent, greatly simplifying the process of making nanoparticles (Kim et al. 2006). Ionic liquids can be used to generate a number of metal nanoparticles, including Au, Ag, Al, Te, Ru, Ir, and Pt (Vollmer et al., 2010; Kamalakannan et al., 2018). Ionic liquids such as (tetraoctylammonium bromide (TOAB) (Mjalli et al., 2014), choline dihydrogen phosphate ([choline][DHP]) (Reslan and Kayser, 2018) can act as a reducing and a shielding agent, which simplifies the synthesis of nanoparticles. Depending on the kind of cations and anions, ionic liquids can either be hydrophilic or hydrophobic. Both hydrophilic and hydrophobic ionic liquids can serve as catalysts due to their ionic nature (Kamalakannan et al., 2018; Ananikov, 2010). In the electrolytic process, the ionic liquid was supplied in place of water without any mechanical stirring.

#### **1.4.1 Biosynthesis of the AuNPs from the plant extracts**

According to Iravani and coworkers, the bio-synthesis of AuNPs using plant extracts involves the use of plant extracts as the reducing and capping agents for the bio-reduction of gold ions to form AuNPs. The author also mentions that this method of synthesis is eco-friendly, cost-effective, and scalable (Iravani, 2011). Biosynthesis of the AuNPs from the plant source is a simple one-pot method. Different parts of the plants are utilised such as bark, leaves, stem, roots, etc. (Ahmed et al., 2016). In order to make extract the parts of the plants are cleaned with distilled water then it is grounded and chopped into fine granules and boiled in distilled water. For purification, various techniques are used (centrifugation, filtration, etc.). The extract is then simply combined with

varying quantities of gold salt solution (Ahmed et al., 2016). Within a few minutes to a few hours, the gold salt solution is reduced into AuNPs. The reaction mixture is held for longer periods of time and can be identified by colour change. The generated AuNPs are then extensively cleaned in water and centrifuged for purity before being used. The entire procedure is easy and environmentally friendly (Santhosh et al., 2022).

#### **1.4.2 Using microorganisms**

Microorganisms such as bacteria and actinomycetes can be used for the green synthesis of AuNPs. Microorganisms have attracted a lot of attention in the field of industrial microbiology. Some of the attractive factors include simple handling and processing, inexpensive growing media, and the capability to adsorb and reduce different metal ions into nanoparticles (Lee et al., 2020; Sharma, 2012). Large-scale microbe growth in bulk fermenters will make it possible to extract more enzymes and different secondary metabolites in a less expensive way. The microbes can be cultured in a less expensive method which makes them environmentally friendly (Siddiqi and Husen, 2016). Bacteria are suitable candidates for the synthesis of nanoparticles due to their explicit availability in the environment, fast growth, and capacity for survival under adverse conditions. Actinomycetes and prokaryotic bacteria have both been employed extensively in the production of AuNPs, either intracellularly or extracellularly (Santhosh et al., 2022). Metal ions can be converted to their corresponding nanoparticles by a number of enzymes, fatty acids, and carbohydrates found inside the bacterial cell. The capability of some bacterial strains to bind and adsorb metal ions and then convert them into nanoparticles using enzymes generated during cellular metabolic processes makes the strains useful in biological processes (Santhosh et al., 2022).

#### **1.4.3 Fungi and algae**

Fungi-based synthesis of AuNPs involves the use of the cell wall of the fungi as a template for the formation of uniform and stable AuNPs (Molnár et al., 2018). This method has several advantages over conventional methods, including a simple and cost-effective synthesis process, low toxicity, and the ability to produce highly stable and uniform nanoparticles. In addition, the use of fungi as a template allows for precise control over the size and shape of the AuNPs, which is critical for their potential applications (Michael et al., 2022). Algae-based synthesis of AuNPs, on the other hand, involves the use of photosynthetic pigments found in algae to reduce gold ions to AuNPs



(Michael et al., 2022). This process is typically carried out in the presence of sunlight, which provides the energy required for the reduction reaction. This method has several advantages, including a low-cost and eco-friendly synthesis process, the ability to produce a large quantity of AuNPs and the potential for scalability (Michael et al., 2022).

## **1.5 Biomedical application of the AuNPs**

AuNPs have many potential biomedical applications due to their unique physical and chemical properties (Milan et al., 2022). AuNPs have a high surface area to volume ratio, which makes them attractive for use in drug delivery and imaging applications (Milan et al., 2022). This is due to a high surface area to volume ratio allows a large number of drugs or imaging agents to be attached to the AuNPs, which increases the efficiency of the drug or imaging agent (Kong et al., 2017b). In addition, a high surface area to volume ratio also allows AuNPs to interact with a larger number of tissues or cells in the body, which can increase the effectiveness of the drug or imaging agent (Kong et al., 2017). AuNPs also have a high melting point, good electrical conductivity, and good biocompatibility, which makes them useful for a variety of other biomedical applications (Hu et al., 2020). The high melting point of AuNPs makes them stable and resistant to degradation, which is important for maintaining the integrity of the drug or imaging agent attached to the AuNPs (Amina & Guo, 2020). The good electrical conductivity of AuNPs allows them to be used in a variety of electrical or magnetic applications, such as MRI or photothermal therapy (Luo et al., 2021). The good biocompatibility of AuNPs means that they are not toxic or harmful to the body, which is important for ensuring the safety of any drugs or imaging agents attached to the AuNPs (Luo et al., 2021),

### **1.5.1 Drug delivery**

Due to their large surface area to volume ratio, AuNPs can be functionalised with a wide range of biomolecules, including proteins, peptides, and DNA (Tiwari et al., 2011). This ability to directly attach to particular cells or tissues makes them effective for targeted drug delivery (Lim et al., 2011). In order to selectively target and deliver drugs to cancer cells, AuNPs, for instance, can be functionalised with ligands that bind to receptors on cancer cells (Bloise et al., 2022). This targeted delivery can increase the overall effectiveness of cancer treatment by lowering the toxicity of chemotherapy medicines to healthy cells (Lim et al., 2011). Additionally, AuNPs can be used to deliver drugs to specific body parts, which are challenging to reach with conventional drug

delivery techniques (De Jong & Borm, 2008). Due to their tiny size, AuNPs may readily cross the blood-brain barrier, a physical barrier that protects the brain from blood flow (Sokolova et al., 2020). In order to cure diseases of the brain like Alzheimer's or brain cancer, AuNPs are a promising method (Khan et al., 2021). The unique physical and chemical characteristics of AuNPs make them suitable for application in the treatment of cancer (Lim et al., 2011). AuNPs have the capability to be used in drug delivery, which would improve the cytotoxic effects of chemotherapy treatments by increasing their absorption into cancer cells. Given that they may be easily found using methods like CT or MRI, AuNPs have also been employed for cancer imaging (Deb et al., 2015). There are a number of possible benefits to using AuNPs for drug delivery. First, AuNPs can enhance the targeted delivery of chemotherapy medications to cancer cells, therefore lowering their toxicity to healthy cells and enhancing the effectiveness of the treatment (Lim et al., 2011). Second, by boosting the absorption of chemotherapy drugs into cancer cells and by making cancer cells more sensitive to the treatments, AuNPs can improve the harmful effects of chemotherapy drugs (Lim et al., 2011). Photothermal therapy, in which AuNPs are used to absorb near-infrared (NIR) light and transform it into heat that may subsequently be utilised to destroy cancer cells, is one application for which they may be used to treat cancer (Lim et al., 2011). Additionally, scientists are attempting to optimise the therapeutic benefits of the nanoparticles by enhancing their size and shape (Mitchell et al., 2021). Overall, research into the use of AuNPs in cancer therapy is vigorous and shows promise as a possible cancer treatment.

### **1.5.2 Imaging**

Magnetic resonance imaging (MRI) and computed tomography (CT) can both employ AuNPs as diagnostic imaging tools (Amina & Guo, 2020). They can be functionalised with contrast agents that can be seen by CT or MRI scanners, allowing medical professionals to more precisely visualise and identify disorders like cancer or cardiovascular disease (Deb et al., 2015). Using CT or MRI scanners, AuNPs may be easily seen due to their great contrast (Popovtzer et al., 2008). Additionally, they may be functionalised with various contrast agents, enabling them for multimodal imaging (Jain et al., 2013). AuNPs may be utilised to simultaneously visualise various features of a disease or tissue, giving more thorough and precise information about the condition. AuNPs can be employed in optical imaging methods like fluorescence microscopy in addition to CT and MRI (Wu et al., 2019). This technique involves the functionalisation of AuNPs with fluorescent molecules, which produce light when exposed to specific light wavelengths

(Swierczewska et al., 2011). This enables medical professionals to see certain cells or tissues within the body, revealing critical details regarding the location and spread of illnesses like cancer. Compared to conventional contrast agents, using AuNPs in imaging provides a number of benefits. Using CT or MRI scanners, AuNPs may be easily seen due to their great contrast (Amina & Guo, 2020b). Additionally, AuNPs can be utilised in conjunction with other treatments, including photothermal therapy, to treat and see illnesses at the same time (Vines et al., 2019). This implies that a more comprehensive approach to healthcare is possible by using AuNPs for both illness diagnosis and treatment.

### **1.5.3 Biosensors**

Biosensors have impacted various fields by providing a quick and reliable way to detect specific analytes. Biosensors use biological elements such as enzymes, antibodies, or nucleic acids to recognise and bind to a specific target molecule, resulting in a measurable signal (Michael et al., 2022). In recent years, nanoparticles produced by algae have emerged as promising candidates for biosensor development due to their unique properties. These nanoparticles can be easily synthesised in large quantities and functionalised with biomolecules to enhance their selectivity and sensitivity (Zheng and Tan, 2020). One potential application of algae-derived nanoparticles is in the detection of adrenaline, a hormone that plays a critical role in the body's response to stress. Elevated levels of adrenaline can indicate conditions such as allergies, heart attacks, cardiac operations, and asthma (Michael et al., 2022). Using algae-derived nanoparticles, scientists have developed a biosensor with remarkable sensitivity for detecting adrenaline in clinical samples. Moreover, the use of algae-derived AuNPs has also been proposed for the detection of cancer (Chaudhary et al., 2020). Different types and numbers of hormones are present in our bodies, and their levels can change in various diseases, including cancer. The detection of these hormones can provide valuable diagnostic information, and AuNPs made from algae could serve as a crucial tool for the detection of cancer (Chaudhary et al., 2020).

## 1.6 Overall objective and specific aims of the thesis

As explained in the literature review written as part of this chapter, there are numerous advantages of using AuNPs in biomedical applications and possibilities of developing green methods for their synthesis. Therefore, the overall objective of this thesis is to produce AuNPs functionalised with hydrophobic coating agents in water and synthesise the latter using greener solvents with the use of simulation software to reduce the number of experimental attempts and more importantly reduce the wastage of chemicals. Specific aims to achieve this main objective are the followings:

- To incorporate green chemistry principles in the organic synthesis of both intermediates and cationic lipophilic phosphonium ligands by using Aspen Plus software to check whether the corresponding reactions can occur in 100% water and obtain reaction conditions (optimal reaction time and temperature).
- To conduct the syntheses of the cationic lipophilic phosphonium ligand and intermediates in the laboratory using greener solvents and the reaction conditions predicted by the Aspen Plus, and to use FTIR for their chemical structure characterisation.
- To develop green synthetic methods to produce cationic lipophilic AuNPs using water as the main solvent, dimethylformamide (DMF) as the reducing agent and the cationic lipophilic phosphonium ligand for the coating, and varying reaction temperature and DMF concentration.
- To characterise cationic lipophilic AuNPs, produced following the green methods developed in this project, using techniques such as UV-Vis spectroscopy and Transmission Electron Microscopy, and compare with same AuNPs synthesised with conventional methods reported in the literature.

# Chapter 2

## Characterisation techniques

### 2.1 Introduction

This chapter provides an overview of the primary characterisation techniques employed for the analysis of phosphonium ligands and functionalised gold nanoparticles. The analytical methods utilised in this study, include Attenuated Total Reflectance-Fourier-transformed Infrared (ATR-FTIR), Melting point, Rotary evaporator, Thin layer chromatography (TLC), Transmission Electron Microscopy (TEM), UV-Visible spectroscopy (UV-Vis), and X-ray Photoelectron Spectroscopy (XPS). Each of these techniques was employed to characterise all ligands and functionalised AuNPs prepared using both conventional and green synthetic methods. The use of these analytical methods ensures a comprehensive understanding of the synthesised materials, their properties, and their potential applications.

### 2.2 Analytical techniques

#### 2.2.1 ATR-FTIR spectroscopy

FTIR analysis of intermediates and final ligand was carried out using a PerkinElmer UATR Two equipped with Spectrum<sup>TM</sup> software (Version 10). A Smart Omni-Sampler (ATR cell with single reflectance diamond crystal) is used for the characterisation of the ligands synthesised using both conventional and green synthetic approaches.

ATR spectroscopy provides valuable information about the chemical structure and functional groups of materials and can measure the amount of light absorbed as it interacts with a sample at the interface between two media, typically the sample and a diamond crystal (Ismail et al., 1997). The diamond crystal serves as a waveguide for the IR light, allowing for the measurement of the IR spectra of samples in contact with it. Total internal reflection is the underlying theory behind ATR spectroscopy, which describes how light is reflected back into a medium from the interface between two mediums with different refractive indices. In ATR spectroscopy, a sample is brought in contact with a crystal that has a higher refractive index than the sample, and a beam of infrared light is focused onto the crystal at a certain angle, known as the critical angle, causing the light to experience total internal reflection (Ismail et al., 1997).



**Figure 2.1.** PerkinElmer UATR Two was used for the analysis of Intermediate #1, Intermediate #2 and the Ligands

Figure 2.1. shows the (ATR-FTIR) spectroscopy setup used in this project. Prior to the analysis, the samples were first dried in an oven at 60°C overnight and then stored in a desiccator to prevent moisture. The instrument was set up by selecting a spectrum range from 4000cm<sup>-1</sup> to 400cm<sup>-1</sup>, fixing the resolution at 4, and selecting the number of scans to 64. A background scan was run to eliminate any environmental effects on the spectrum. Then a small quantity of the dried sample (Intermediate #1, Intermediate #2, and the Ligand), was taken and spread over the top of the diamond crystal in the ATR unit. The sample was then pressed and the pressure in the gauge bar was selected between 80-100, and the sample was scanned to obtain the spectrum. The sample's capacity to absorb particular IR light wavelengths is correlated with the intensity of the IR light that passes through the sample. Functional groups of the sample are then determined from the spectrum (Ismail et al., 1997).

### **2.2.2 Melting point**

Stuart Melting point SMP10 was used for the analysis of the melting point of the intermediates. An electrothermal melting point apparatus is a laboratory instrument used to determine the melting point of a solid substance. This temperature is a fundamental physical property of the substance that can provide important information about its nature, purity, and composition (Sharma 2021).



**Figure 2.2.** Melting point apparatus

To determine the melting point of a substance, a small amount of intermediates was placed in a capillary tube and inserted into the melting point apparatus the substance was then heated at a controlled rate as shown in Figure 2.2. The temperature was continuously monitored until the substance begins to melt. The temperature at which the substance completely melts is recorded as its melting point.

### **2.2.3 Rotary Evaporator**

Rotavapor R-210 was used for the extraction of Intermediate #2. A rotary evaporator is an instrument generally used to separate the solvent from the sample by continuous distillation, in addition to the continuous distillation of volatile solvents it is used for concentration, crystallisation, drying, separation, and solvent recovery. They have applications in various fields such as pharmaceuticals, chemicals and biotechnology-based industries. Various components are involved in the working of the rotary evaporator (Elgie, 2022).

The schematic representation of the Rotary Evaporator is shown in Figure 2.3. The rotary evaporator utilises this principle to evaporate/ remove and recover organic solvents from a sample by applying mild heat (40 – 60<sup>0</sup>C) to the sample in a water bath while simultaneously creating a vacuum in the system to lower the pressure. The vapours produced from the sample are then condensed back into a liquid form in a cooled condenser and collected in a flask for further analysis or use (Elgie, 2022).



**Figure 2.3.** Instrumentation of the rotary evaporator

Rotary evaporator is used for the extraction of Intermediate #2 using the conventional method and Intermediate #1 using the green method.

#### **2.2.4 Thin layer chromatography TLC**

Thin layer chromatography (TLC) was performed on Merk silicagel plates using mixtures of dichloromethane: methanol as an eluent system. This simple chromatographic method was used to check the progress of the reaction carried out to obtain Intermediate #1, Intermediate #2, and the ligand, by monitoring the emergence of a product or the elimination of a reactant (Thin Layer Chromatography, n.d.). The schematic representation of the TLC is shown in Figure 2.4.

A small amount of the solution of Intermediate #1 and Intermediate #2 and ligand is transferred into one end of the TLC plate using a micropipette the spotting sample evaporates very quickly and leaves behind a spot on the plate. The TLC plate is placed in a shallow pool of the 90:10 of DCM and methanol solution and the solvent moves up the plate by capillary rise. Reactants and products with different polarities within the first spot will migrate to different positions away from the original spot. Once the separation was completed, the TLC plate was dried and placed in the



glass containing iodine. After a short period of the time dark brown spots corresponding to the reactants and the products were observed.

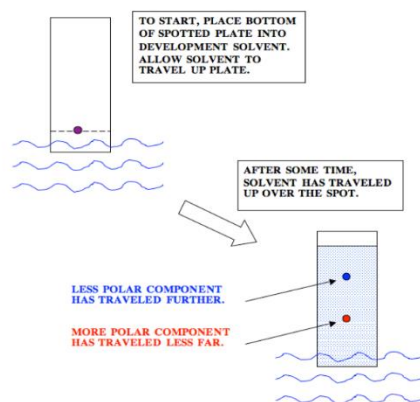


**Figure 2.4.** Schematic representation of TLC (Sathya, 2017)

### 2.2.5 Transmission Electron Microscope (TEM)

The Jeol 2100F Field Emission Gun Transmission Electron Microscope was used for the characterisation of the samples synthesised by both conventional and green synthetic methods and to obtain information about their size.

In general, a microscope consists of several parts which include a source for illumination, a condenser lens to converge the beam from the source to the sample, an objective lens to magnify the image, and a projector lens to project the image onto an image plane. The wave nature of the electron is used to obtain the image of the sample in an electron microscope. The lenses used in electron microscopes are electromagnetic in nature. TEM is a powerful tool for investigating the morphology and properties of materials at the atomic and molecular levels (Zuo and Spence, 2016). The working of a TEM involves a beam of high-energy electrons passing through a very thin sample, interacting with the atoms in the sample, and producing an image on a detector.

Figure 2.5. shows the schematic diagram of the Transmission electron microscope (TEM). The electron beam is generated by an electron gun, which accelerates electrons towards the sample. An array of electromagnetic lenses that operate as microscope lenses focus and shape the electron beam in a manner similar to an optical microscope. As the electron beam passes through the sample, which then interacts with the electrons in the atoms and the crystal structure of the sample

that causes scattering and absorption of the electrons. The scattered electrons and transmitted electrons from the sample are then collected by the detector, which then converts the electron signal into an image (Zuo and Spence, 2016).

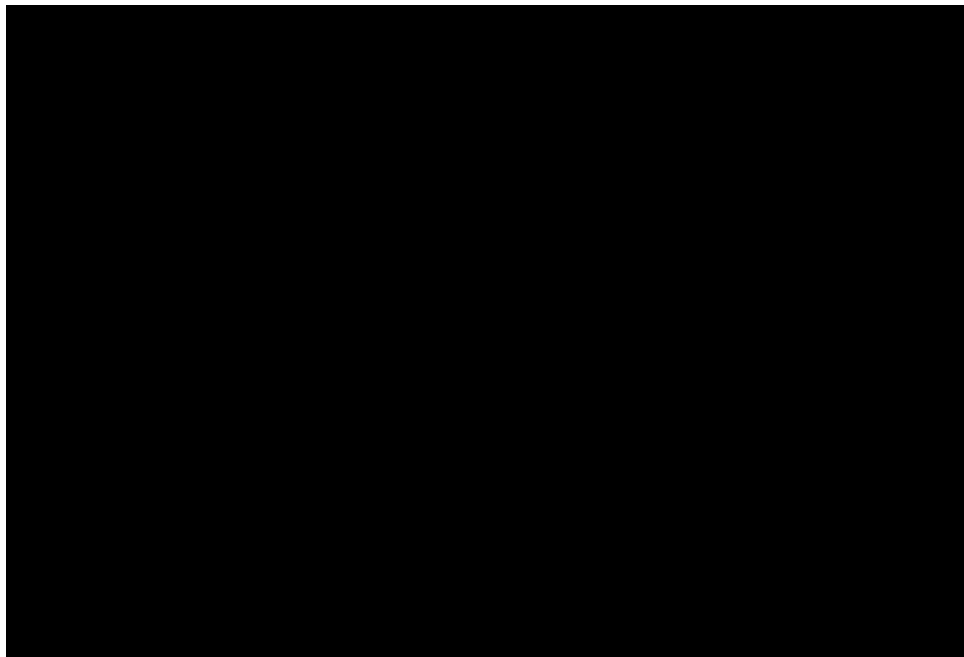


**Figure 2.5.** Schematic representation of TEM (PeakD, n.d.)

Sample preparation for TEM analysis, involves dilution of the AuNPs colloidal solution. These were performed by adding 1  $\mu\text{l}$  of the AuNPs solution to 100  $\mu\text{l}$  of DI water. This ensures that the concentration of the AuNPs is appropriate for the subsequent sample preparation. After dilution, the AuNPs were centrifuged to remove any large aggregates or debris. The supernatant was deposited onto the carbon-coated copper grid. The sample is then allowed to dry, once dried the copper grid was placed under a magnifying glass in order to remove large fibres and other contaminants as these may interfere with the imaging. Finally, the TEM grid is loaded onto the TEM column and imaging parameters are optimised to obtain clear and detailed images of the nanoparticles. The imaging conditions were optimised for the sample by adjusting the electron beam current, focus, and aperture to get a clear image. For the analysis of the particle size, two TEM images of each sample were analysed by counting 150 particles corresponding to each samples using the ImageJ software and are plotted using the Origin 2023 software.

### **2.2.6 UV-Visible spectroscopy**

A Perkin-Elmer 25 UV-Vis spectrophotometer was used for the characterisation of the functionalised AuNPs prepared using both conventional and green synthetic methods. Samples were analysed in the wavelength range from 400 to 700nm, with a resolution of 1 nm.

UV-Visible spectroscopy is a type of absorption spectroscopy in which a molecule absorbs light in the ultra-violet range. Surface Plasmon resonance (SPR) is a phenomenon that occurs when light interacts with a metal surface, such as gold and excites the collective oscillation of free electrons, known as surface plasmons. Gold nanoparticles can exhibit SPR, which is commonly used for sensing and detection applications. In the case of gold nanoparticles, the SPR occurs at a specific wavelength and is dependent on the size, shape, and composition of the nanoparticle. When the wavelength of incident light matches the SPR wavelength of the gold nanoparticles, the intensity of the scattered light is greatly enhanced, making them visible under a microscope or other imaging techniques (Amendola et al., 2017). On absorption of the light by the molecule, electrons are excited from their ground state to a higher energy state. Molecules containing electrons or non-bonding electrons (n-electrons) can absorb energy in the form of ultraviolet light to excite these electrons to higher anti-bonding molecular orbitals. The more easily excited the electrons are, the longer the wavelength of light they can absorb. The amount of light absorbed by the sample depends on the chemical composition of the sample and the wavelength of light used. Different molecules have different energy levels and absorb light at different wavelengths, which allows for the identification and quantification of the components of a sample. The UV-Vis spectrophotometer can also be used to measure the concentration of a particular component in a sample, as the amount of light absorbed is directly proportional to the concentration of the component (Skoog et al., 2023).



**Figure 2.6.** Perkin-Elmer 25 UV-Vis spectrophotometer was used for the analysis of the colloidal gold nanoparticles

The principle of UV-visible spectroscopy is based on the Beer-Lambert law, which states that the absorbance of a solution is directly proportional to the concentration of the absorbing species and the path length of the sample. Figure 2.6. depicts the UV-Vis spectrophotometer used for the analysis of the colloidal AuNPs. For the characterisation of the samples, different dilutions of the synthesised samples were used. The colloidal gold nanoparticles were diluted with 1ml in 9ml of solvent, for the green synthesis different ratios of the DMF and DI water were used, and for the conventional method, 100 % DI water is used as the solvent.

For the data collection process, specific parameters were specified, including the wavelength range (400-700nm), the number of scans (64), and the type of spectrum (absorption). The subsequent step involved selecting the appropriate reference sample, depending on the method of synthesis employed, whether conventional or green. For the conventional method, 100% of DI water was chosen as the reference/ blank, while for the green synthesis, various ratios of DMF and DI water (1:5 and 1:2) were used. Prior to the analysis, background scanning was performed by placing the reference/ blank in one sample holder and leaving the other sample holder empty. This step ensures that any signals arising from the instrument or the environment are subtracted from the final spectrum. After the background scanning, the synthesised colloidal gold nanoparticle solution was placed in one sample holder, while the reference/ blank was kept in the sample holder. The analysis was then carried out to acquire the UV-Vis spectrum.

## 2.2.7 X-ray photoelectron spectroscopy (XPS)

X-ray Photoelectron Spectroscopy (XPS) measurements were made on a KRATOS SUPRA Photoelectron Spectrometer at 10 KV and 20 mA using a monochromatic Al  $K\alpha$  X-ray source (1486.6 eV). The take-off angle was fixed at 90°. Three drops of AuNP sample were deposited on a clean Al foil surface and let to dry at room temperature, and then mounted on a standard sample stud employing double sided adhesive tape. On each sample, the data were collected from three randomly selected locations, and the area corresponding to each acquisition was 400  $\mu\text{m}$  in diameter. Each analysis consisted of a wide survey scan (pass energy 160 eV, 1.0 eV step size) and a high-resolution scan (pass energy 20 eV, 0.1 eV step size) for component speciation. All experiments were conducted in triplicate. The binding energies of the peaks were determined using the C 1s peak at 284.6 eV. The software CasaXPS 2.3.17 (Fairley, 2014) was used to fit the XPS spectra peaks.

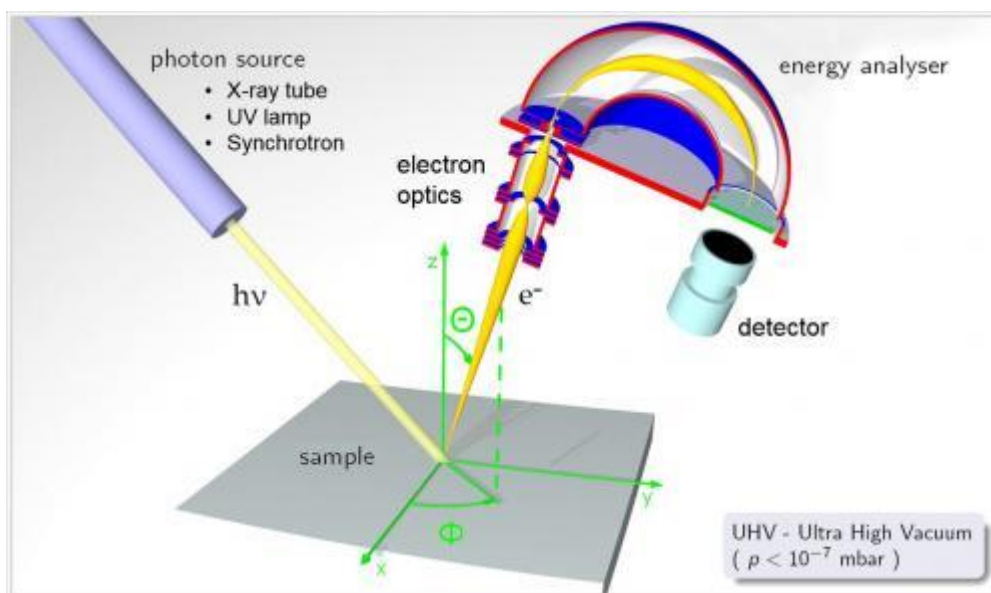


**Figure 2.7.** X-ray Photoelectron Spectroscopic technique (West Campus Materials Characterisation Core, n.d.)

## Chapter 3

# Green synthesis of phosphonioalkylthiosulfate ligand - Aspen modelling to experimental trials

### 3.1 Introduction

Phosphonioalkylthiosulfate ligands, such as triphenylphosphoniopropylthiosulfate zwitterion, can be used as capping agents to functionalise AuNP as reported in the literature (Ju-Nam et al., 2012; Ju-Nam et al., 2016). The triphenylphosphoniopropylthiosulfate zwitterion synthetic route is based on a three-stage process as shown in the in Figure 3.1. This procedure is referred to the Conventional Route in this thesis. In the first stage, hydroxylpropyltriphenylphosphonium salt (from now on referred as **Intermediate #1**) is synthesised by reacting TPP with bromopropanol in ACN under reflux conditions. In the second stage, Intermediate #1 crystals, obtained from the first stage, are reacted with hydrobromic acid also under reflux conditions for several hours to produce  $\omega$ -bromopropyltriphenylphosphoniumbromide (**Intermediate #2**). Purification of the latter is normally carried out using organic solvents such as DCM. In the third and final stage, Intermediate #2 is reacted with sodium thiosulfate in a 1:1 ratio of ethanol:water. This mixture is left under reflux conditions for several hours to obtain final product triphenylphosphoniopropylthiosulfate zwitterion (**Ligand**).

The main aim of this part of the project was to incorporate green chemistry principles in the organic synthesis of both intermediates and Ligand. However, due to the time constrains, this concept was only applied to Reaction # 1 (Figure 3.1). Prior attempting a green synthesis of Intermediate #1 in the laboratory, Aspen Plus software was used to check whether Reaction #1 can occur in greener solvents and duration (reaction time). The approach of modelling Reaction #1 first to predict and obtain reaction conditions could potentially save time spent in the laboratory, reduce the number of experimental attempts and more importantly reduce the wastage of chemicals.

Aspen Plus is a powerful and widely used process simulation software in the fields of chemical engineering and process chemistry. This software provides chemical engineers with a comprehensive toolkit to model and optimise chemical processes, from the early stages of process

design. Users can create process flowsheets, compute thermodynamic and transport parameters, simulate unit operations, and improve process performance using the software (Haydary, 2019).

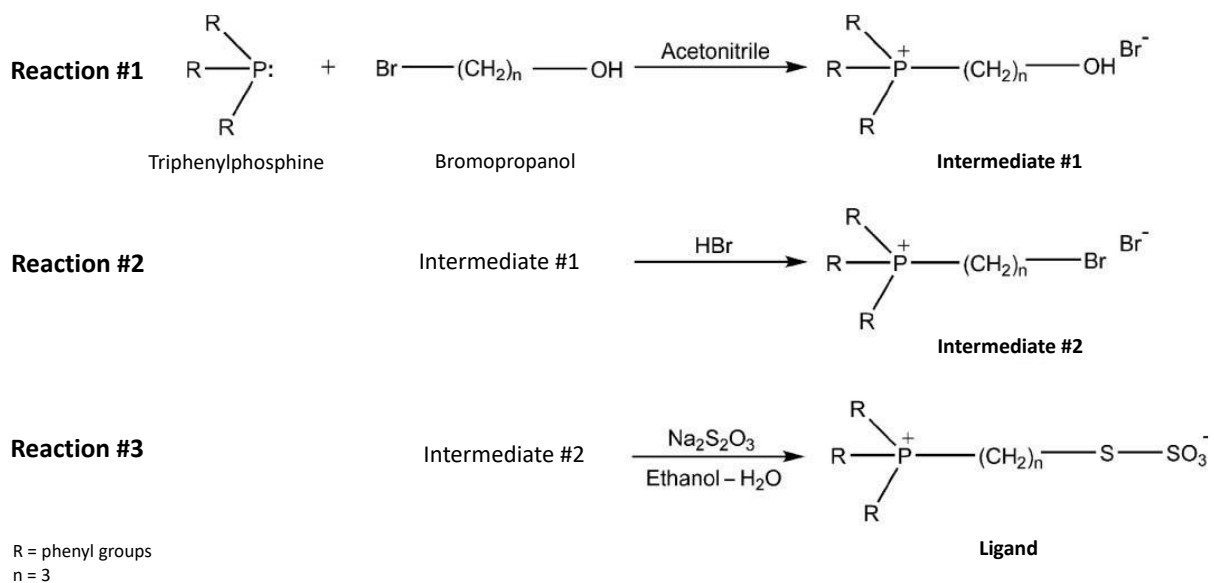


**Figure 3.1.** Conventional Route (three-stage process) to produce Intermediate #1, Intermediate #2 and Ligand (triphenylphosphoniopropylthiosulfate zwitterion).

Aspen Plus users can develop, execute, and analyse complex process simulations due to its user-friendly interface. Creating informed decisions about components such as equipment selection, process design, and operating conditions is one of the main advantages of adopting Aspen Plus. This approach can help to cut costs, increase efficiency, guarantee safety and reliability, and discover possible bottlenecks by modelling a chemical process. They can also assess various scenarios and enhance process performance. This simulation tool also aids engineers in evaluating a process financial viability, including capital and operational expenses, by offering thorough cost estimates and financial evaluations. Aspen Plus has a variety of uses, including process synthesis, optimisation, and precise engineering. A broad variety of process types, including distillation, absorption, evaporation, reaction, heat transfer, and many more, may be handled by the programme (Al-Malah, 2017; Haydary, 2019).

Aspen Plus allows users to create their own process model, beginning with the flow sheet and specifying the chemicals involved in the reaction and operating condition. During the simulation, all the necessary calculations to solve a reaction, and predict its behaviour can be obtained. Once

the calculations are completed, Aspen Plus software will display the result stream by stream and also unit by unit, making the analysis of reactions easy to follow.

Before starting the Aspen Plus work for this project, synthesis of both Intermediate #1 and #2, and Ligand was carried out following the Conventional Route reported by Ju-Nam and co-workers (Ju-Nam, et al., 2016), with the aim to obtain the Ligand to produce functionalised AuNPs using greener methods (Chapter 4), and deeper understanding of the Conventional Route, to aid the simulation work and design of a greener protocol to obtain the intermediates and Ligand. Experimental results from the Conventional Route, simulation work and its corresponding experimental attempt to obtain Intermediate #1, using a newly designed greener route, are outlined in this Chapter 3. The latter also includes the materials and methods, a detailed explanation of the modelling approach and a discussion of corresponding experimental work carried out in the laboratory.

## **3.2 Materials and methodology**

### **3.2.1 Chemicals**

Triphenylphosphine ( $\text{P}(\text{C}_6\text{H}_5)_3$ , TPP), bromopropanol ( $\text{C}_6\text{H}_7\text{BrO}$ ), acetonitrile (ACN), sodiumthiosulfate ( $\text{Na}_2\text{S}_2\text{O}_3$ ), ethanol, dichloromethane (DCM) were bought from Sigma-Aldrich and hydrobromic acid from Fisher. All chemicals and reagents used in the entire study were of analytical grade. All the chemicals were used without further purification. Finally, deionised water (DI water) was obtained from the Millipore Direct-Q Water Purification system (resistivity  $18.2 \text{ M}\Omega\cdot\text{cm}$  at  $25 \text{ }^\circ\text{C}$ ; total organic carbon (TOC)  $\leq 5 \text{ ppb}$ ).

### **3.2.2 Synthesis of triphenylphosphoniopropylthiosulfate zwitterion (Ligand) using the Conventional Route**

#### **3.2.2.1 Synthesis of hydroxypropylphosphonium salt (Intermediate #1)**

The synthesis of Intermediate #1 was done accordingly to the previously published study by Ju-Nam et al., 2016). In order to synthesise Intermediate #1, 1g (3.8 mmol) of TPP and 3ml (30.2 mmol) of bromopropanol were mixed with 15ml of ACN in a round bottom flask. A few amounts of anti/bump granules were added to the mixture, which was then placed in a reflux condenser setup for five hours. The solution was transferred into a conical flask and sealed with paraffin tape. The flask was then kept overnight to allow the crystal formation. The crystals were filtered and



washed with DCM to remove any impurities. The filtered crystals were then dried overnight in an oven at 60°C.

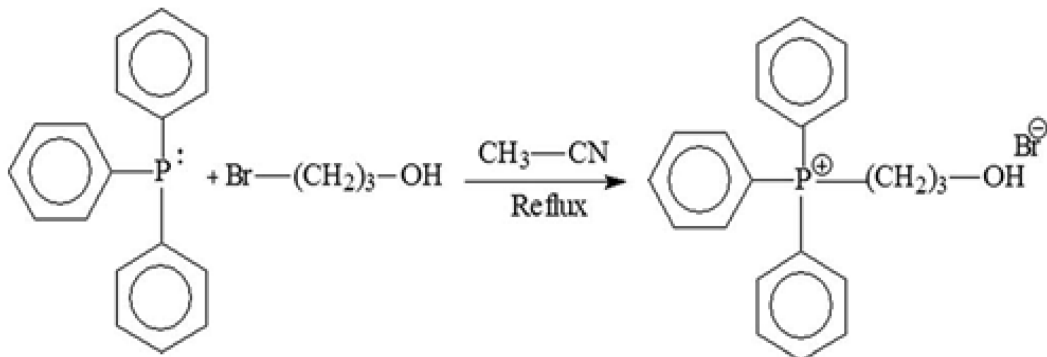


**Figure 3.2.** Reaction #1 for the synthesis of Intermediate #1 (Ju-Nam et al., 2016)

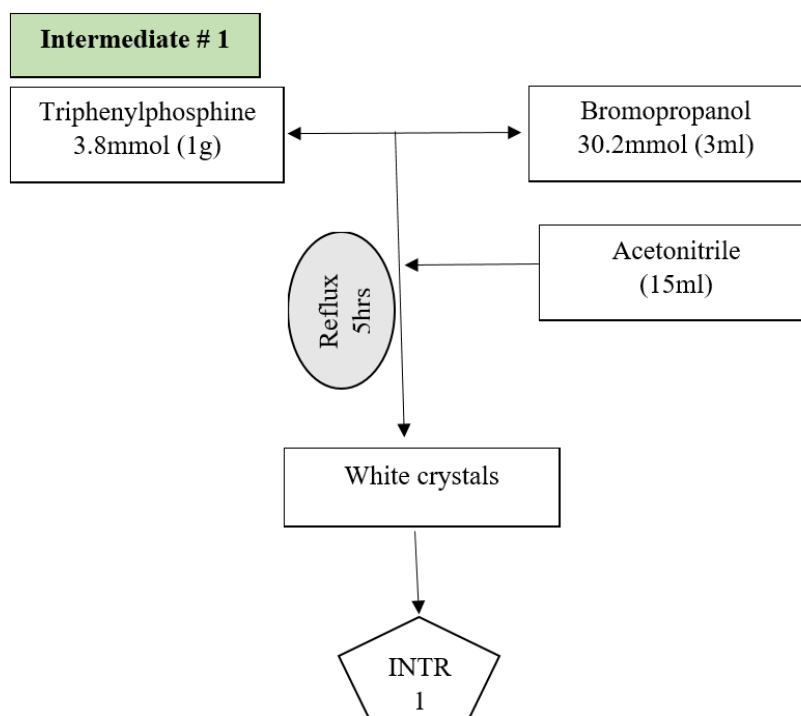


**Figure 3.3.** Flowchart representation for the synthesis of Intermediate #1.

### 3.2.2.2 Synthesis of $\omega$ -bromopropyltriphenylphosphoniumbromide (Intermediate #2)

In order to synthesise Intermediate #2 (Ju-Nam et al., 2016), 1g of hydroxylpropylphosphonium salt (Intermediate #1) was weighed and mixed with 15ml of hydrobromic acid in a conical flask, the mixture was kept for reflux for five hours. The solution was then left overnight to cool down. After cooling, the solution was transferred to a separating funnel, and 20 ml of DCM was added, followed by thorough shaking to generate two layers of the solution. The DCM layer was separated from the bottom aqueous layer, and this process was repeated three times with the addition of 20 ml of DCM to the aqueous layer after each separation step. 1g of magnesium sulfate was then added to the top layer of the separated DCM mixture until it becomes a clear solution to remove the moisture from the mixture. The solution was filtered and washed with DCM, and the resulting solution was connected to a rotary evaporator to remove the solvent. The rotary evaporator works on the principle of distillation under reduced pressure, as described in the previous chapter. Crystals formed at the bottom of the round bottom flask were scrubbed and dried in the oven at 60°C.

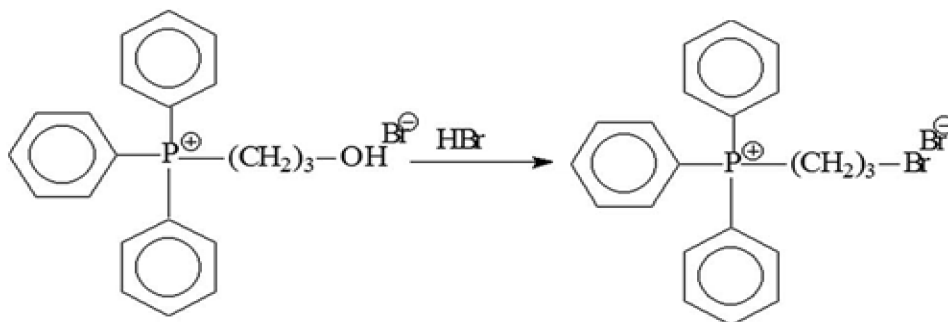


**Figure 3.4.** Reaction #2 for the synthesis of Intermediate #2 (Ju-Nam et al., 2016)

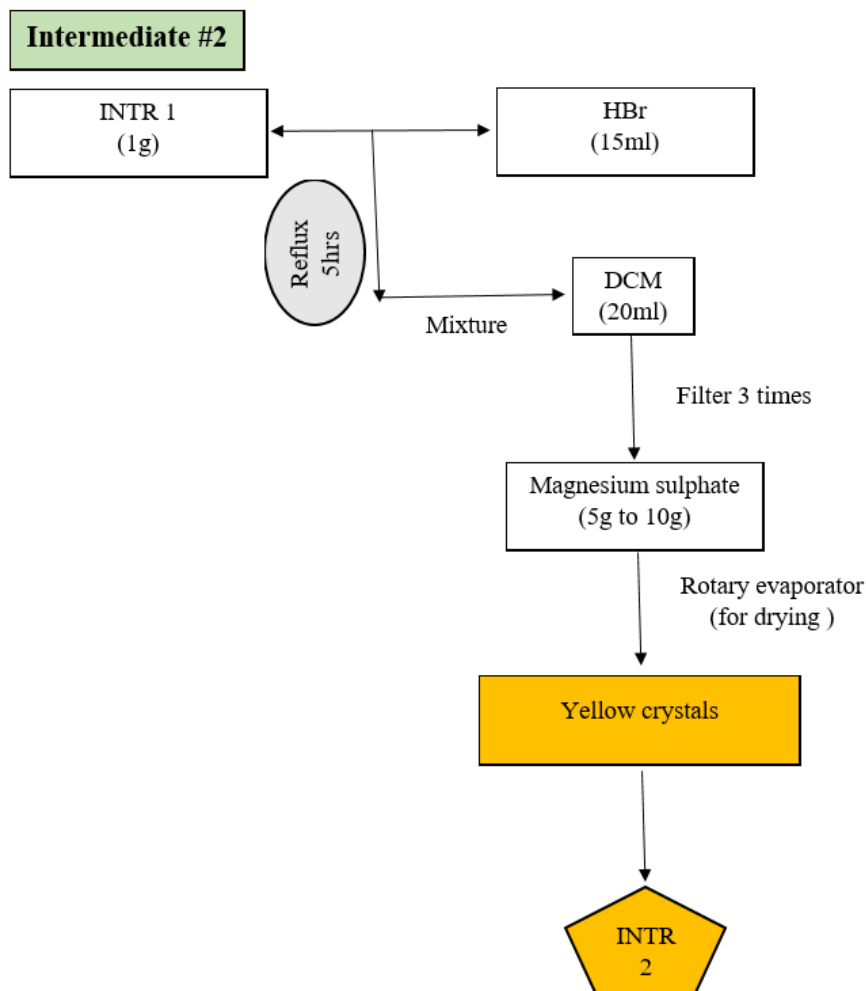


**Figure 3.5.** Flowchart representation for the synthesis of Intermediate #2

### 3.2.2.3 Synthesis of triphenylphosphoniopropylthiosulfate zwitterion (Ligand)

In order to synthesise the Ligand (Ju-Nam et al., 2016), about 1g of  $\omega$ -bromopropyltriphenylphosphoniumbromide (Intermediate #2) was taken and mixed with 5ml of ethanol in a vial. Approximately 0.8g of sodium thiosulfate was taken in a separate beaker, and mixed with 5ml of deionised water, and sonicated to form a clear solution. The solution thus formed was mixed with Intermediate #2 in ethanol and was refluxed for five hours. The solution was then transferred into a conical flask and left undisturbed overnight to allow the crystal formation. In order to promote more crystal growth, 10ml of hot deionised water was added into the conical flask and was kept in an ice bath for a few minutes. The crystals were then washed

with a mixture of cold ethanol and deionised water in a 1:1 ratio and the crystals were filtered and kept overnight in the oven at 60°C.

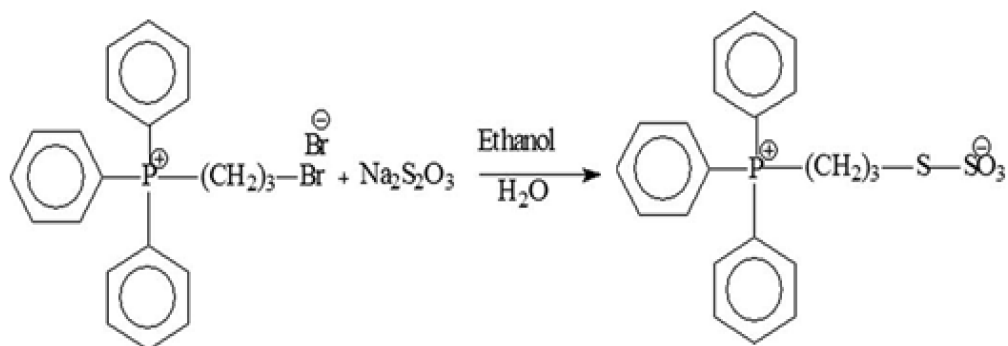


**Figure 3.6.** Reaction #3 for the synthesis of Ligand (Ju-Nam et al., 2016)

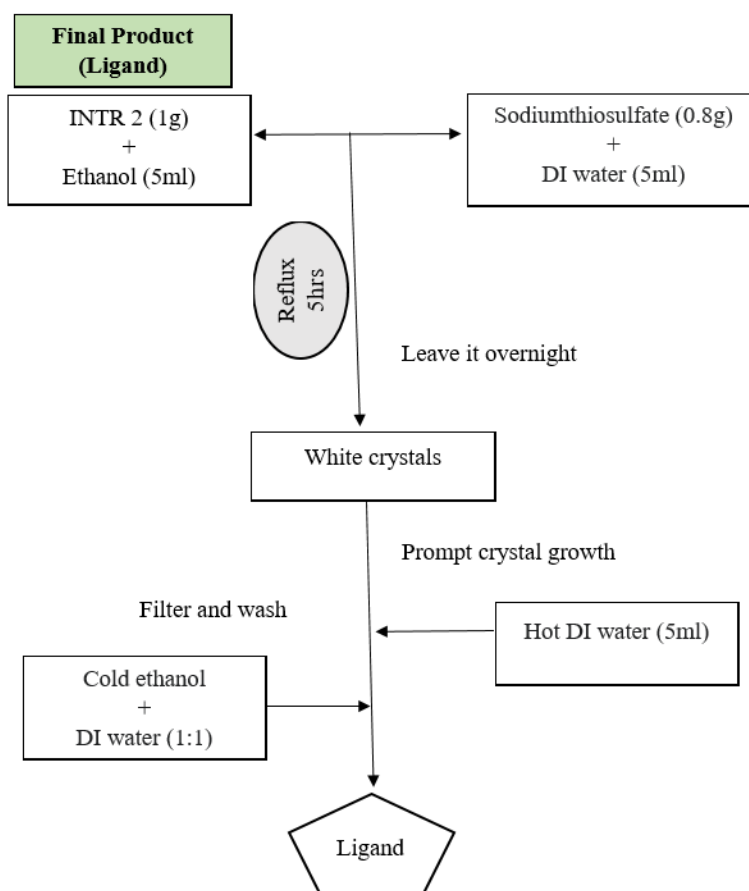


**Figure 3.7.** Flowchart representation for the synthesis of Ligand

### 3.2.3 Aspen Plus simulation of Reaction #1

A process simulation model for the green synthesis of Intermediate #1 was developed using Aspen Plus version 9.0. The primary objective was to check whether Reaction #1 occurs or not when 100% water is used as the main solvent. The non-random two-liquid (NRTL) thermodynamic model was chosen as it is recommended for chemical systems that include both polar and non-polar components. This NRTL model is suitable for a process involving multiple solvents. Simulation model for Reaction #1 using the Conventional Route was developed before modelling the green route. The conventional components, including ACN and bromo-propanol, were specified for the simulation of Reaction #1. Since the Aspen component databases did not include phosphonium salts, these compounds had to be user-defined and entered using a combination of chemical property calculations, estimations, and assumptions, in order to ensure the simulation runs effectively. In the literature or chemical databases, not all of the critical properties for TPP are available. The critical properties of the compounds were found using the Joback Method as cited in the literature (Jha et al., 2016). The Conventional and Green reaction routes for Intermediate #1 were simulated in continuous and in batch modes. The simulation environment included one CSTR unit in steady-state mode for continuous, and a batch flowsheet was generated to create a batch version of the process.

In order to run the simulations for Reaction #1, for both Conventional and Green routes, the Joback method approach was used in this project. Several equations were used in order to find the following parameters for some of the chemicals involved in Reaction #1: normal boiling point, critical temperature, critical pressure, critical volume, critical compressibility, acentric factor, freezing point, heat of formation, Gibbs energy of formation, heat of vaporisation, heat of fusion, and heat capacity.

Joback method is a group contribution method that uses basic structural information of the chemicals such as a list of simple functional groups, adds parameters to these functional groups, and calculates the thermo-physical and transport properties (Fernández et al., 2022). The Joback method is a technique used to determine the typical boiling point of a chemical compound. This property is predicated based on the idea that a typical boiling point of a compound may be estimated using information from its molecular structure, molecular weight, carbon number, and functional group composition. The Joback technique is frequently used in the field of Chemical

Engineering as it is a quick and effective approach to calculate the typical boiling point of a chemical compound without the requirement of experimental data. The normal boiling point is a crucial design factor for heat exchangers, distillation columns, and other process unit operations. Therefore, this knowledge is helpful for process design and optimisation (Fernández et al., 2022). The Joback approach is based on statistical correlations found in a vast database of substances, and the quality and quantity of the data affect the method's accuracy (Csemány et al., 2021). The explanation of the Joback method applied for this project is outlined below.

### 3.2.3.1 Joback method

As previously mentioned, Joback method available in CheCalc.com was used to find the following parameters for some of the chemicals involved in Reaction #1, for both Conventional and Green routes: normal boiling point, critical temperature, critical pressure, critical volume, critical compressibility, acentric factor, freezing point, heat of formation, Gibbs energy of formation, heat of vaporisation, heat of fusion, and heat capacity. The equations that the program use are outlined below.

#### Normal boiling point:

The normal boiling point ( $T_{NBP}$ ) is defined as "the temperature at which the vapour pressure of the liquid is equal to the standard atmospheric pressure of 1atm, where boiling occurs and it is the temperature at which the liquid changes into a vapour state and begins to boil under the standard conditions of pressure" (Chang, 2019). This temperature is a characteristic property of a substance and can be used to identify and distinguish it from other substances.

$$T_{NBP} (K) = 198 + \sum T_{b,i} \quad (3.1)$$

where  $T_{b,i}$  is the boiling point of each component.

#### Critical temperature:

The critical temperature ( $T_c$ ) is the highest temperature at which the substance can exist as a liquid, regardless of the pressure applied to it. At this temperature, the substance vapour pressure is equal to the pressure of the substance and then the substance is said to be at its critical point (Laidler, et al., 2019). The equation is as follows:

$$T_c \text{ (K)} = T_{NBP} \div (0.584 + 0.965 \times \sum T_{c,i} - (\sum T_{c,i})^2) \quad (3.2)$$

where  $T_{NBP}$  and  $T_{c,i}$  is the normal boiling point and critical temperature of each component.

### **Critical pressure:**

The critical pressure ( $P_c$ ) is the maximum pressure at which a substance can exist in a state between liquid and gas, known as the critical point. Beyond this pressure, the substance will not condense into a liquid regardless of the temperature. Critical pressure is a characteristic property of a substance and depends on its molecular structure and interactions (Laidler et al., 2019). The equation is as follows:

$$P_c \text{ (bar)} = (0.113 + 0.0032 \times N_A - \sum P_{c,i})^{-2} \quad (3.3)$$

where  $N_A$  is number of atoms in the molecular structure,  $P_{c,i}$  is the critical pressure of each component.

### **Critical volume:**

The critical volume ( $V_c$ ) is the volume occupied by a substance at its critical point. The critical point is the temperature and pressure at which a substance can exist in a state between liquid and gas, and beyond this point, the substance will not condense into a liquid regardless of the temperature and pressure. The critical volume is a characteristic property of a substance and depends on its molecular structure and interactions. It is used in various fields, including thermodynamics, phase diagrams, and engineering, to study and understand the behaviour of materials (Cengel and Boles, 2014).

$$V_c \text{ (cm}^3\text{/mol)} = 17.5 + \sum V_{c,i} \quad (3.4)$$

where  $V_{c,i}$  is the critical volume of each component.

### **Critical compressibility:**

Critical compressibility ( $Z_c$ ) is a measure of the change in volume of a substance as a function of pressure at its critical point. It is defined as the fractional change in volume per unit pressure at the critical point and is a fundamental property of a substance. The critical compressibility of a substance is related to its molecular structure and interactions and is an important parameter in

thermodynamics and phase diagrams. It provides information about the behaviour of a substance at high pressure (Cengel and Boles, 2014). The equation is as follows,

$$Z_c = (P_c \times V_c)/(R \times T_c) \quad (3.5)$$

where  $R$  is the gas constant,  $P_c$  is the critical pressure and  $V_c$  is the critical volume.

### **Acentric factor:**

The acentric factor ( $\omega$ ) is defined as the ratio of the deviation of a substance's vapour pressure from that of an ideal gas to the vapour pressure of the ideal gas at a given temperature. It is a measure of the deviation from ideal behaviour and is related to the shape, size, and intermolecular interactions of the substance's molecules. The acentric factor ranges from 0 for an ideal gas to 1 for a highly non-ideal substance (Cengel and Boles, 2014). The Lee-Kesler method can be used to estimate the acentric factor.

$$\omega = \alpha/\beta \quad (3.6)$$

$$\alpha = -\ln(P_c) - 5.92714 + 6.09648/\theta + 1.28862 \times \ln(\theta) - 0.169347 \times \theta^6 \quad (3.7)$$

$$\beta = 15.2518 - 15.6875/\theta - 13.4721 \times \ln(\theta) + 0.43577 \times \theta^6 \quad (3.8)$$

The factor  $\theta$  can be obtained by using the following equation:

$$\theta = T_{NBP}/T_c \quad (3.9)$$

where  $T_{NBP}$  is the normal boiling point,  $T_c$  is the critical temperature and  $P_c$  is the critical pressure.

### **Freezing point:**

The freezing point ( $T_m$ ) is the temperature at which a liquid changes into a solid due to the loss of thermal energy. At the freezing point, the heat absorbed by the substance is used to overcome the attractive forces between the molecules, causing the liquid to transition into a solid state. The freezing point of a substance is a characteristic property that depends on the type of substance and its molecular structure. For a pure substance, the freezing point is a constant value at a given pressure. However, for solutions, the freezing point can be depressed or raised relative to the pure solvent due to the presence of solute particles, which interfere with the formation of a solid crystal structure (Cengel and Boles, 2014).



$$T_m (\text{K}) = 122.5 + \sum T_{m,i} \quad (3.10)$$

where  $T_{m,i}$  is the freezing point of each component.

**Heat of formation (ideal gas, 298 K):**

The heat of formation ( $H_{formation}$ ) of an ideal gas is the amount of energy required to form the gas from its constituent elements in their standard states. For an ideal gas, the heat of formation is equal to zero as the ideal gas is considered to be composed of point-like particles with no intermolecular interactions, and therefore, no energy is required to bring the particles together to form the gas (Cengel and Boles, 2014).

$$H_{formation} (\text{kJ/mol}) = 68.29 + \sum H_{form,i} \quad (3.11)$$

where  $H_{formation,i}$  is the heat of formation of each component.

**Gibbs energy of formation (ideal gas, 298 K):**

The Gibbs energy of formation ( $G_{formation}$ ) of an ideal gas is the change in Gibbs energy that occurs when a substance is formed from its constituent elements in their standard states. For an ideal gas, the Gibbs energy of formation is equal to zero as the ideal gas is considered to be composed of point-like particles with no intermolecular interactions, and therefore, no energy is required to bring the particles together to form the gas (Cengel and Boles, 2014).

$$G_{formation} (\text{kJ/mol}) = 53.58 + \sum G_{form,i} \quad (3.12)$$

where  $G_{formation,i}$  is the Gibbs energy of formation of each component and  $H_{formation,i}$  is the heat of formation of each component.

**Heat of vaporisation (at normal boiling point):**

The heat of vaporisation ( $\Delta H_v$ ), (also known as the enthalpy of vaporisation) at the normal boiling point is the amount of energy required to convert a given amount of a liquid into a gas at the normal boiling point, usually measured in units of joules per mole (J/mol). The normal boiling point ( $T_{NBP}$ ) is the temperature at which the vapour pressure of a liquid is equal to one atmosphere (101.325 kPa). The heat of vaporisation is an important physical property of a substance and is closely related to its molecular structure, size, and intermolecular interactions. In general, substances with strong intermolecular forces, such as hydrogen bonding or dipole-dipole interactions, have higher

heat of vaporisation values compared to substances with weaker intermolecular forces (Cengel and Boles, 2014). Reidel's equation can be used to estimate a liquid's heat of vaporisation at its normal boiling point.

$$\Delta H_v \text{ (kJ/mol)} = 1.092 \times R \times T_{NBP} \times (\ln(P_c) - 1.013)/0.930 - T_{NBP}/T_c \quad (3.13)$$

where  $R$  is the gas constant,  $T_{NBP}$  is the normal boiling point,  $P_c$  is the critical pressure and  $T_c$  is the critical temperature.

### Heat of fusion:

The heat of fusion ( $\Delta H_{fusion}$ ), also known as the enthalpy of fusion, is the amount of energy required to convert a given amount of a solid into a liquid at its melting point, usually measured in units of joules per mole (J/mol). The heat of fusion is an important physical property of a substance and is closely related to its molecular structure, size, and intermolecular interactions. In general, substances with strong intermolecular forces, such as hydrogen bonding or dipole-dipole interactions, have higher heat of fusion values compared to substances with weaker intermolecular forces (Cengel and Boles, 2014).

$$\Delta H_{fusion} \text{ (kJ/mol)} = -0.88 + \sum H_{fus,i} \quad (3.14)$$

where  $H_{fus,i}$  is the enthalpy of fusion of each component.

### Heat capacity:

The heat capacity of an ideal gas ( $C_p$ ) is the amount of heat required to raise the temperature of a given quantity of the gas by a certain amount, usually measured in units of Joules per Kelvin per mole (J/K/mol). For an ideal gas, the heat capacity can be calculated using the ideal gas law. The heat capacity of an ideal gas is temperature-independent, which means it does not change with temperature. This is in contrast to real gases, which deviate from ideal gas behaviour due to intermolecular interactions, and due to a temperature-dependent heat capacity (CheGuide and Dash; Property Estimation Joback Method, n.d.).

$$C_p \text{ (J/mol.K)} = A + B \times T + C \times T^2 + D \times T^3 + E \times T^4 + F \times T^5 + G \times T^6 \quad (3.15)$$

where A, B, C, D, E, F, G are the regression coefficients and T is the temperature.

### 3.2.3.1.1 Critical properties required for Reaction #1 simulation

In the modelling of Reaction #1 using Aspen Plus software, it was noted that some important properties of the TPP and the product (Intermediate #1) were not found in the software database. This made it difficult for the software to accurately predict the reaction. Despite some available data in the database, it was not sufficient to run the simulation successfully. Therefore, the TPP and Intermediate #1 were defined as user-defined compounds and the physical and chemical properties were entered manually. The counterion Br<sup>-</sup> was also separately entered manually. To estimate the missing properties of the TPP and Intermediate #1, the Joback method follows similar works reported in the literature (Jha et al., 2016). The Joback method was used to estimate the properties of these compounds, and the results were tabulated for reference. Specific heat capacities of TPP and Intermediate #1 were calculated using the equation (3.15) and the regression coefficients found in the Knovel online library.

### 3.2.3.2 Continuous mode simulation

A continuous Stirred Tank Reactor (CSTR) is one type of reactor used for the continuous mode simulation of Reaction #1 using Aspen Plus in this thesis. CSTR is a type of chemical reactor that is used for continuous processing. Reagents, reactants, and solvents are continuously fed into the reactor, while the products of the reaction exit simultaneously. The reactor is designed with effective mixing capabilities and operates under steady-state conditions with uniform properties. Ideally, the output composition is equal to the composition of the material within the reactor, which is determined by the reaction rate and the residence time. In instances where the reaction is slow or when immiscible or viscous liquids are present which require high agitation, multiple CSTR units can be connected together to form a cascade (Mettler-Toledo International Inc. all rights reserved, 2022).

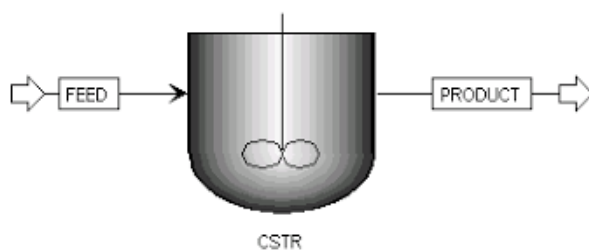


**Figure 3.8.** Representation of the CSTR reactor

### 3.2.3.3 Batch mode simulation

The Batch Reactor is the other type of reactor used for the simulation of Reaction #1 Using the Aspen Plus in this thesis. The batch reactor is a sophisticated model that simulates batch or semi-batch reactions. These types of reactors are used when the reaction kinetics are known to continue until a specified stop criterion is met (Soroush and Kravaris, 1993). A semi-batch reactor, on the other hand, can have a combination of a vent product stream and continuous feed streams. The vent product stream exits through a vent accumulator, which continuously captures the vapour vent produced over time (Soroush and Kravaris, 1993). The continuous feed streams maintain a constant composition, temperature, and flow rate until a time profile for the flow rate is specified. Unlike steady-state processes, batch operations are dynamic, with variables such as temperature, composition, and flow rate changing over time (Soroush and Kravaris, 1993). To integrate the Batch Reactor with steady-state flow sheets, it is necessary to use time-averaged streams.

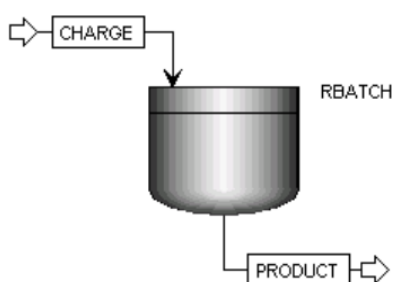


**Figure 3.9.** Representation of the Batch reactor

### 3.2.3.4 Simulation of Reaction #1 using the CSTR and the Batch reactors (Conventional Route)

Simulation of Reaction #1 in continuous mode (using CSTR reactor) was performed by setting the temperature of the feed as 25<sup>0</sup>C and the total flow rate was fixed to be 600 mol/hr which includes 564 mol/hr of ACN, 30 mol/hr of bromopropanol, and 6 mol/hr of TPP. After setting the initial condition of the feed the next step was to set the conditions for the reactor. Initial operating conditions were set for the reactor were 80<sup>0</sup>C at 1 bar. The valid phase was set to be a vapour-liquid phase and the volume of the reactor taken was 40 litres. After setting the required parameters for the reactor the next step was to set the parameters of Reaction #1 for the synthesis of the

Intermediate #1. Simulation of Reaction #1 in batch mode (using a Batch reactor) was performed by setting the temperature of the feed as 25<sup>0</sup>C and the total flow rate was fixed to be 600 mol/batch which includes 564 mol/batch of ACN, 30 mol/batch of bromopropanol, and 6 mol/batch of TPP. The initial operating conditions and reactor volume used for the simulation in batch mode were the same ones used for continuous mode.

### **3.2.3.5 Simulation of Reaction #1 using CSTR reactor (Green Route)**

The approach shown in section 3.2.3.4. was followed to obtain feasible reaction conditions from the Aspen simulation and develop a greener route for Reaction #1. For the Green Route simulation, a water stream was included in the Aspen model. Reaction #1 simulation was done in continuous mode only.

### **3.2.4 Synthesis of Intermediate #1 in the laboratory using 100% water (Green Route):**

Reaction #1 was performed in the laboratory using 100% water and other reaction conditions from Aspen Plus simulation. Green synthesis of the Intermediate #1 was carried out by mixing 1g (3.8 mmol) of TPP and 3ml (30.2 mmol) of bromopropanol in a 10 ml water in a round-bottomed flask. The reaction time was 5 hours. To promote uniform boiling to the reaction, a small quantity of anti/bump granules was added to the mixture, which was then refluxed for a period of five hours. The resulting solution was transferred to a conical flask and sealed with paraffin tape and kept undisturbed overnight. The solution was transferred to a separating funnel, and 20 ml of DCM was added, followed by thorough shaking to generate two layers of the solution and purify Intermediate #1. The DCM layer was separated from the bottom aqueous layer, and this extraction process was repeated three times. To obtain a clear solution, magnesium sulfate was added to the DCM solution, and it was filtered and washed using DCM into a round-bottomed flask. The solution was subjected to a rotary evaporator to obtain the product as crystals. These were gently scraped out using a spatula and dried in an oven at 60<sup>0</sup>C.

### 3.3 Results and Discussions

#### 3.3.1 Characterisation of the Intermediate #1, Intermediate #2 and Ligand obtained following Conventional Route

As previously mentioned, Ligand was synthesised following the Conventional Route to be able to design a greener approach for Ligand production. The conventional synthetic method involves three chemical reactions, the production of two intermediates and the Ligand. After carrying out all three reactions and corresponding purification steps, crystals of Intermediates #1 and #2 and Ligand was obtained as shown in Figure 3.10. The synthesis of the Ligand using the Conventional Route not only help to understand the reactions involved and the reagents used for the Aspen simulation work but also help design a greener synthetic route. However, due to the time constrains, Reaction #1 was the only one considered in the design of a greener approach. The Ligand synthesised in this part of the project was also used in the work carried out in the synthesis of cationic lipophilic AuNPs using a green method (Chapter 4).

Both intermediates and Ligand were characterised using ATR-FTIR spectroscopy technique.

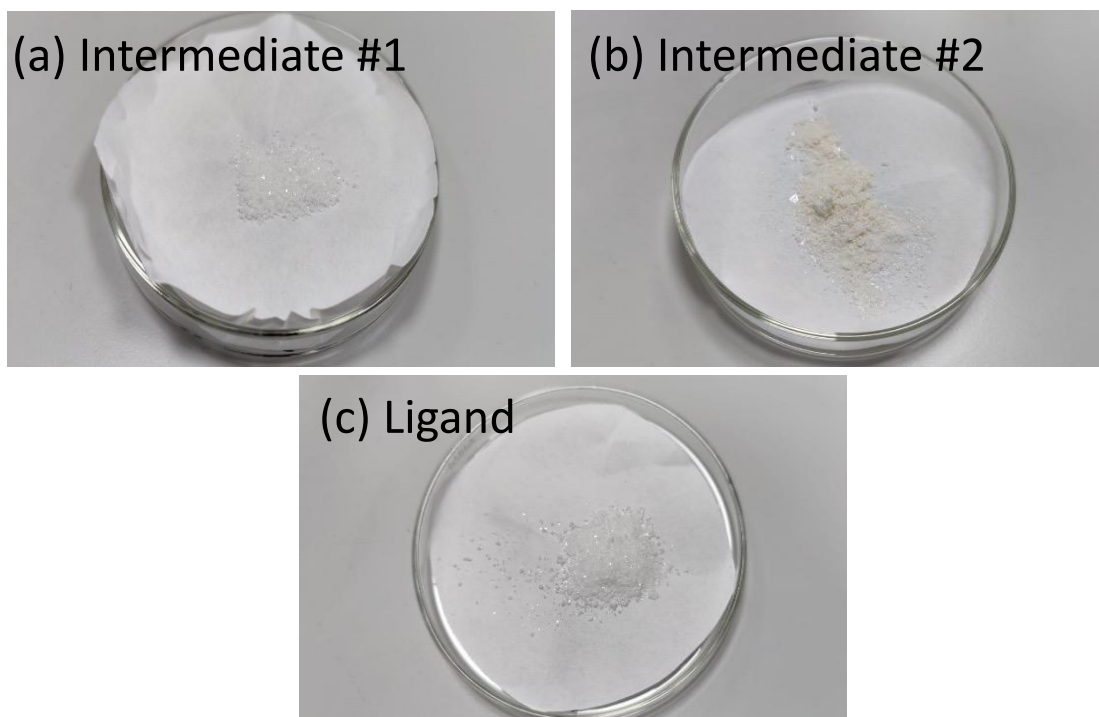


**Figure 3.10.** Crystals of (a) Intermediate #1, (b) Intermediate #2, (c) Ligand obtained using the Conventional Route of synthesis.

### 3.3.1.1 ATR-FTIR spectroscopy analyses of Intermediates #1 and #2 and Ligand

Attenuated Total Reflectance-Fourier-transformed Infrared Spectroscopy (ATR-FTIR) is a technique used to identify and analyse chemical compounds by measuring the infrared absorption or emission spectra of a sample (Kalmodia et al., 2015). This technique is based on the interaction of infrared light with the chemical bonds in a substance, which causes vibrations in the bonds and results in the absorption or emission of specific frequencies of infrared radiation (Kalmodia et al., 2015).

Analysis of the ATR-FTIR was made for both intermediates and the Ligand to confirm the presence of their characteristic functional groups. Each recorded spectrum is the average of 64 scans with a spectral resolution of  $4\text{ cm}^{-1}$  from  $400$  to  $4000\text{ cm}^{-1}$  on a dried sample, with a background spectrum recorded before each analysis. Spectra were measured and analysed and fitted using Origin 2023 software. The infrared (IR) spectrum of a chemical compound can provide valuable information about the functional groups and chemical bonds present in the molecule. Peaks in the infrared spectrum corresponding to Intermediate #1 provide information about the chemical structure of the molecule (Figure 3.11. (a)). The peak at  $3322\text{ cm}^{-1}$  is characteristic of the O-H stretching vibration of an alcohol (-OH) functional group. This indicates the presence of an alcohol group in the molecule. The peak at  $2885\text{ cm}^{-1}$  corresponds to the C-H stretching in the alkyl chain of the molecule. This suggests the presence of an alkyl chain. The peak at  $1436\text{ cm}^{-1}$  is indicative of the C=C stretching of an alkene or aromatic ring. The peak at  $1115\text{ cm}^{-1}$  corresponds to the P-C stretching vibration (Ju-Nam et al., 2012). This suggests the presence of a phosphine functional group in the molecule. For Intermediate #2 (Figure 3.11. (b)) the peak observed at  $690\text{ cm}^{-1}$  corresponds to the stretching vibration of the C-Br bond, while the peak at  $1105\text{ cm}^{-1}$  is indicative of the P-C bond. Furthermore, the peak observed at  $1435\text{ cm}^{-1}$  is associated with the presence of the C=C bond in the molecule. Finally, the peak observed at  $2890\text{ cm}^{-1}$  is attributed to the stretching of the C-H bond (Ju-Nam et al., 2016). Infrared spectrum of the Ligand shows various characteristic peaks that provide information about the chemical structure of the molecule (Figure 3.11. (c)). The peak at  $1440\text{ cm}^{-1}$  indicates the presence of C-H groups in the alkyl chains of the zwitterion. The peak at  $1230\text{ cm}^{-1}$  is associated with the C-S bond, while the peak at  $1210\text{ cm}^{-1}$  is indicative of the S=O bond. In addition, the presence of aromatic C-H bonds is evident in the range of  $2900\text{-}3100\text{ cm}^{-1}$  (Sigma Aldrich, ir-spectrum-table). All the infrared results obtained

in this project, correspond well with those reported by Ju-Nam and co-workers in their work on the synthesis of triphenylphosphinealkylthiosulfate zwitterions (Ju-Nam et al., 2012; Ju-Nam et al., 2016).

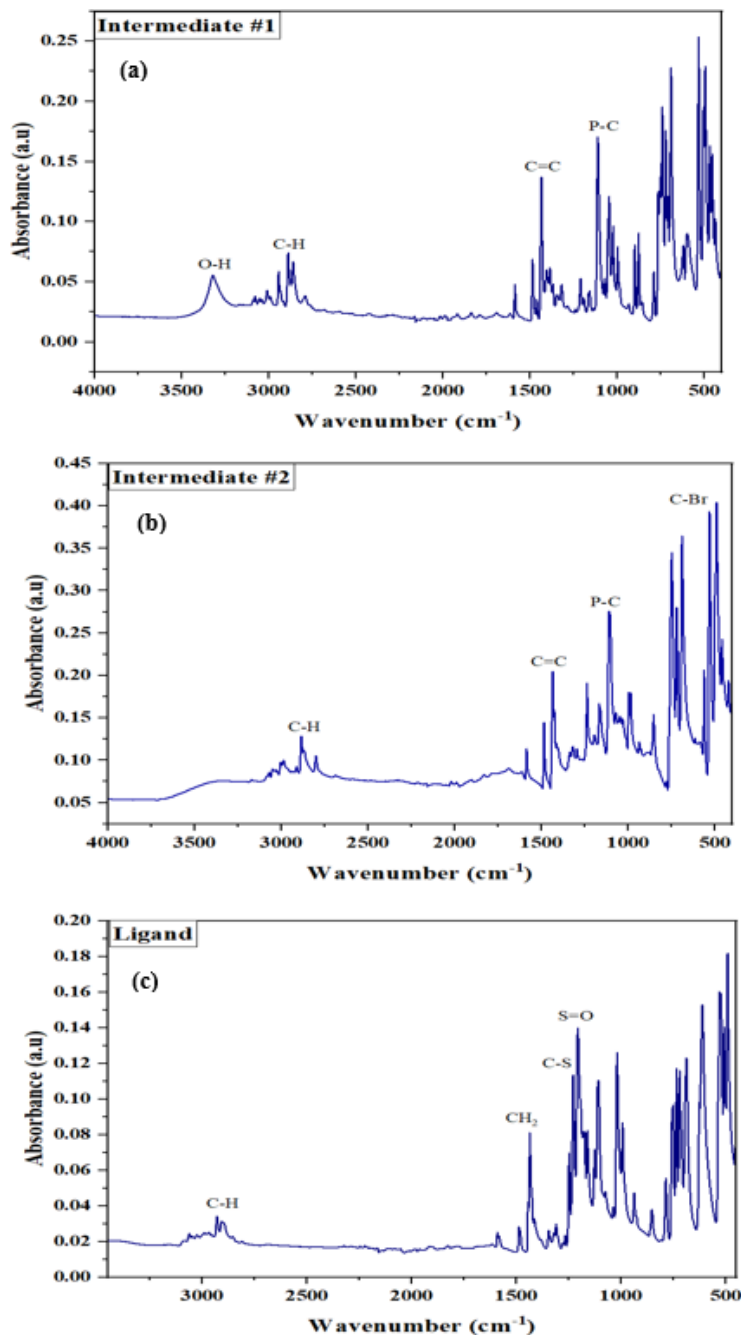


**Figure 3.11.** Infrared spectra of (a) Intermediate #1, (b) Intermediate #2, (c) Ligand obtained using ATR-FTIR technique.

As mentioned before, one of the main aims of this MSc project was to design a greener method



for conventional organic reactions by replacing conventional organic solvents with more environmentally friendly solvents, such as water. In order to showcase this, the strategy used was to employ simulation tools, like the one used for this study, Aspen Plus before planning any experimental work in the laboratory. The results from the Aspen modelling on Reaction #1 are outlined in the following sections.

### 3.3.2 Aspen simulation of Reaction #1: estimated properties for TPP and Intermediate #1 (Conventional Route) using Joback method

The properties of TPP and Intermediate #1 required for the Aspen Plus simulation of Reaction #1 were estimated by using the Joback method. For this, the chemical structures of Intermediate #1 and TPP were used to obtain element counts for carbon and hydrogen atoms. This data was inputted to the Joback method (CheCalc.com), which uses the equations mentioned in section 3.2.2.1., to obtain the estimated properties for both compounds. This approach is used in similar works reported in the literature (Jha et al., 2016). The results are shown in Table 3.1. and Table 3.2. All these critical properties of both Intermediate #1 and TPP were further utilised for the simulation of Reaction #1.

**Table 3.1.** Estimated properties for TPP using the Joback method (CheCalc.com)

SI no.	PROPERTIES OF TPP		
1	Molecular Weight	g/mol	231.31
2	Normal Boiling Point, $T_{\text{nbp}}$	K	691.98
3	Critical Temperature, $T_c$	K	1109.73
4	Critical Pressure, $P_c$	bar	25.08
5	Critical Volume, $V_c$	cm <sup>3</sup> /mol	728.50
6	Critical Compressibility, $Z_c$		0.1980
7	Acentric Factor, $\omega$		-0.0064
8	Freezing Point	K	355.5
9	Heat of Formation, (Ideal Gas 298 K)	kJ/mol	238.93
10	Gibbs Energy of Formation	kJ/mol	385.53
11	Heat of Vaporisation at $T_{\text{nbp}}$	kJ/mol	45.29
12	Heat of Fusion	kJ/mol	22.82

**Table 3.2.** Estimated properties for Intermediate #1 using the Joback method (CheCalc.com)

SI no.	PROPERTIES OF INTERMEDIATE #1		
1	Molecular Weight	g/mol	290.4
2	Normal Boiling Point, $T_{nbp}$	K	853.50
3	Critical Temperature, $T_c$	K	1183.04
4	Critical Pressure, $P_c$	bar	19.98
5	Critical Volume, $V_c$	cm <sup>3</sup> /mol	924.50
6	Critical Compressibility, $Z_c$		0.1878
7	Acentric Factor, $\omega$		0.4443
8	Freezing Point	K	433.77
9	Heat of Formation, (Ideal Gas 298 K)	kJ/mol	-31.03
10	Gibbs Energy of Formation	kJ/mol	221.59
11	Heat of Vaporisation at $T_{nbp}$	kJ/mol	73.64
12	Heat of Fusion	kJ/mol	32.99

These critical properties are shown in Table 3.1. and 3.2. were estimated and used as inputs to the Aspen for the simulation of Reaction#1. In particular, data for Intermediate #1, such as acentric factor, freezing point, and critical pressure among others were predicted and obtained from the Joback method as there were not available in the Aspen database. Some of the data corresponding to TPP were found in the mentioned database. The estimated properties were crucial to successfully run the simulation of Reaction #1.

### 3.3.3 Specific heat capacity of TPP and Intermediate #1

Specific heat capacities of TPP at different temperatures (150-500 K) were calculated using the corresponding regression coefficients (A, B, C, D, E, F, G) found in the Knovel online library (Table 3.3), and the  $C_p$  equation shown below (Valderrama and Rojas 2009).

$$C_p \text{ (J/mol.K)} = A + B \times T + C \times T^2 + D \times T^3 + E \times T^4 + F \times T^5 + G \times T^6$$

Here A, B, C, D, E, F, G are the regression coefficients.

**Table 3.3.** Regression coefficients for TPP from Knovel library.

<b>A</b>	<b>B</b>	<b>C</b>	<b>D</b>	<b>E</b>	<b>F</b>	<b>G</b>
324.0535	-2.4343	0.01328	-2.6E <sup>-05</sup>	2.47E <sup>-08</sup>	-1.2E <sup>-11</sup>	2.24E <sup>-15</sup>

**Table 3.4.** Specific heat capacity obtained for TPP, temperature range: 150 - 500 K.

Temperature in K	Heat capacity [J/(mol K)]
150	182
160	183
170	185
180	188
190	192
200	196
220	206
240	218
260	231
280	245
300	259
320	274
340	289
360	303
380	317
400	330
420	342
440	353
460	364
480	373
500	381

The specific heat capacities for Intermediate #1 were assumed to be the same as the ones calculated for TPP (Table 3.4). The reason for this was that no regression coefficients corresponding to Intermediate #1 were available in the literature. This assumption seemed sensible as both compounds have similarities in their chemical structure. Specific heat capacities for TPP and Intermediate #1 were crucial inputs for the Aspen simulation of Reaction #1.

### 3.3.4 Aspen simulation of Reaction #1 using CSTR reactor (Conventional-Route)

Reaction #1 following the Conventional Route was successfully simulated using CSTR reactor. For thermodynamic modelling of the experimental data, the built-in NRTL model was used. The approach followed in this part of the study was similar to the modelling carried out for dibenzothiophene using phosphonium-based ionic liquid, reported in the literature (Jha et al., 2016). According to the results obtained from the Aspen simulation shown in Table 3.5. The reaction of 30 moles/hr of bromopropanol and 6 moles of TPP in the presence of 564 moles/hr of ACN solvent, yields 0.64 moles/hr of Intermediate #1 (approximately 208 grams) and 0.64 moles/hr of Br<sup>-</sup> counterion. The initial conditions of the first reactor were set at 85<sup>o</sup>C and 1 bar. The reaction was assumed to occur only in the liquid phase (reagents are completely dissolved when the reaction reaches 85<sup>o</sup>C). The simulation did not show errors when Reaction #1 was run under a CSTR model. The stream results are shown in Table 3.5. below.

**Table 3.5.** Stream results of Reaction #1 using CSTR reactor

Parameters	R1in	R1out	R1in	R1out
	Mole Flow kmol/hr	Mole Flow kmol/hr	Mass Flow kg/hr	Mass Flow kg/hr
ACN	0.564	0.564	23.1536	23.153
Bromo-propanol	0.03	0.0293	4.1697	4.0797
Br <sup>-</sup> counterion	0	0.00064	0	0.0517
INTER#1	0	0.00064	0	0.2082
TPP	0.006	0.00535	1.5738	1.4039
<b>Total</b>	<b>0.6</b>	<b>0.6</b>	<b>28.8972</b>	<b>28.897</b>

### 3.3.5 Aspen simulation of Reaction #1 using Batch reactor (Conventional-Route)

Conventional Route for the synthesis of Intermediate #1 was modelled in Aspen using Batch reactor and at different stop times. Based on the results from Table 3.6, it is evident that both mole and mass of Intermediate #1 and Br<sup>-</sup> counterion increase for every batch as the stop time of the reactor increases. At a stop time of 5 hours, a significant portion of TPP has reacted to form the desired product (Intermediate #1). Moreover, from the results obtained from the batch mode simulation, the amount of Intermediate #1 remains constant after 4 hours. In addition, the stream result for Reaction #1 indicates that 1.7 moles per batch of Intermediate #1 are produced along with an equivalent amount of Br<sup>-</sup> counterion for the stop time of 1 hour. Furthermore, by increasing the stop time to 4 hours, the simulation predicts an increase in product yield (4.27 moles per batch). Approximately 546.4 grams per batch of Intermediate #1 is obtained for Reaction #1 for the stop time of 1 hour, according to the simulation results. A considerable amount of Intermediate #1, 1372.9 grams per batch, was achieved when the stop time was 5 hours (reaction time).

**Table 3.6.** Comparison of Reaction #1 using batch reactor at different stop times (ST), 1-5hrs.

Parameters	Units	R1 In	R1out Batch (ST:1)	R1out Batch (ST:2)	R1out Batch (ST:3)	R1out Batch (ST:4)	R1out Batch (ST:5)
<b>Mole Flow</b>	<b>kmol/batch</b>	0.6	0.6	0.6	0.6	0.6	0.6
ACN	kmol/batch	0.564	0.564	0.564	0.564	0.564	0.564
<b>Bromo-propanol</b>	kmol/batch	0.03	0.02829	0.0271	0.02632	0.02572	0.02573
<b>Br<sup>-</sup> counterion</b>	kmol/batch	0	0.00170	0.00286	0.00368	0.00427	0.00427
<b>INTR #1</b>	kmol/batch	0	0.00170	0.00286	0.00368	0.00427	0.00427
<b>TPP</b>	kmol/batch	0.006	0.00429	0.00314	0.00232	0.00173	0.00173
<b>Mass Flow</b>	<b>kg/batch</b>	28.8972	38.5007	38.5007	38.5007	38.5007	38.5007
ACN	kg/batch	23.1536	32.7571	32.7571	32.7571	32.7571	32.7571
<b>Bromo-propanol</b>	kg/batch	4.1697	3.93346	3.77178	3.65802	3.5760	3.5760
<b>Br<sup>-</sup> counterion</b>	kg/batch	0	0.13584	0.22879	0.29419	0.34132	0.34132
<b>INTR #1</b>	kg/batch	0	0.54640	0.92028	1.18333	1.37290	1.37290
<b>TPP</b>	kg/batch	1.5738	1.12787	0.82275	0.60806	0.45335	0.45335
<b>Total</b>	kg/batch	28.8971	38.50067	38.5007	38.5007	38.50067	38.5006

### **3.3.6 Comparison of simulations carried out in continuous and batch modes (Conventional Route)**

Aspen simulations were done for Reaction #1 following the Conventional Route, and results are presented in Tables 3.5. and 3.6. indicate that the Batch reactor generated more amount of Intermediate #1 in 5 hours under the same experimental conditions when compared to the CSTR. According to the batch mode simulation, the amount of product generated in 5 hours stop time or reaction time is 1.3729 kg, whereas when looking at the result obtained in the continuous mode simulation, the amount of Intermediate #1 generated in 5 hours is approximately 1 kg (0.2082 kg/hr multiplied by 5 hours). However, in both simulations, the amounts of bromopropanol in mass that remain unreacted (see corresponding outputs in Tables 3.5. and 3.6.) are quite significant. The Aspen simulations were carried out using a scale-up of the molar ratios used in laboratory scale reactions to produce Intermediate #1. Analysing the results obtained from Reaction #1 modelling following the Conventional Route, the amounts of reactants that are normally used could be re-assessed even for Reaction #1 carried on small scale. The reaction is typically carried out with 1:2 TPP:bromopropanol molar ratio. It might be worth trying to simulate Reaction #1 with a molar ratio of 1:1, and try to replicate it if better results are obtained in the simulation. More encouraging results were obtained for Reaction #1 modelled in batch mode. Event though, the amount of bromopropanol consumed after 5 hours of reaction time is small (IN 4.1697 kg, OUT 3.5760 kg, Table 3.6) and similar to the results obtained from the continuous mode simulation, it can be observed that the TPP amount consumed is more significant in batch (IN 1.5738 kg, OUT 0.4335 kg) than in continuous mode simulation (IN 1.5738 kg/hr, OUT 1.4039 kg/hr). From these findings, batch mode simulation of Reaction #1 following the Conventional Route could potentially generate more realistic results.

### **3.3.7 Aspen simulation of Reaction #1 using CSTR reactor (Green Route)**

Water is often considered the greenest and safest solvent option for chemical processes, especially when the goal is green synthesis. To investigate the potential for using water as a solvent in the synthesis of Intermediate #1 (Reaction #1), the effect of replacing organic solvent ACN with water was studied by using the Aspen Plus simulation tool. Specifically, different concentrations or ratios of ACN and water were used for this work. Changes in reaction output were observed as the water concentration increased from 0 to 100%, as shown in Table 3.7. An additional stream of

water was introduced to the simulation and CSTR, in order to compare the reaction kinetics of Reaction #1 at different concentrations of water and ACN. The simulation was carried out using pure ACN and 100% water. The results from Table 3.7. indicates that both the mole flow and mass flow of Intermediate #1 were higher for the 100% water mixture compared to the other reactions modelled. This suggests that water could potentially have a more significant impact on the reaction kinetics than ACN for the synthesis of the Intermediate #1.

**Table 3.7.** Reaction #1 using CSTR reactor with different concentrations of Water and Acetonitrile (ACN)

Parameters	Units	100%ACN R1 In	100%ACN R1 out	100% water R1 In	100% water R1 out
<b>Mole Flow</b>	kmol/hr	0.6	0.6	0.6	0.6
<b>ACN</b>	kmol/hr	0.564	0.564	0	0
<b>Bromo- propanol</b>	kmol/hr	0.03	0.029352	0.03	0.02772
<b>Br<sup>-</sup> counterion</b>	kmol/hr	0	0.000647	0	0.00228
<b>INTR#1</b>	kmol/hr	0	0.000647	0	0.00228
<b>TPP</b>	kmol/hr	0.006	0.005352	0.006	0.00372
<b>WATER</b>	kmol/hr	0	0	0.564	0.564
<b>Mass Flow</b>	kg/hr	28.8972	28.8972	28.8972	15.9042
<b>ACN</b>	kg/hr	23.1536	23.1536	0	0
<b>Bromo- propanol</b>	kg/hr	4.169	4.07973	4.169	3.85311
<b>Br<sup>-</sup> counterion</b>	kg/hr	0	0.05175	0	0.18204
<b>INTR#1</b>	kg/hr	0	0.20817	0	0.73221
<b>TPP</b>	kg/hr	1.5738	1.40391	1.5738	0.97623
<b>WATER</b>	kg/hr	0	0	10.152	10.1606
<b>Total</b>	kg/hr	28.8964	28.89716	15.8948	15.9040

### 3.3.8 Green synthesis of Reaction #1 using Aspen simulation outputs

In the current study, the green synthesis of Intermediate #1 was investigated by replacing 100% ACN with 100% water as the main reaction solvent. The Aspen Plus simulation results indicated that this green synthetic method was feasible. Due to the encouraging results are shown in Table 3.7. synthesis of Intermediate #1 was carried out in the laboratory (small scale) using 100% water, at 85<sup>0</sup>C and atmospheric pressure to replicate operating conditions from the Aspen simulation. As the Green Route simulation for Reaction #1 was only done in continuous mode, the reaction times were trialled, 5 and 10 hours. Even though the main aim of this experimental work was to show that some organic synthesis can be done in 100% water, DCM extractions were carried out to purify the product after the reaction was completed. The author of this thesis understands that this purification approach is not the greenest. However, the synthesis of Intermediate #1 using the greenest solvent possible, 100% water was achieved. Crystals of Intermediate #1 were obtained following the Green Route and are shown in Figure 3.12.

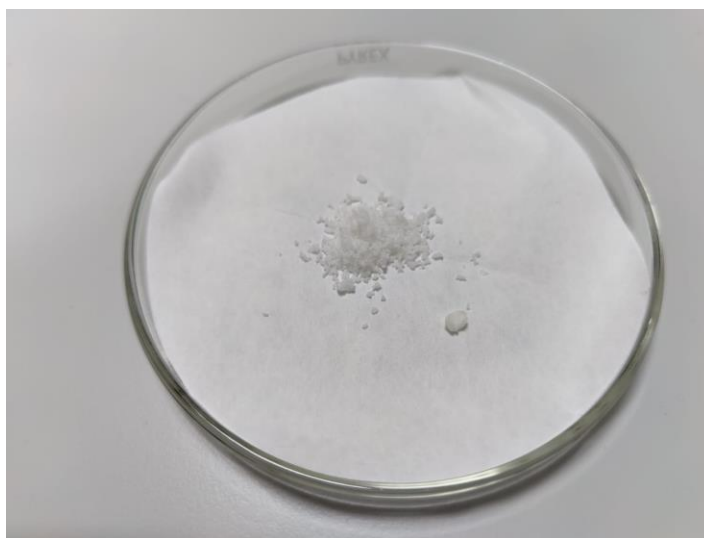


**Figure 3.12.** Crystals obtained for the Intermediate #1 using the Green Route.

To further confirm the successful synthesis of Intermediate #1 using the Green Route, the ATR-FTIR spectra was taken for Intermediate #1 obtained in 5 and 10 hours. The infrared spectra were exactly the same. The key comparison, however, was done when the spectrum of Intermediate #1 produced following the Green Route was contrasted with the spectrum of Intermediate #1



produced following the Conventional Route (Figure 3.13). The comparison of the infrared spectra of the two Intermediates #1 indicated that the peaks were in perfect match, which confirmed that Intermediate #1 was successfully synthesised using 100% water as the solvent. The spectrum corresponding to Intermediate #1 produced from the Green Route, showed peaks of functional groups characteristics from Intermediate #1 chemical structure. The peak corresponding to O-H stretching vibration can be observed at  $3322\text{ cm}^{-1}$ . This indicates the presence of an alcohol group in the molecule. The peak at  $2885\text{ cm}^{-1}$  corresponds to the C-H stretching in the alkyl chain of the molecule. This suggests the presence of an alkyl chain. The peak at  $1436\text{ cm}^{-1}$  is indicative of the C=C stretching of an alkene or aromatic ring. The peak at  $1115\text{ cm}^{-1}$  corresponds to the P-C stretching vibration (Ju-Nam et al., 2012; Ju-Nam et al., 2016).

This result is significant as it shows that the green synthetic method is viable in certain organic syntheses like the one showcased in this thesis. The use of water as the solvent in conventional organic reactions could potentially have several advantages, such as the reduction of chemical use and toxic chemical waste. The latter is a significant environmental concern associated to conventional chemical processes.

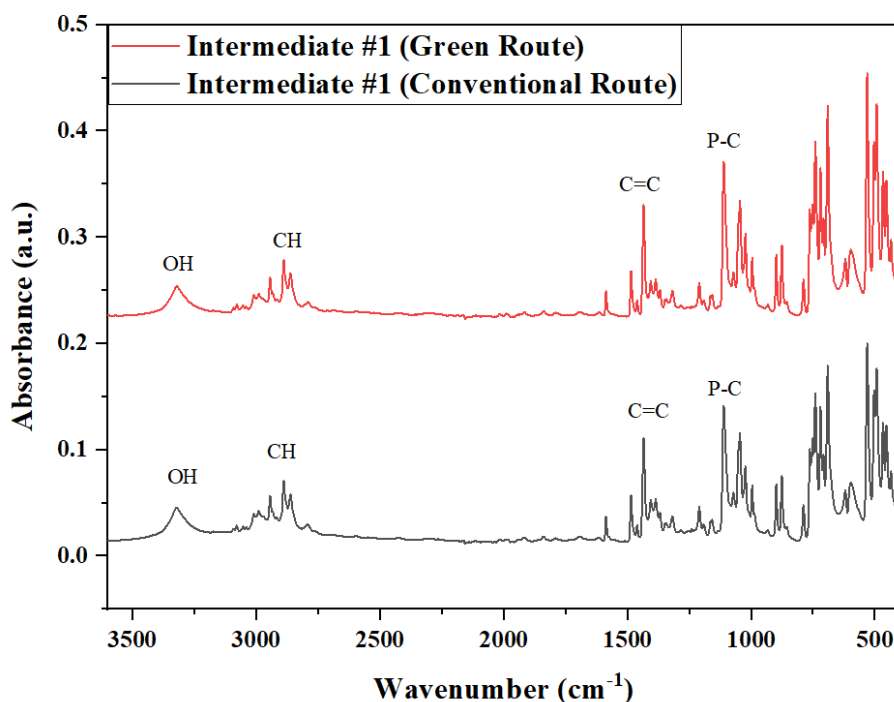


**Figure 3.13.** FTIR spectrum of the synthesised Intermediate #1 with 100 % water

## Chapter 4

# Green synthesis of the cationic lipophilic AuNPs

### 4.1 Introduction

In this chapter, the green synthesis of AuNPs functionalised with triphenylphosphonothiosulfate zwitterion (Ligand) is outlined. All bottom-up approaches and colloidal AuNP synthesis reported in the literature involves the reduction of  $\text{Au}^{3+}$  to  $\text{Au}^0$  and subsequent functionalization (Barrow, 2013). The latter can occur through the sulfur-Au bonding, sulfur coming from the coating agent or ligand based on thiolate containing compounds, also known as "sulfido-ligands". Gold is a highly unreactive metal and is not typically known to form chemical bonds with sulfur (Barrow, 2013). However, it is possible to form gold-sulfur bonds, when gold is in one of its reduced forms (gold (I)) (Barrow, 2013).

Previously reported green methods for AuNP synthesis mainly begin with the preparation of a gold precursor solution, which either contains gold chloride or another gold salt that is dissolved in a solvent generally water. Then the mixture is heated to a particular temperature and the reducing agent is added to the solution. The most common reducing agents used for green synthesis of AuNPs in their colloidal form is sodium borohydride ( $\text{NaBH}_4$ ) (Hammami et al., 2021), glutathione (GSH) (Mao et al., 2010), ascorbic acid (Sun et al., 2009), sodium citrate (Ji et al., 2007), dimethylformamide (DMF) (Pastoriza-Santos and Liz-Marzán, 2009b). The latter is a polar aprotic solvent with a high boiling point, the C=O and C-N bonds make the molecule polar, and it is aprotic as it does not have O-H or N-H bonds in its chemical structure. DMF can act as a reducing agent by providing electrons to reduce the gold ions to metallic gold (Pastoriza-Santos and Liz-Marzán, 2009b).

The size and shape of the AuNPs can be controlled by adjusting the reaction conditions such as the concentration of the gold ions and reducing agent, temperature and reaction time (Amina and Guo, 2020). AuNPs can have different shape distributions depending on the temperature (25 - 90°C): triangular, pentagonal, hexagonal, and spherical (Shankar et al., 2004; Starnes et al., 2010). An increase in the temperature and salt concentration can trigger the development of nanoparticles. The colour change is caused primarily by a shape difference represented by the absorbance peak in the visible spectral (Bhaskaran et al., 2019). By using higher concentrations of the gold ions and

the reducing agent, AuNPs of uniform and small size can be obtained. In contrast, by using lower concentrations of the gold ions and the reducing agent, larger and more irregular AuNPs can be obtained (Hammami et al., 2021). Additionally, by increasing the reaction temperature, the rate of the reduction reaction increases, resulting in smaller and more uniform AuNPs (Hammami et al., 2021).

As part of this MSc by Research project, a green synthetic method was developed to produce functionalised AuNPs using water as the main solvent, DMF as the reducing agent and the Ligand for the coating, and varying reaction temperatures. The challenge of this method development was to design a green approach to manufacture AuNPs functionalised with a hydrophobic ligand, like the one synthesised for this project and explained in Chapter 3 (Ligand). AuNPs functionalised with the Ligand using the method previously reported by Ju-Nam and co-workers (Ju-Nam et al., 2012) were produced for comparison purposes. This synthesis uses dichloromethane as the main solvent to obtain the colloidal gold. This method is referred to as the conventional method from this point onwards and for clarity. This chapter outlines all experimental details and results obtained from the green method development.

## **4.2 Materials and Methods**

### **4.2.1 Chemicals**

Potassium gold (III) chloride ( $\text{KAuCl}_4$ ), N,N-dimethylformamide (DMF), dichloromethane (DCM), and sodium borohydride ( $\text{NaBH}_4$ ) were purchased from Sigma-Aldrich. Ligand triphenylphosphoniopropylthiosulfate zwitterion was synthesised in-house (as described in Chapter 3). All chemicals and reagents used in the entire study were of analytical grade. All the chemicals were used without further purification. Finally, deionised water (DI water) was obtained from the Millipore Direct-Q Water Purification system (resistivity  $18.2 \text{ M}\Omega\cdot\text{cm}$  at  $25^\circ\text{C}$ ; total organic carbon (TOC)  $\leq 5 \text{ ppb}$ ).

### **4.2.2 Synthesis of cationic lipophilic AuNPs**

#### **4.2.2.1 Conventional Method**

In order to prepare cationic lipophilic AuNPs following the Conventional Method, protocols previously reported by (Ju-Nam et al., 2006; Ju-Nam et al., 2012) were followed. 0.1041g (0.25mmol) of Ligand, 0.04534g (0.12mmol) of  $\text{KAuCl}_4$  were weighed and mixed with 20ml of

dichloromethane (DCM) in a conical flask. The solution was kept stirring overnight at room temperature. The reduction of gold (III) to gold (0) in the presence of phosphonium Ligand was carried out, as shown in Figure 4.1. by adding drop by drop a freshly prepared NaBH<sub>4</sub> solution (0.054g of NaBH<sub>4</sub> was added to 3ml DI water). After a few minutes of reaction, 20 ml of DI water was added to the mixture to promote the transfer of cationic lipophilic AuNPs from the organic phase (DCM) to the aqueous phase. Three samples were produced following the Conventional Method.

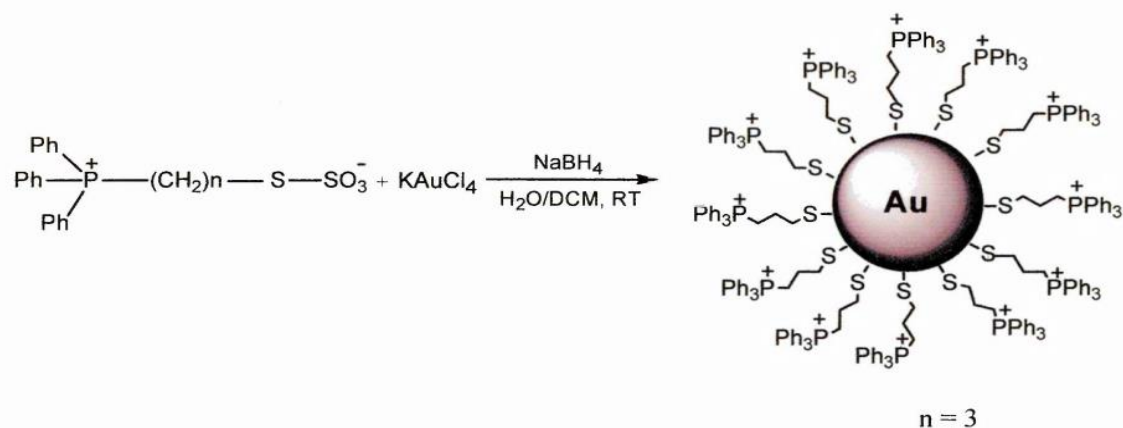


**Figure 4.1.** Synthesis of cationic lipophilic AuNPs using the conventional method (Ju-Nam et al., 2006).

#### 4.2.2.2 Green Methods

In order to develop a green synthesis method, two ways of chemical mixing were trialed in the laboratory. These are outlined below in Green Method #1 and Green Method #2 subsections. Six samples were prepared (three replicates were produced for each sample) following these two methods. Additional to the mixing of chemicals, reaction temperature, and DMF concentration were varied.

**Green Method #1:** In this method, 0.0416g (0.1mmol) of the Ligand was mixed with 20 ml of DI water in a three-neck round bottom flask. The mixture was sonicated until a clear solution was obtained. The flask was then connected to a condenser in the reflux setup. Some samples were heated at 80°C and others at 100°C for a period of 5 hours, and the temperature was maintained constant throughout the reaction. Next, a mixture of 0.0128g (0.034mmol) of KAuCl<sub>4</sub> in 5ml of DI water was prepared and was sonicated to dissolve lumps of the KAuCl<sub>4</sub> salt. After 1 hour, this

mixture was added drop by drop to the boiling solution of Ligand and DI water. After another hour, 10 ml of DMF was added drop by drop to the mixture, and the solution was maintained under reflux for another 2 hours. A deep purple colour solution was the indication of reaction completion.

**Green Method #2:** In this method, 0.0416 g (0.1mmol) Ligand and 0.0128 g (0.034mmol) of  $\text{KAuCl}_4$  were added and mixed in 30 ml of solution of DMF:DI water (ratios of 1:5 and 1:2) in a three-neck round bottom flask. The mixture was then sonicated until a uniform clear pale yellow solution was obtained. The flask was then connected to a reflux condenser setup and heated. Some samples were heated at 80°C and others at 100°C for a period of 5 hours. During this time, the temperature was maintained constant. Colour change at each stage of the reaction was noted. The reaction was stopped when a deep purple solution was obtained.

### **Samples:**

As previously mentioned, six samples were produced using Green Method #1 and Green Method #2. Preparation and differences between samples are outlined below.

Samples 1, 2, 3 and 4 were synthesised using Green Method #1. Samples 1 and 2 were prepared at a temperature of 100°C, and Samples 3 and 4 at 80°C. The ratio of DMF:DI water was varied for each sample. For Samples 1 and 3, the ratio used was 1:2 (DMF:DI water), while for Samples 2 and 4, the ratio used was 1:5 (DMF:DI Water). The amounts of Ligand and  $\text{KAuCl}_4$  salt used in all syntheses were kept the same as mentioned in Green Method #2. The main aim of varying the ratio of DMF:DI water and temperature, was to investigate the effect of these parameters on the AuNP size and shape.

### **Sample 5 and Sample 6**

Both Samples 5 and 6 were synthesised using the Green Method #2. Both samples were prepared using DMF:DI water ratio of 1:2. However, the temperature of the syntheses was varied between the two samples. Sample 5 was prepared at the temperature of 80°C and Sample 6 at 100°C. The amounts of the Ligand and  $\text{KAuCl}_4$  salt used were kept the same as specified in Green Method #1. All reaction conditions for all six samples are summarised in Table 4.1.

**Table 4.1.** Temperatures and DMF:DI water ratio used for all six samples of AuNPs.

SI No.	Sample	Total volume 30ml		Temperature (°C)	Green Method used
		DMF (ml)	H <sub>2</sub> O (ml)		
1	Sample 1	10	20	100	1
2	Sample 2	5	25	100	1
3	Sample 3	10	20	80	1
4	Sample 4	5	25	80	1
5	Sample 5	10	20	80	2
6	Sample 6	10	20	100	2

Samples 1, 2, 3, 4 and 5 were characterised using techniques described in Chapter 2, UV-Vis spectroscopy, XPS, and TEM. Whereas Sample 6 was only analysed using UV-Vis spectroscopy technique.

## 4.3 Results and Discussions

### 4.3.1 UV-Visible spectroscopy analysis

UV-Vis absorption spectroscopy has been employed to study the optical characteristics of nanoparticles. In the present study, all cationic lipophilic AuNPs prepared using the Conventional as well as Green synthetic methods were analysed using a Perkin-Elmer 25 UV-Vis spectrometer, as described in Chapter 2. The wavelength range used for the analysis was 400-700 nm, with a resolution of 1 nm. UV-Vis absorption spectroscopy is a powerful tool for characterising the optical properties of nanoparticles. For all AuNP samples prepared in this project, absorption bands were observed in the visible region, around 520 nm, indicating the successful formation of AuNPs and suggesting that the cationic lipophilic AuNPs could be between 2-10 nm in diameter, according to the literature (Daniel and Astruc, 2004). It is important to note that there are slight differences between AuNPs prepared using Green Method #1 and Green Method #2. This could be due to variations in the reaction conditions, such as temperature, and DMF concentration, which could also affect the size, shape, and stability of the nanoparticles.

#### 4.3.1.1 UV-Vis spectroscopy analysis of cationic lipophilic AuNP solutions obtained using the Conventional Method

The initial step in characterising AuNPs involves observing a colour change in the solution, which is visible to the naked eye. This colour change is attributed to the surface plasmon resonance (SPR) band of the particles (Ramalingam, 2019) in the UV spectrum of the solution. In the Conventional Method, the addition of  $\text{NaBH}_4$  to the mixture causes a color change from cloudy white to wine red, as shown in Figure 4.2.

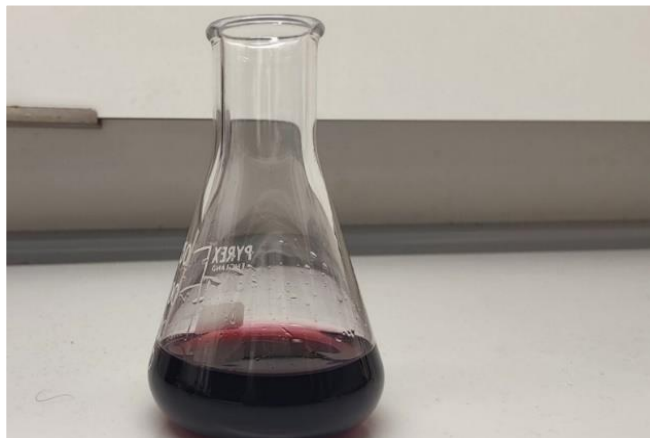


**Figure 4.2.** Cationic lipophilic AuNP solution prepared following the Conventional Method using  $\text{NaBH}_4$  as the reducing agent.

Results from the UV-visible analysis provide evidence of the AuNP formation. The colloidal solutions containing the functionalised AuNPs (cationic lipophilic AuNPs) were dark purple in colour. The UV-Vis spectrum is shown in Figure 4.3. the absorption band is centred at the wavelength of 525 nm. According to the relation between the absorption and the particle size of the AuNPs published in the literature, the particle sizes can be between 3 and 5 nm in diameter (Ju-Nam et al., 2006; Zuber et al., 2016). The UV-visible absorption band of AuNPs is controlled by a number of factors such as the shape and size of the metal nanoparticles. AuNPs exhibit a distinct optical property referred to as localised surface plasmon resonance (LSPR) in which light is incident on a metal surface. The excited electrons on the metal nanoparticle surface create an electromagnetic field that can interact with the incident light, leading to the absorption of certain wavelengths of light. The absorption band, also known as the SPR band is typically observed in the visible region of the spectrum. Spherical AuNPs will typically have an SPR peak at around 520 nm, while anisotropic nanoparticles such as rods or triangles will have a peak at a different wavelength ranging from 520 to 550 nm (Chen et al., 2010). The particle size and shape of the

cationic lipophilic AuNPs obtained following the Conventional method have been reported in previous works found in the literature (Ju-Nam et al., 2006; Ju-Nam et al., 2012). The authors reported that these nanoparticles were  $3.0 \pm 1.2$  nm in size, and spherical in shape from the TEM analyses.

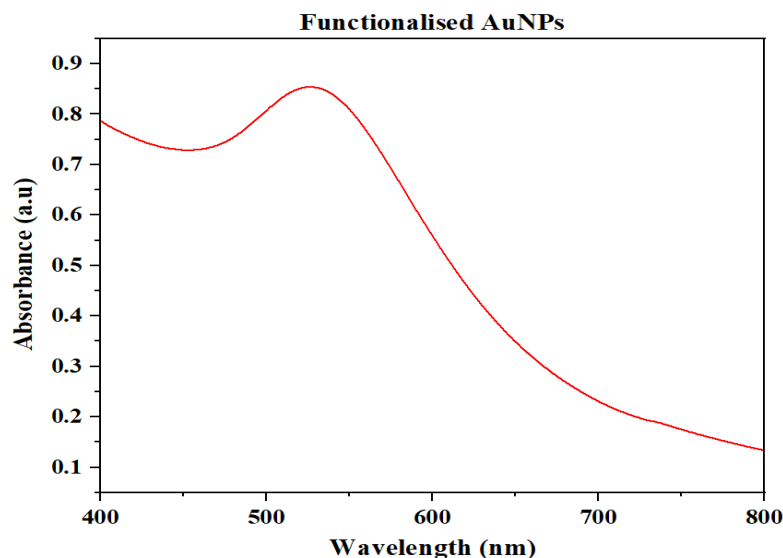


**Figure 4.3.** Absorption spectra of the functionalised AuNPs via Conventional Method.

The stability of the cationic lipophilic AuNPs was also monitored using the UV-Vis technique. Figure 4.4. shows the UV-visible spectra of the same AuNP colloidal solution prepared following the Conventional Method, over a period of four months. The absence of any observable changes in the position of the absorption peaks, centered at 525 nm indicates that the functionalised or cationic lipophilic AuNPs were able to maintain their stability over the four-month period. This finding suggests that the functionalised AuNPs can be reliably used over an extended period without any significant changes in their optical properties. As per earlier research, organic disulfides and alkylthiosulfates S-S bonds may be cleaved in solution in the presence of a reducing agent, releasing organic thiolates that subsequently attach to the surface of the particle (Lukkari et al., 1999). Therefore, it can be assumed that the S-S bond of the Ligand (triphenylphosphoniopropylthiosulfate zwitterion) would be cleaved under the reductive conditions employed in the Conventional Method. The gold salt and Ligand were reduced in the presence of  $\text{NaBH}_4$  for the formation of cationic lipophilic AuNPs.



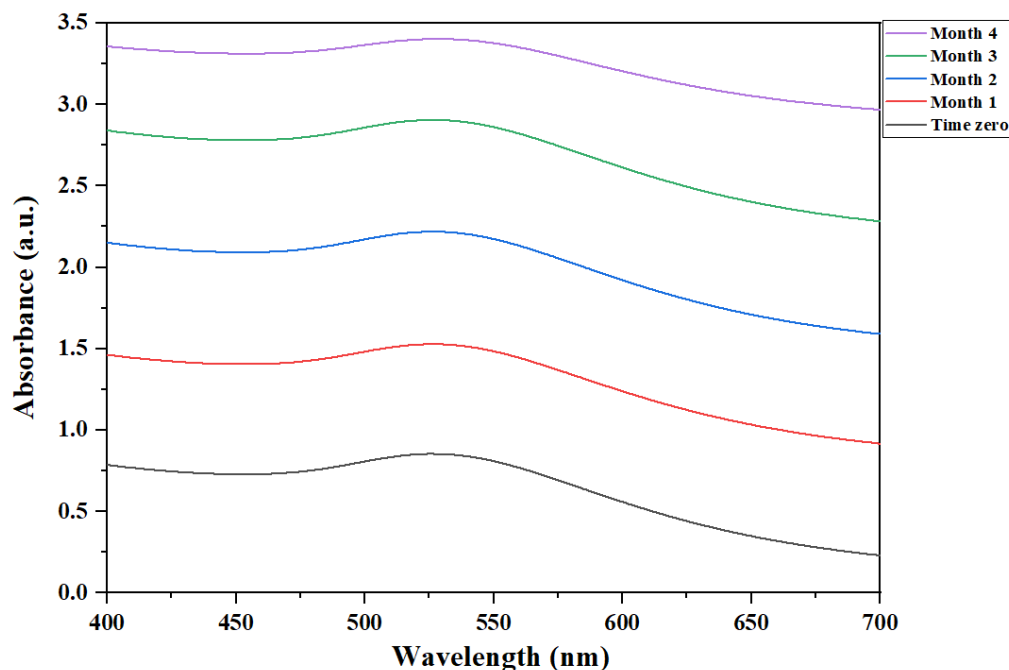


**Figure 4.4.** UV-visible spectra of functionalised AuNPs with after 1, 2, 3, and 4 months (solutions made using same dilution)

#### 4.3.1.2 UV-Vis spectroscopy analysis of cationic lipophilic AuNP solutions obtained using the Green Methods

Absorption spectra of the functionalised AuNPs synthesised via two green synthetic methods (**Green Method #1 and Green Method #2**) are shown in Figure 4.5. During the synthesis, a visible colour change was observed during the progression of the reaction from pale yellow to colourless when the temperature reached 50°C, in all six samples. A further colour change was observed after 2 hours of reaction with a colour change from colourless to pale purple. At the completion of the 5-hour reaction, the colour deepened from pale to dark purple, which indicated that the reduction of Au<sup>3+</sup> to Au<sup>0</sup> took place, and hence, the formation of cationic lipophilic AuNPs.

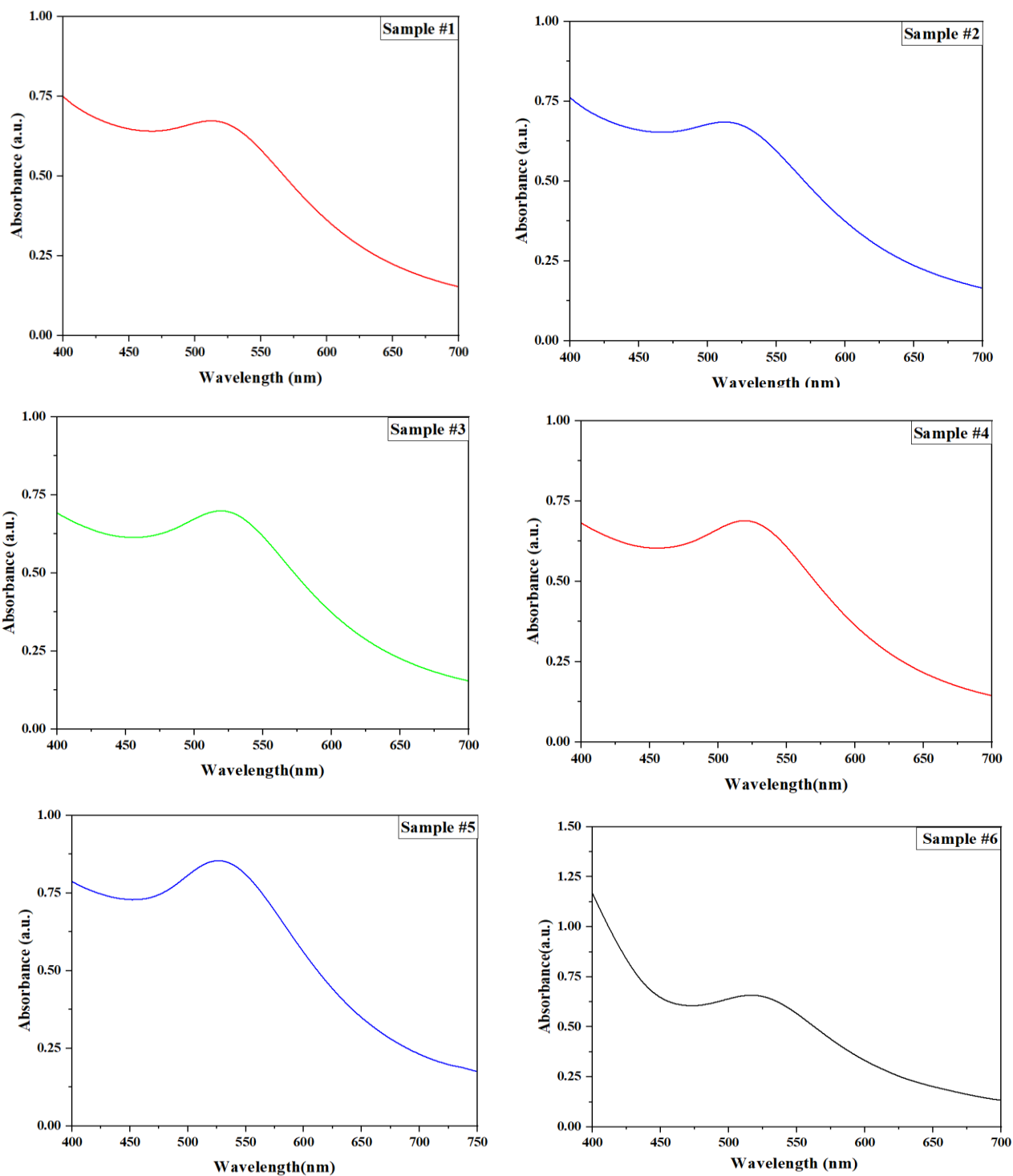


**Figure 4.5.** UV-Vis Spectra of Sample 1 (100<sup>0</sup>C, 1:2 DMF:DI water), Sample 2 (100<sup>0</sup>C, 1:5 DMF:DI water), Sample 3 (80<sup>0</sup>C 1:2 DMF:DI water), Sample 4 (80<sup>0</sup>C, 1:5 DMF: DI water) and Sample 5 (80<sup>0</sup>C, 1:2 DMF:DI water), Sample 6 (100<sup>0</sup>C, 1:2 DMF:DI water).

Samples 1, 2, 3 and 4 were prepared following Green Method #1. Sample 1 and Sample 2 were prepared at 100°C, and higher DMF concentration in Sample 1. SPR bands can be observed at 513 nm in both cases. Sample 3 and Sample 4 were synthesised at 80°C and higher concentration of DMF in Sample 3. The SPR bands for Samples 3 and 4 appear at 517 nm. A shift in the absorption bands were observed when the reaction temperature was lower (80°C). This shift observed between samples could be attributed to the concentration of DMF, which can act as the reducing agent (Pastoriza-Santos and Liz-Marzán, 2009). However, this theory can be discarded when only looking at the results from the UV-Vis spectroscopy analysis, as Sample 1 and Sample 2 are prepared at 100°C and different DMF concentrations. The corresponding SPR bands appear at 513 nm in both cases. Similar results were obtained in the case of Sample 3 and Sample 4. Figure 4.5. also shows UV spectrum of Sample 5 sample 6 and the SPR bands appeared at 525 nm. A small shift of the SPR band can be noted in this case. This may be due to the mixing order of the reactants (Green Method #2). To assess the potential effect of different concentrations of DMF used in this study, results from TEM work were analysed and discussed in detail in the following sections of this Chapter 4.

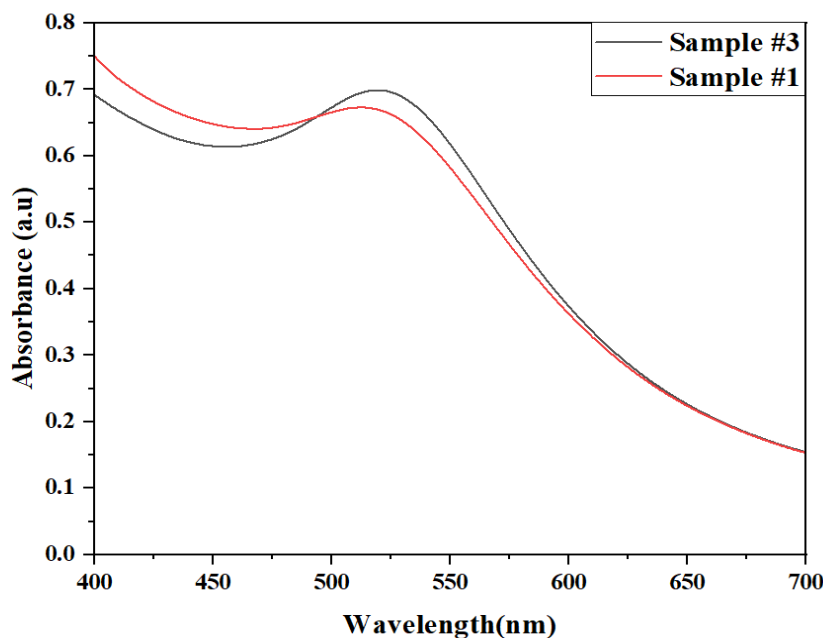


**Figure 4.6.** Comparison of the absorption spectra corresponding to different synthesis temperatures Sample #1 100°C and Sample #3 80°C.

The shift in SPR bands observed in spectra from Samples 1 and 2, and Samples 3 and 4, can be attributed to the faster reduction of the AuNPs themselves at higher reaction temperatures (100<sup>0</sup>C), which can lead to changes in their shape, size, and SPR peak position (Bondarchuk et al, 2013). According to He and co-workers (He et al., 2005), the absorption band of AuNPs shifts to lower wavelengths with an increase in reaction temperature. This can be observed when comparing Sample 1 and Sample 3 as shown in Figure 4.6.

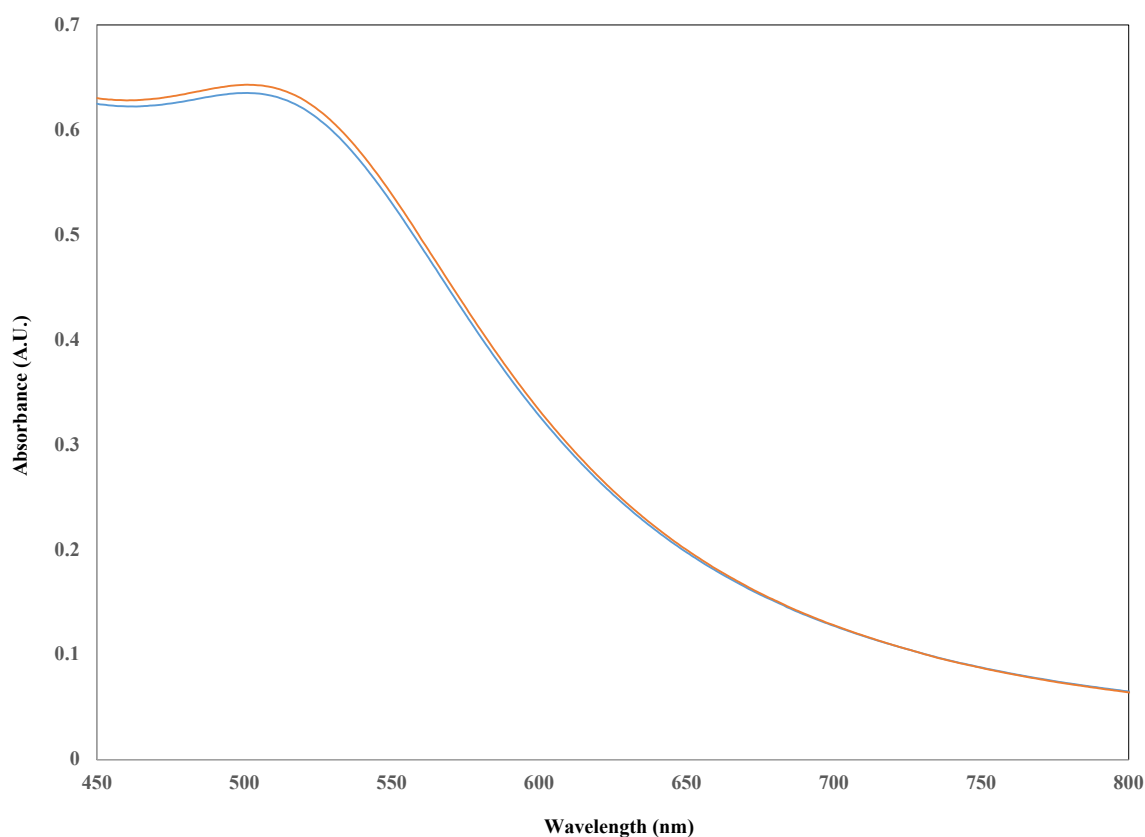


**Figure 4.7.** UV-visible spectra of functionalised AuNPs (Sample 1) produced following Green Method #1 (red line – time 0, blue line – time 6 months)

Stability study was conducted by monitoring Sample 1. Figure 4.7. shows the UV spectra taken at time 0 and after 6 months. The SPR peak remained the same (513 nm).

### **4.3.2 TEM analysis of cationic lipophilic AuNPs synthesised following Green Methods**

As previously mentioned, TEM is a widely used microscopic technique for the characterisation of nanoparticles, as it provides high-resolution images for particle size and morphology analysis. In this project, TEM was used to characterise the cationic lipophilic AuNPs produced following the Conventional Method and the Green Method (explained in Section 4.2.2.2, using different experimental conditions, such as chemical mixing, DMF concentration and temperature), in order to determine their size and shape. TEM micrographs were obtained using a Jeol 2100F Field Emission Gun Transmission Electron Microscope, from the Experimental Techniques Centre (ETC) at Brunel University. All samples were diluted first (1:100 AuNP:DI water) and then centrifuged prior TEM analysis. From the centrifuged solution, one drop of the reaction mixture was deposited on a 1000-mesh carbon-coated copper grid. The latter was then dried for approximately 1 hour (air drying) before TEM imaging. Particle size analysis was conducted by examining a minimum of 100 particles per sample from the TEM images using ImageJ software.

#### **4.3.2.1 TEM analysis of the cationic lipophilic AuNPs synthesised using Conventional Method**

From Figure 4.8.(a), it is clear that AuNPs functionalised with the Ligand following the Conventional Method (biphasic DCM:water method) are spherical in shape. Most particles examined for this sample were within a distribution range of 2.75 - 4.75 nm (Figure 4.8. (b)). This confirms the observations made when analysing the corresponding UV-Vis spectrum (SPR band 525 nm, Figure 4.3.). After examining the diameter of 100 particles (taken from several images), the calculated mean diameter was  $3.33 \pm 0.45$  nm in diameter. There is evidence of particles of < 2.5 nm and *circa* 5 nm diameters present in the colloidal AuNP sample when looking at the particle size distribution shown in Figure 4.8.(b). This may be due to the type of method used to produce the cationic lipophilic AuNPs. The Conventional Method is based on a biphasic or two-phase solvent method. The solvent system used was DCM:water. The functionalised AuNPs are synthesised at room temperature. This may affect the particle size distribution of the sample, but also the addition and amount of NaBH<sub>4</sub> (reducing agent). The results obtained in this part of the study aligned well with the ones reported in the literature on the Conventional Method (Ju-Nam et al., 2006, Ju-Nam et al., 2012).

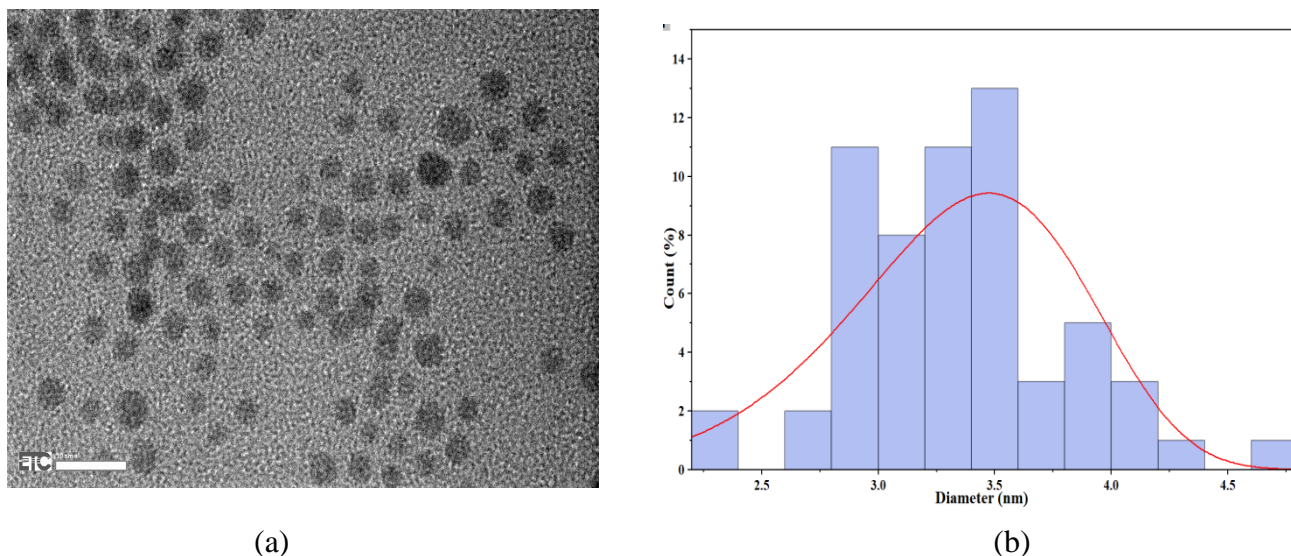
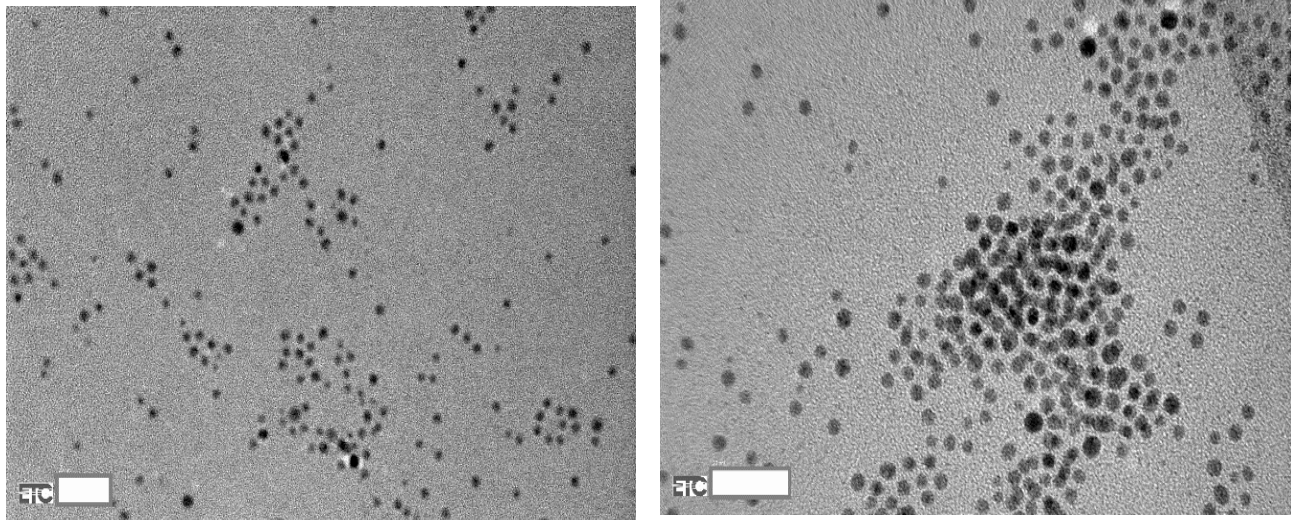


**Figure 4.8.** (a) TEM image of cationic lipophilic AuNPs (image scale: 10 nm), (b) particle size distribution of the functionalised AuNPs via Conventional Method

#### 4.3.2.2 TEM analysis of the cationic lipophilic AuNPs synthesised via Green Methods

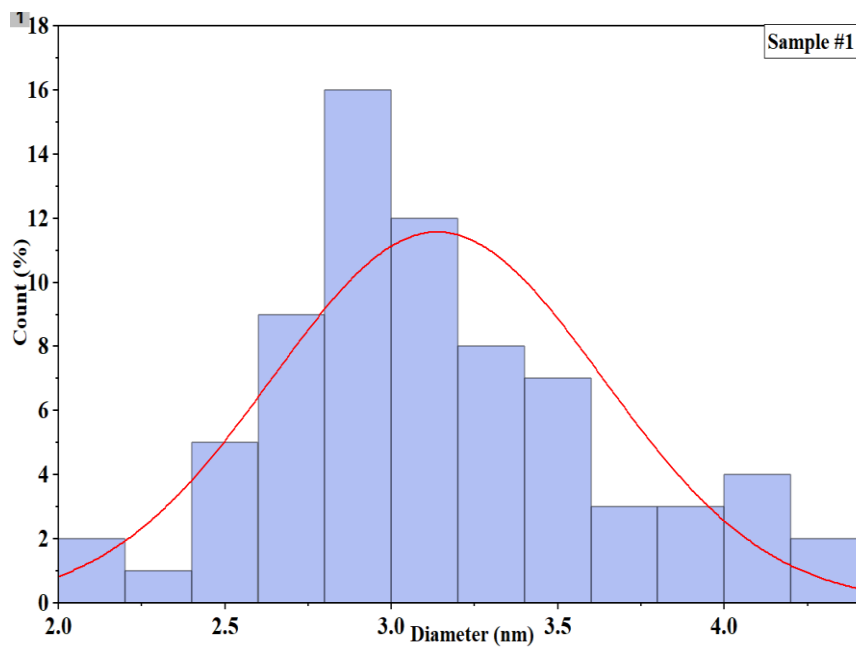
TEM studies showed that all the samples are spherical in shape (Figure 4.9. - 4.13.), the particle size of all the samples reveals that AuNPs prepared from different DMF concentrations at different temperatures produces particle of different size and distribution. The images showed that the AuNPs were well-dispersed and spherical in shape, with a narrow size distribution. The size of the particles was determined by measuring the diameter of the core, which was found to be in the range of 2-10 nm, consistent with the results obtained from UV-Vis absorption spectroscopy. In contrast, different passivation kinetics of the ligands corresponding to different temperatures can be used to explain variations in particle size distribution for the different Samples (Lohse et al., 2010; Fealy et al., 2011; Singh et al., 2010; Zhang et al., 2009). From Table 4.3 AuNPs prepared at 100<sup>0</sup>C produces particle of smaller size and at 80<sup>0</sup>C produce particles of larger size.

## Sample 1



(a)

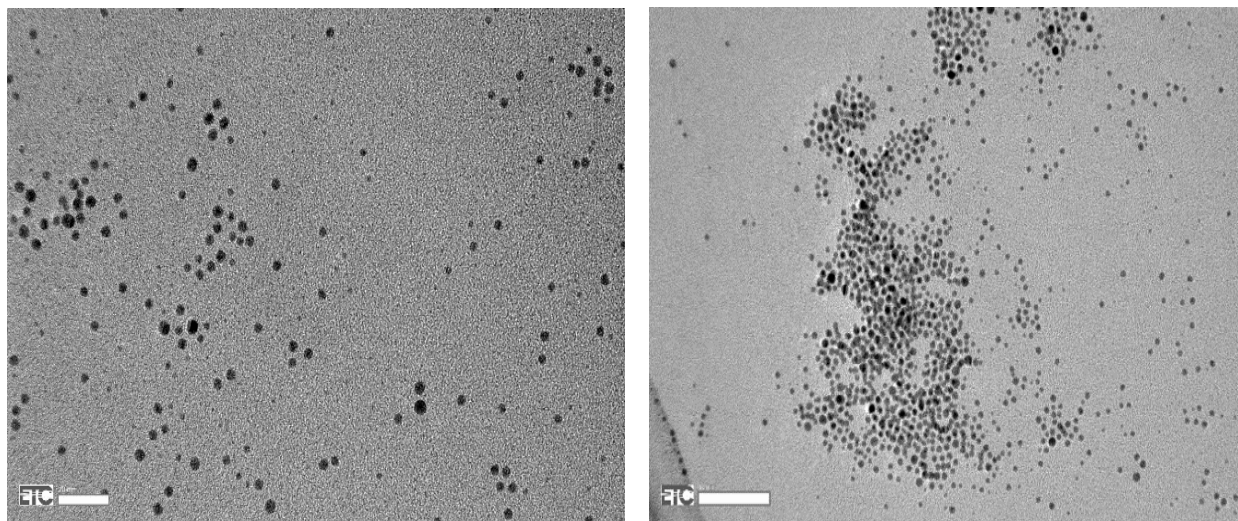
(b)



(c)

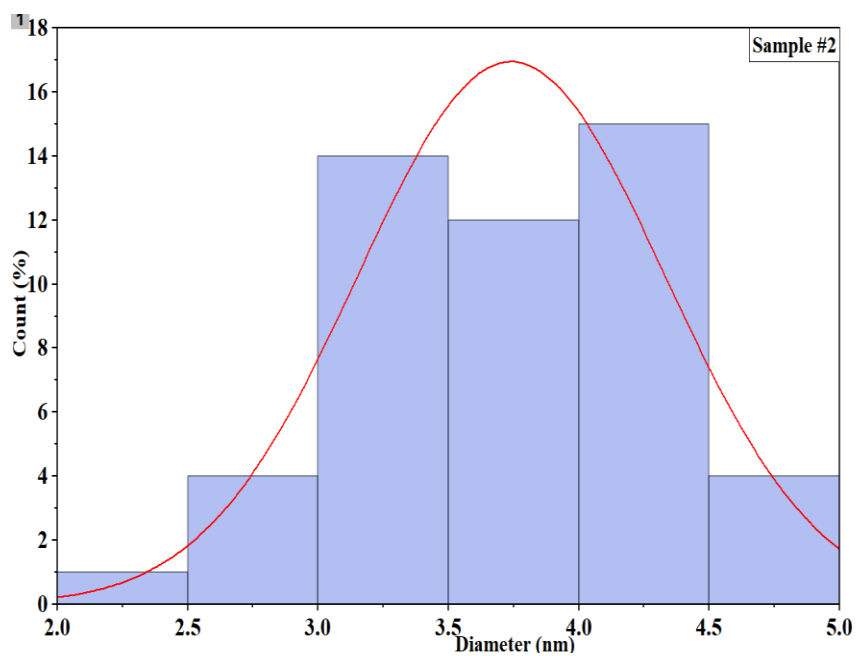
**Figure 4.9.** (a), (b) TEM micrographs (images scale: 20 nm) of Sample #1 (100<sup>0</sup>C, 33%DMF), and (c) particle size histograms of AuNPs synthesised by Green Method #1. Mean particle size  $3.13 \pm 0.5\text{nm}$ , in each histogram 200 nanoparticles were counted

## Sample 2



(a)

(b)

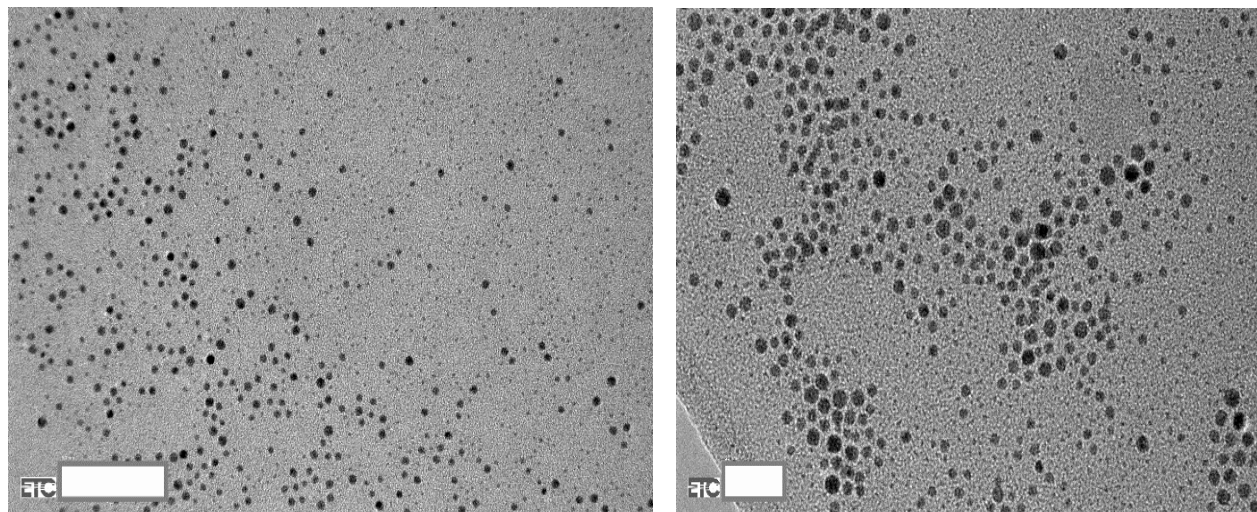


(c)

**Figure 4.10.** (a), (b) TEM micrographs (image (a) scale: 20 nm, image (b) scale: 50 nm) of Sample #2 (100<sup>0</sup>C, 16% DMF), and (c) particle size histograms of AuNPs synthesised by Green Method #1. Mean particle size  $3.74 \pm 0.6\text{nm}$ , in each histogram 200 nanoparticles were counted.

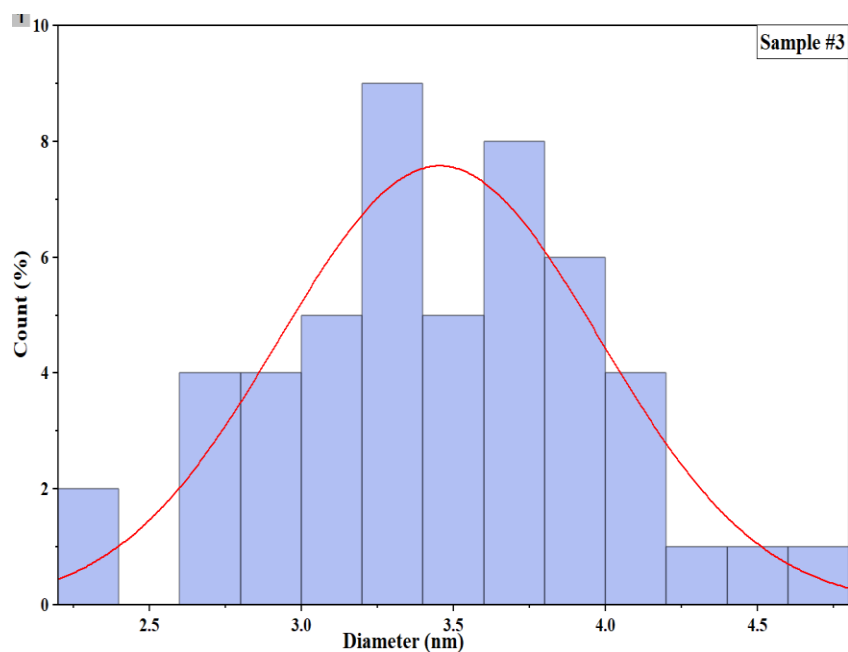


### Sample 3



(a)

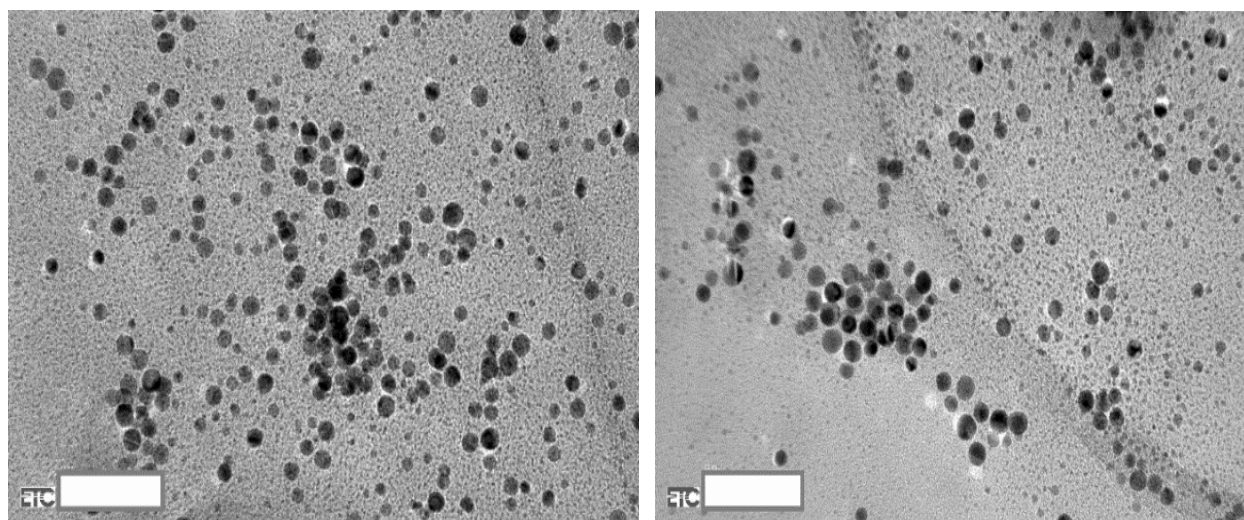
(b)



(c)

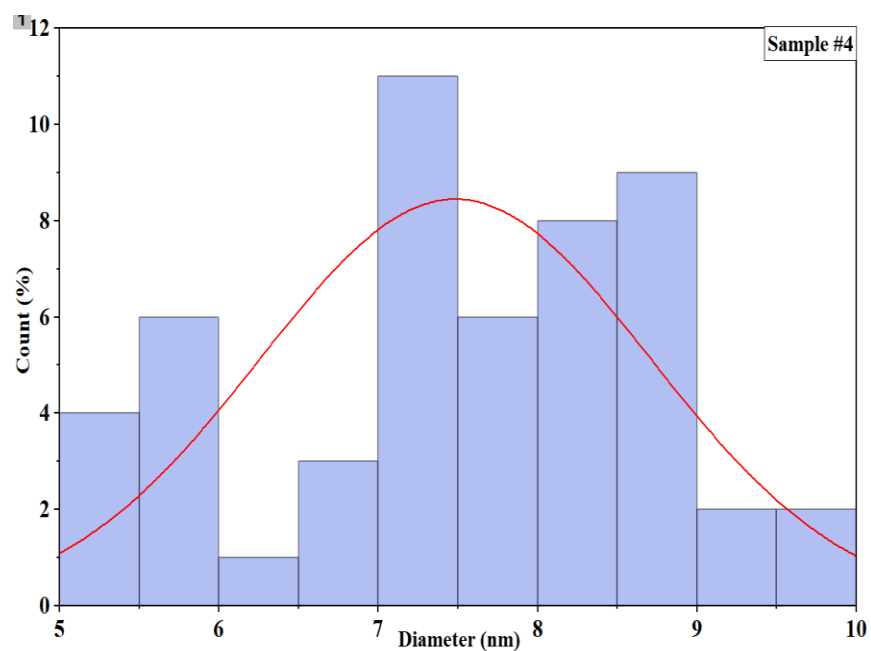
**Figure 4.11.** (a), (b) TEM micrographs (image (a) scale: 50 nm, image (b) scale: 20 nm) of Sample #3 (80°C 33% DMF), and (c) particle size histograms of AuNPs synthesised by Green Method #1. Mean particle size  $3.45 \pm 0.5$ nm, in each histogram 200 nanoparticles were counted.

## Sample 4



(a)

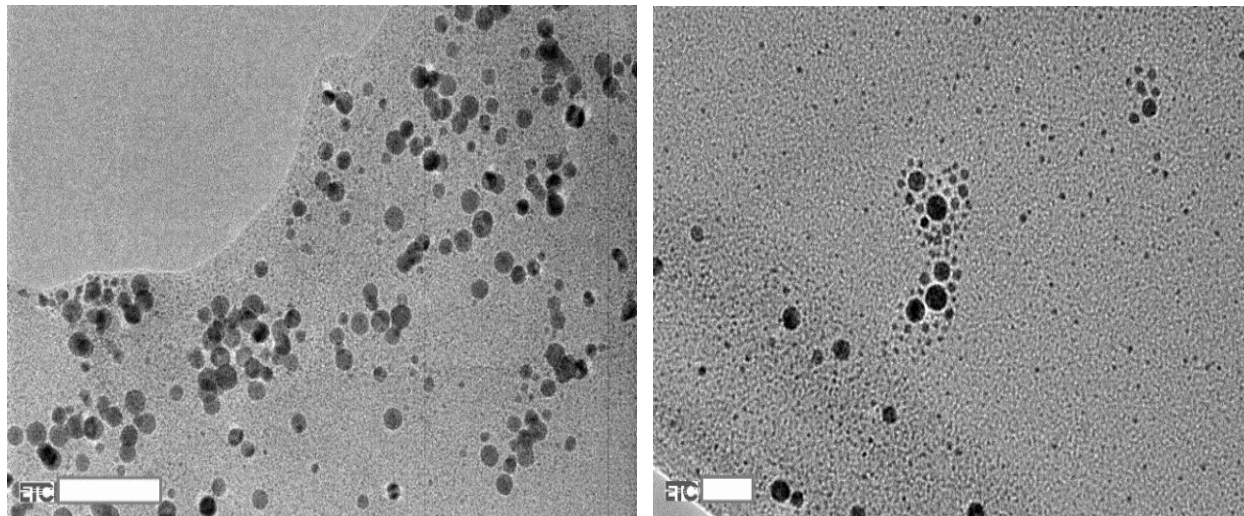
(b)



(c)

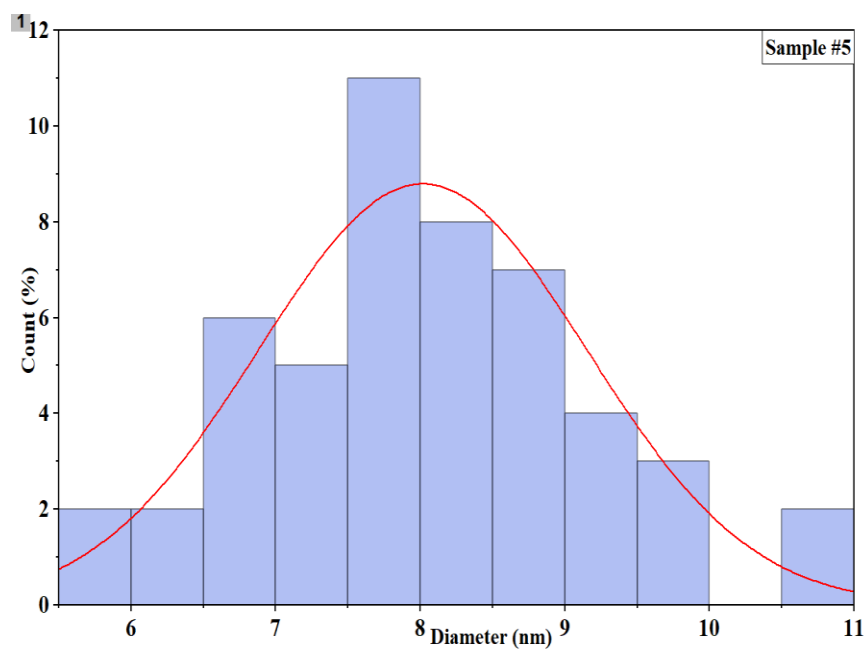
**Figure 4.12.** (a), (b) TEM micrographs (images scale: 25 nm) of Sample #4 (80<sup>0</sup>C, 16% DMF), and (c) particle size histograms of AuNPs synthesised by Green Method #1. Mean particle size  $7.52 \pm 0.97$ nm, in each histogram 200 nanoparticles were counted.

## Sample 5



(a)

(b)



(c)

**Figure 4.13.** (a), (b) TEM micrographs (image (a) scale: 15 nm, and image (b) scale: 20nm) of Sample #5 (80°C, 33% DMF) and (c) particle size histograms of AuNPs synthesised by Green Method #2. Mean particle size  $8.01 \pm 1.1$ nm, in each histogram 200 nanoparticles were counted.

**Table 4.2.** Average particle size of AuNPs synthesised at different temperatures and various concentrations of DMF.

Sample	Temperature (°C) Green Method (GM)	DMF:DI water	Mean particle size (nm)
1	100 (GM #1)	1:2	3.13 ± 0.5
2	100 (GM #1)	1:5	3.74 ± 0.6
3	80 (GM #1)	1:2	3.45 ± 0.5
4	80 (GM #1)	1:5	7.52 ± 0.97
5	80 (GM #2)	1:2	8.01 ± 1.1

The temperature of the synthesis of the AuNPs has a high impact on the size of the AuNPs. As the temperature increases the particle size decreases (Mountrichas et al., 2014). Higher temperature results in fast reaction rates and more rapid nucleation leading to small particle size (Tran et al., 2016b). Higher concentrations of reducing agent (DMF) can lead to the formation of smaller nanoparticles when comparing Sample 1 (3.13 ± 0.5 nm) and Sample 2 (3.74 ± 0.6 nm). However, a more significant difference can be noted when comparing Sample 3 (3.45 ± 0.5 nm) and Sample 4 (7.52 ± 0.97 nm), which were produced following the same Green Method #1 at 80°C (Table 4.3). More reductive ions will be available in the solution to reduce the gold ions, resulting in small particle sizes (Tran et al., 2016b). According to the results gathered in Table 4.2. when the reaction temperature is kept at 100°C as in the case of Samples 1 and 2, the particle sizes seem to be determined by the temperature more than the reducing agent concentration. On the contrary, when the reaction temperature is reduced to 80°C (Samples 3 and 4), the particle sizes may be more influenced by the DMF concentration. Similar results were reported by Tran and co-workers when they studied the effect of sodium citrate concentration in AuNP synthesis (Tran et al., 2016b). When analysing the data from Sample 3 (3.45 ± 0.5 nm) and Sample 5 (8.01 ± 1.1 nm), particle size differences may be attributed to the mixing order of the reactants, and not so much to the temperature and DMF concentration, which are kept the same in both cases.

The initial step in the procedure for the synthesis of functionalised AuNPs should be the adsorption of the ligand on the surface of the growing particles then the thiosulphate is transformed into thiolate. Research on the production of monolayers on gold surfaces using alkylthiosulfates

demonstrates the significance of the hydrolysis by trace amounts of water present in the solvent (Fealy et al., 2011; Pillai and Freund., 2011). The cationic lipophilic AuNPs described were synthesised using an excess amount of water in a two-phase water/dimethyl formamide combination. On the growth of AuNPs, the cleavage of the thiosulfate S–S bonds by the addition of the reducing agent (Ju-Nam et al, 2012), and this process is fast at higher temperatures and this leads to the formation of the small size particle distribution (Tran et al., 2016b).

### 4.3.3 XPS analysis of the cationic lipophilic AuNPs produced following Green Method #1

In order to determine the elemental composition of the cationic lipophilic AuNPs (Sample 1 produced following Green Method #1, 1:2 DMF:DI water, at 100<sup>0</sup>C) and probe the nature of Au-S bonds, the AuNPs were studied by XPS spectroscopy. Wide survey spectra of AuNPs showed signals due to Au<sub>4d</sub>, and Au<sub>4f</sub>, C<sub>1s</sub>, S<sub>2s</sub> and S<sub>2p</sub>, and weaker signals due to P<sub>2p</sub>, Cl<sub>2s</sub>, K<sub>2s</sub>, Cl<sub>2p</sub> and Al<sub>2p</sub>, as can be seen in Figure 4.14. The presence of Aluminium is due to the Sample holder where the Samples were deposited, whereas the presence of Potassium and Chlorine are due to the initial potassium tetrachloroaurate used for the synthesis of the AuNPs.

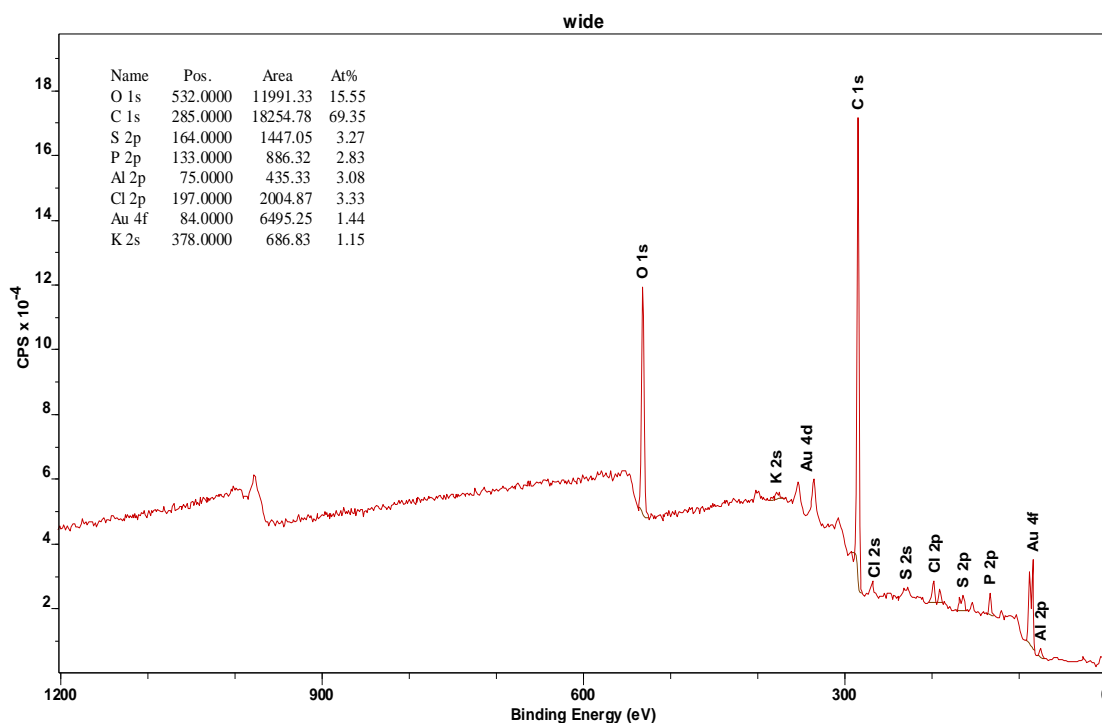


**Figure 4.14.** XPS survey spectrum of the cationic lipophilic AuNPs (from Sample 1).

The Au<sub>4f</sub> XPS signal is a doublet for Au (4f<sub>7/2</sub>) and Au (4f<sub>5/2</sub>), with binding energies *circa* 84.0 and 87.6 eV, respectively (Wagner et al., 1979). The high resolution Au<sub>4f</sub> spectrum of the phosphonium-AuNP is shown in Figure 4.15.

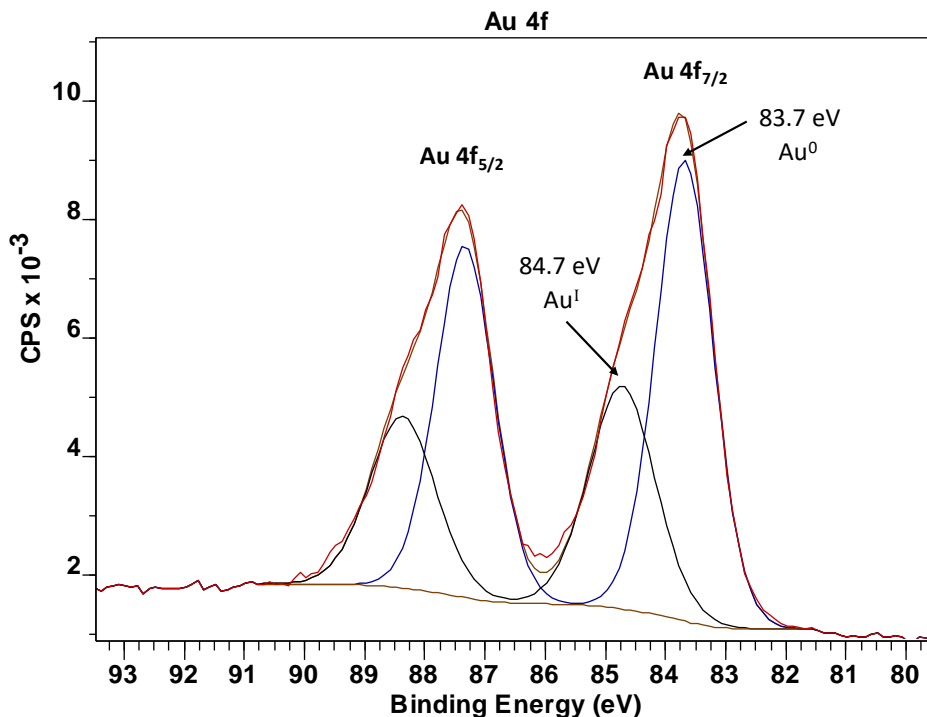


**Figure 4.15.** XPS high resolution spectrum for Au<sub>4f</sub> of the AuNPs, with corresponding peak deconvolution to assess the local chemical environment of this element.

The Au<sub>4f</sub> XPS spectrum of the nanoparticles showed the contribution of two different Au<sub>4f</sub> doublets, with values of Au(4f<sub>7/2</sub>) at 83.7 and 84.7 eV respectively (Figure 4.15.). The binding energy of the first peak observed at 83.7 eV tends toward the value seen for a surface layer of bare Au (83.6 eV (van der Putten et al., 1996). The value at 84.7 eV is close to the value reported by Yee *et al.* at 84.2 eV (Yee et al., 2003), for AuNPs capped with dodecane thiol. AuNPs containing surface atoms in the Au(I) oxidation state show a 4f XPS peak at 84.9 eV (McNeillie et al., 1980). The presence of these two peaks in the phosphonium-AuNPs indicates that the bulk of the gold atoms is in the Au(0) oxidation state (peak at 83.7 eV) and the surface Au atoms are bound to sulphur (Au-S) and have an oxidation state of +1 (peak at 84.7 eV).

The XPS S<sub>2p</sub> peak is a doublet from the closely spaced spin-orbit components S(2p<sub>3/2</sub>) and S(2p<sub>1/2</sub>) ( $\Delta = 1.16\text{eV}$ , intensity ratio = 0.511), with binding energies *circa* 164.0 eV for the peak of S(2p<sub>3/2</sub>)

from elemental sulphur (Lindberg et al., 1970; NIST 2000). The high resolution S<sub>2p</sub> spectrum of the phosphonium-AuNP is shown in Figure 4.16.

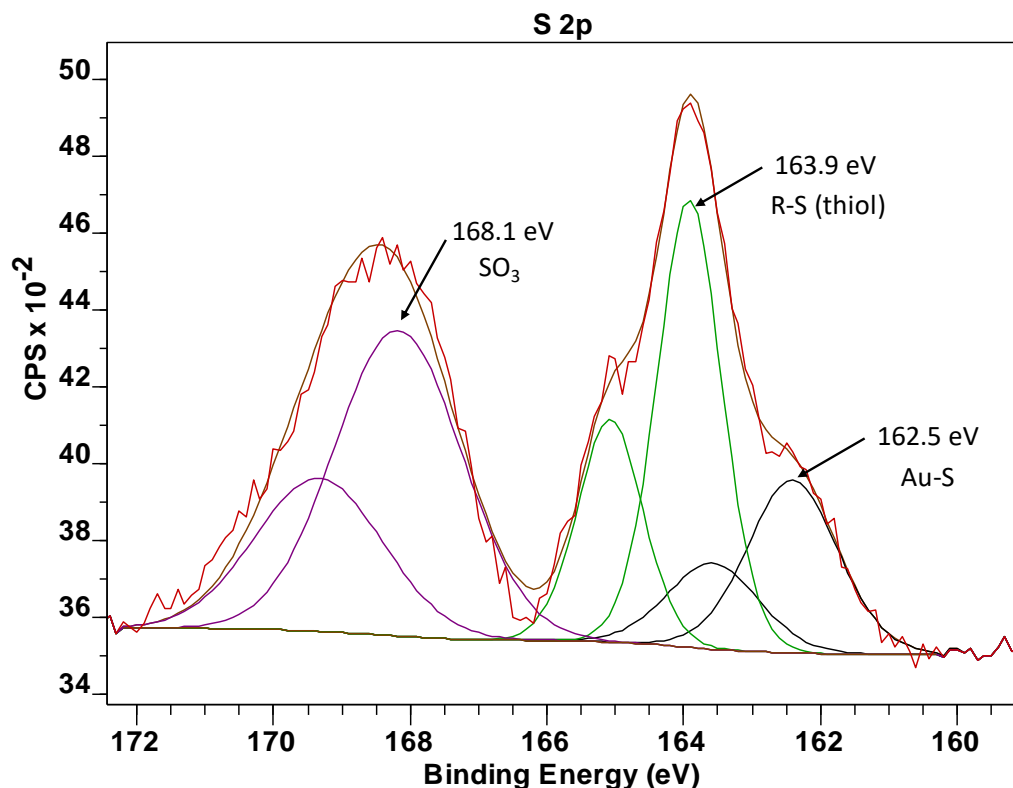


**Figure 4.16.** XPS high resolution spectrum for S<sub>2p</sub> of the AuNPs, with corresponding peak deconvolution to assess the local chemical environment of this element.

For the AuNPs, the high-resolution spectrum of S<sub>2p</sub> suggested the presence of at least three S species. As can be seen from Figure 4.16, the binding energies of the S(2p<sub>3/2</sub>) component of each doublet are 162.5 eV, 163.9 eV and 168.1 eV.

For thiol compounds attached to Au nanoparticles, Au-S-C, the S(2p<sub>3/2</sub>) has been previously reported at 162.6 eV (Gobbo et al., 2013). This correlates very well with the observed S(2p<sub>3/2</sub>) peak at 162.5 eV in the synthesised cationic lipophilic AuNPs, indicating the alkylthiolate bond to gold. The peak observed at 163.9 eV has been assigned to the bond R-S (thiol). This value is in agreement with binding energies previously reported for R-S bonds at 168.8 eV (Beamson and Briggs, 1992; NIST 2000). These results confirm the cleavage of the sulfur-sulfur bond in the phosphonioalkylthiosulfate zwitterions during the synthesis following Green Method #1, with the

concomitant expulsion of  $\text{SO}_3^-$  (or some other sulfur species derived from it), at the ligand/Au interface.

The observed S(2p<sub>3/2</sub>) peak with the binding energy of 168.1 eV is likely to be due to both remaining traces of the original ligand, and surface-bound sulfonate species,  $\text{RSO}_3^-$ , formed by air oxidation of the alkylthiolate bound to gold (Ju-Nam et al., 2012).



## Chapter 5

### Conclusions and Recommendations

The development of a greener method to produce cationic lipophilic AuNPs and a greener reaction route to synthesise organic compounds such as hydroxylpropyltripheylphosphonium salt (Intermediate #1) was achieved by replacing organic solvents, such as DCM and ACN with a more environmentally friendly solvent like water.

For the green synthesis of Intermediate #1, a novel approach for method development was employed, which consisted of the use of Aspen Plus simulation software to model Reaction #1, prior to planning experimental work in the laboratory. First, a process simulation model for the Conventional Route to produce Intermediate #1 (Reaction #1: TPP and bromopropanol are mixed in 15 mL of ACN, and subjected to reflux conditions for 5 hours). Subsequently, the resulting solution was left undisturbed overnight, facilitating the formation of hydroxylpropyltriphenyl phosphonium salt.) was developed using Aspen Plus version 9.0.

The model for Reaction #1 was carried out as a scaled-up reaction by using different reactors such as CSTR and Batch. In the case of the latter, different stop times were evaluated and more encouraging results were obtained for Reaction #1 modelled in batch mode. These results showed that batch mode simulation of Reaction #1 following the Conventional Route could potentially generate more realistic results closer to the ones normally obtained at the laboratory scale. The final objective of this simulation work was to check whether Reaction #1 could occur or not when 100% water was used as the main solvent for the reaction. For that, an Aspen Simulation of Reaction #1 using 100% water was performed using the CSTR reactor (continuous mode). The results indicated that the mass flow of Intermediate #1 was higher for 100% water (0.73221 kg/hr) compared to the ones modelled with 100% ACN (0.20817 kg/hr). This suggests that water could potentially have a more significant impact on the reaction kinetics than ACN for the synthesis of Intermediate #1.

Reaction #1 was performed in the laboratory using 100% water and the product crystals were characterised using ATR-FTIR spectroscopy technique. The peaks corresponding to the Intermediate #1 synthesised using 100% of water as the solvent is in perfect agreement with the

one synthesised using 100% ACN. This confirms the formation of Intermediate #1 using the green solvent (water).

In order to obtain more concrete and realistic operating conditions to be used and replicated in the laboratory experiments, a simulation model in batch mode for Reaction #1 can be created as part of future potential work. Also, rather than using online tools such as CheCal, the Joback method work and calculations of critical parameters are recommended to be carried out using the corresponding equations. The author of this thesis also recommends improving the purification step for Intermediate #1 synthesised following Green Route. One of the options to remove the water and make this process greener to obtain the product crystals could be the use of a freeze-drying technique.

For the second part of the project, cationic lipophilic AuNPs were synthesised using two routes, Conventional Method and the Green Method. No simulation work was carried out in this case. Laboratory work was planned from the start. Functionalised AuNPs synthesised in-house were characterised using different techniques such as UV-Visible spectroscopy, TEM and XPS. Cationic lipophilic AuNPs were obtained by capping AuNPs using phosphoniopropylthiosulfate zwitterion (Ligand). Firstly, the Ligand, capping agent for the nanoparticles, was synthesised in a 3-step process. Crystals were obtained at the end of each stage. The formation of the intermediates and the Ligand was confirmed using the ATR-FTIR spectroscopic technique. The colloidal solution of cationic lipophilic AuNPs synthesised via the Conventional Method remained stable over a period of four months (525 nm), with no wavelength shift in the spectra obtained from the UV-Vis analyses, and no other signs of aggregation. Previously documented data by Ju-Nam et al. 2012 shows that nanoparticles synthesised through this process can remain stable for long periods of time, up to 6 months. The particle sizes of the cationic lipophilic AuNPs were determined using the TEM analysis. The obtained particles were spherical in shape with a mean particle size of  $3.33 \pm 0.45$  nm in diameter. The Conventional Method for nanoparticle synthesis was used to aid the development of the Green Method to produce cationic lipophilic AuNPs.

Functionalised AuNPs are synthesised following two routes, Green Method #1 and Green Method #2. The difference between the methods was in the mixing order of the reactants. For Green Method #1, ligand was mixed with 20 ml of DI water heated under reflux conditions (80 and

100°C). After 1 hour, a solution containing KAuCl<sub>4</sub> dissolved in 5 ml of DI water was added drop by drop into the boiling mixture. After another hour, 10 ml of DMF was gradually added dropwise to the reaction mixture. The solution continued to undergo reflux for an additional 2 hours, ensuring the completion of the reaction. In Green Method #2 ligand and KAuCl<sub>4</sub> were mixed in 30 ml of solution of DMF:DI water (ratios of 1:5 and 1:2) and heated under reflux conditions (80 and 100°C). The temperature was maintained constant throughout the reaction of 5hrs. Six samples were prepared by following two green methods. The formation of the AuNPs was confirmed with the SPR peaks, with values between 513-525 nm. The wavelengths of the maximum absorbance peak values decrease when the reaction temperature increases (from 80 to 100°C). This can be attributed to the decrease in the particle size and rapid nucleation at higher temperatures. The results from TEM analyses showed that: (i) the mixing order of the reactants were affecting the particle sizes at the reaction temperature of 80°C, (ii) temperature determines the size of the particles when the reaction is carried out at 100°C, (iii) the concentration of DMF affects this particle feature when the reaction is kept at 80°C. Finally, Sample 1 prepared following Green Method #1 (100°C, 1:2 DMF:DI water) showed to be stable over a period of 6 months.

In order to determine the elemental composition of the cationic lipophilic AuNPs (Sample 1 produced following Green Method #1, 1:2 DMF:DI water, at 100°C) and probe the nature of Au-S bonds, the AuNPs were studied by XPS spectroscopy. Typical binding energies corresponding to gold atoms were found, Au(0) (peak at 83.7 eV) and Au(+1) atoms at the surface (peak at 84.7 eV). Evidence of thiol compounds attached to AuNPs was observed with a binding energy of 162.5 eV, corresponding to S(2p<sub>3/2</sub>). This was a clear indication the alkylthiolate bond to gold Au-S-C was present in functionalised AuNPs produced following the newly developed green method.

Synthesis of cationic lipophilic AuNPs using greener routes was demonstrated in this thesis. However, greener alternatives to DMF must be found, as this solvent and reducing agent is a toxic chemical. Especially, if these nanoparticles are aimed to be used in biomedical applications. Alternatives of greener reducing agents that could be used in future works are ascorbic acid and glutathione.

# Appendices

## Appendix A

### ATR-FTIR spectra obtained during the synthesis of the ligand

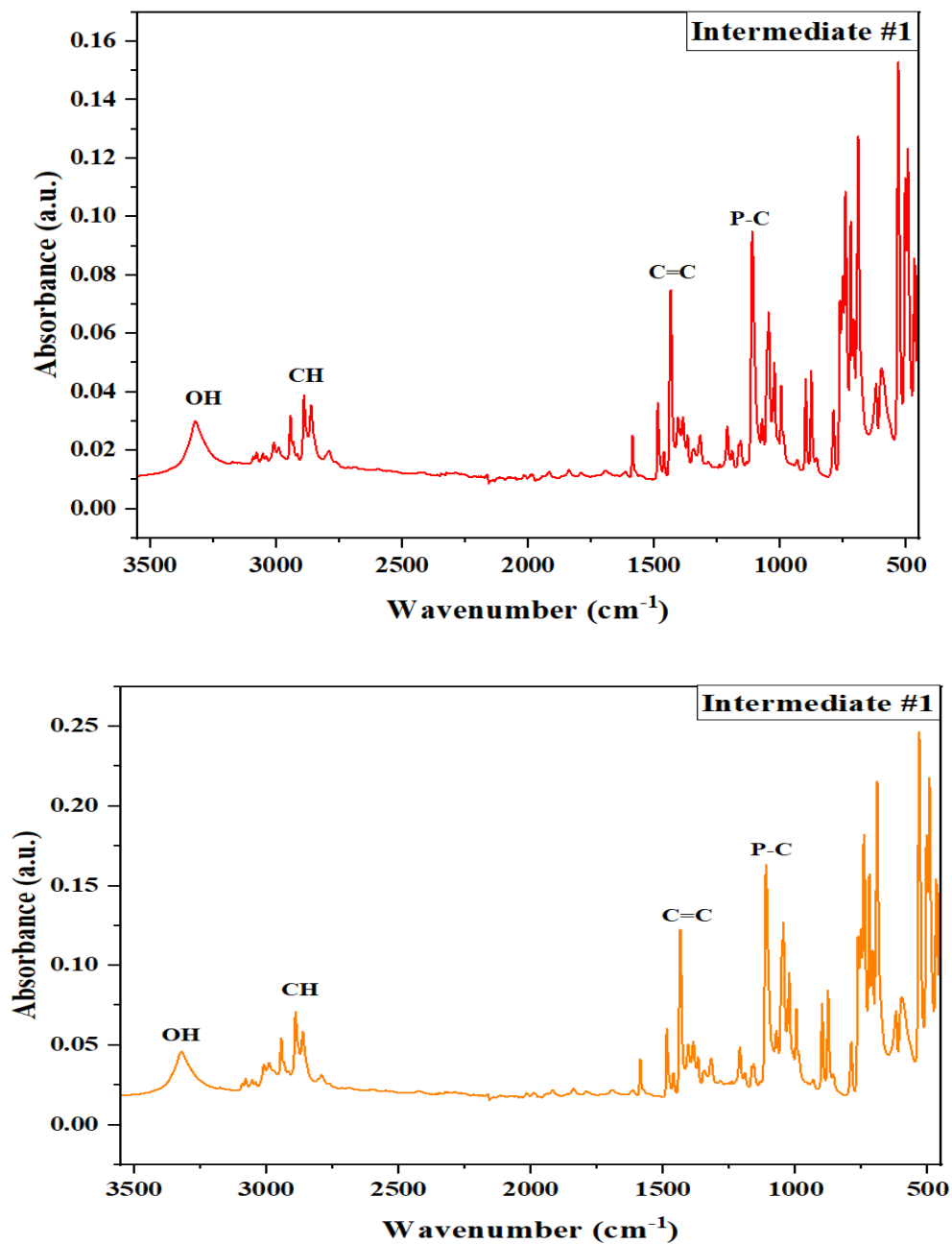


**Figure A1** ATR-FTIR spectra of two different batches of the Intermediate #1 using Conventional Route

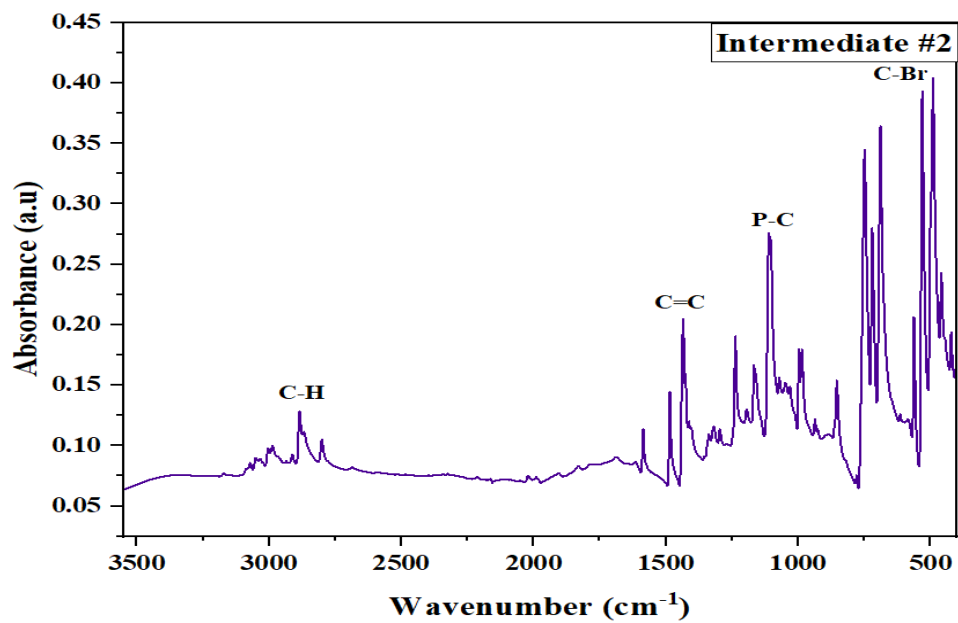
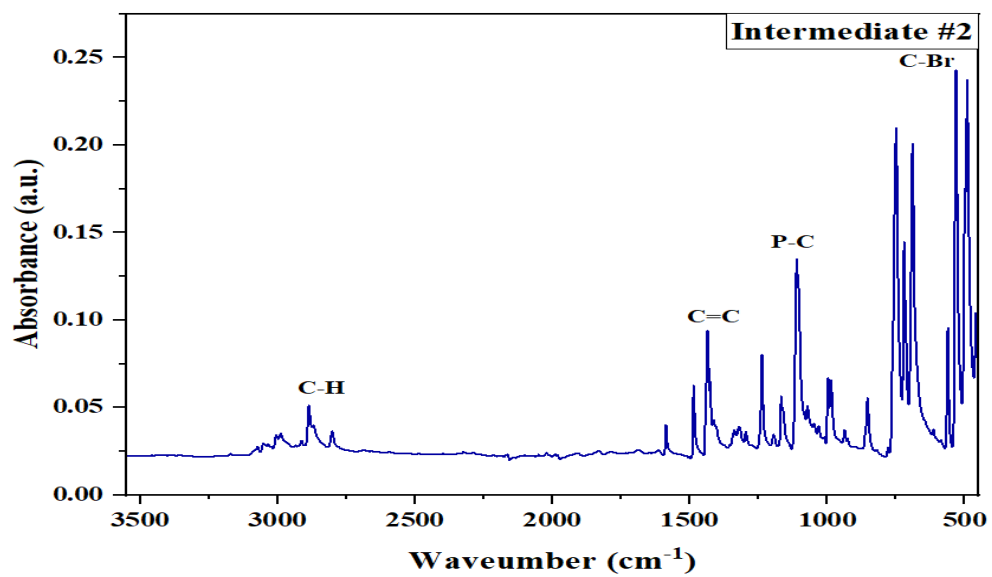


**Figure A2** ATR-FTIR spectra of two different batches of the Intermediate #2 using Conventional Route

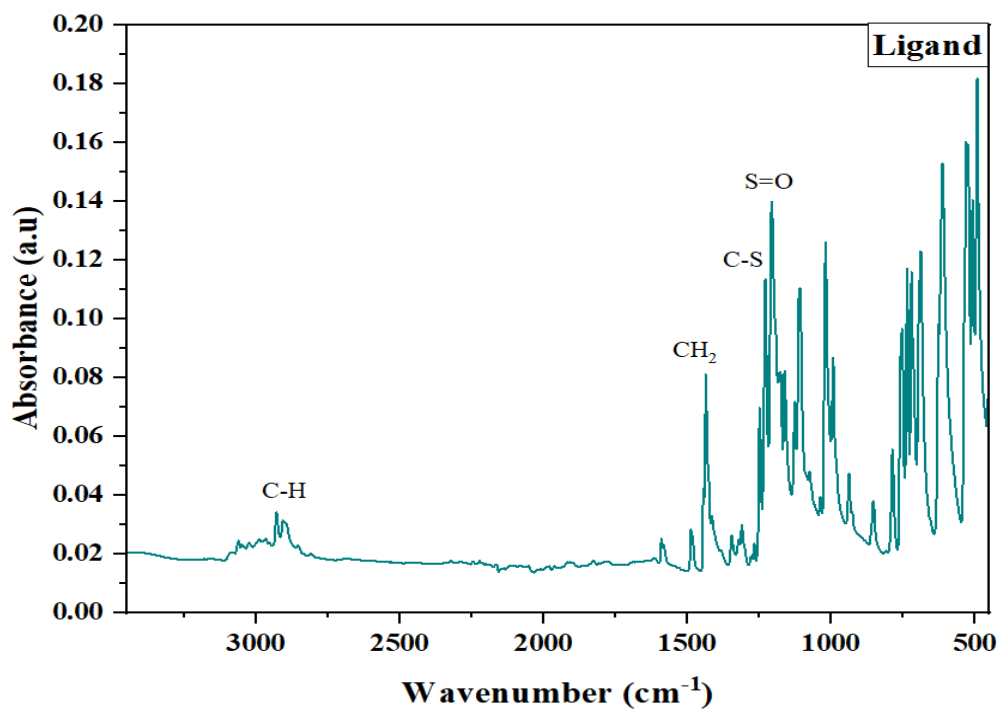
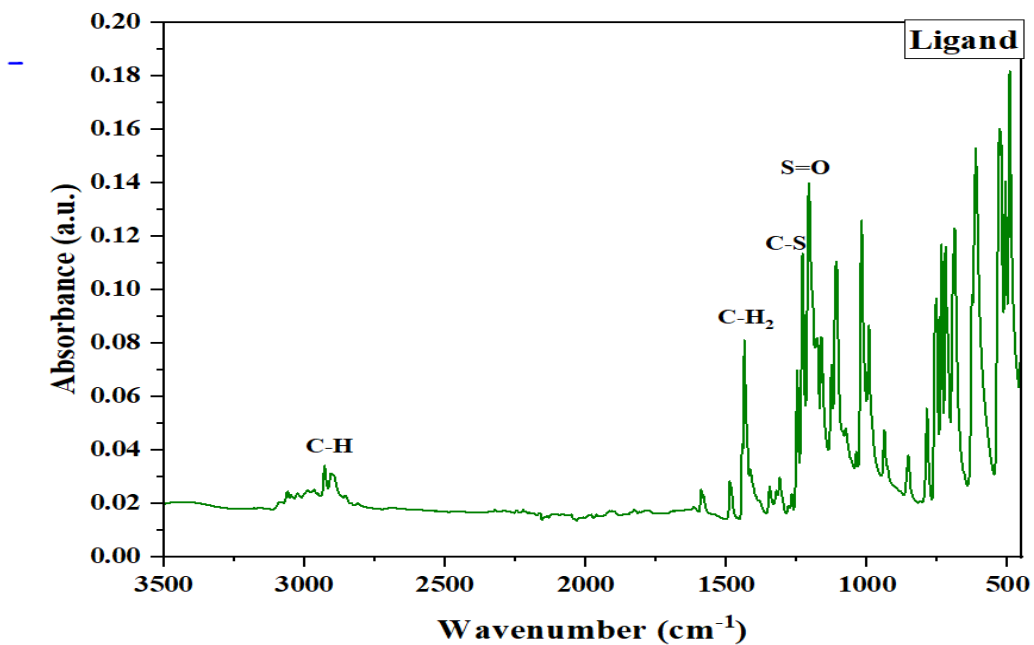


Figure A3 ATR-FTIR spectra of two different batches of the Ligand

## Melting Point studies

- Melting point of the Intermediate #1 – 228<sup>o</sup>C
- Melting point of the Intermediate #2 – 229<sup>o</sup>C
- Melting point of the Ligand – 245<sup>o</sup>C

## Appendix B

### TEM IMAGES (Green Route)

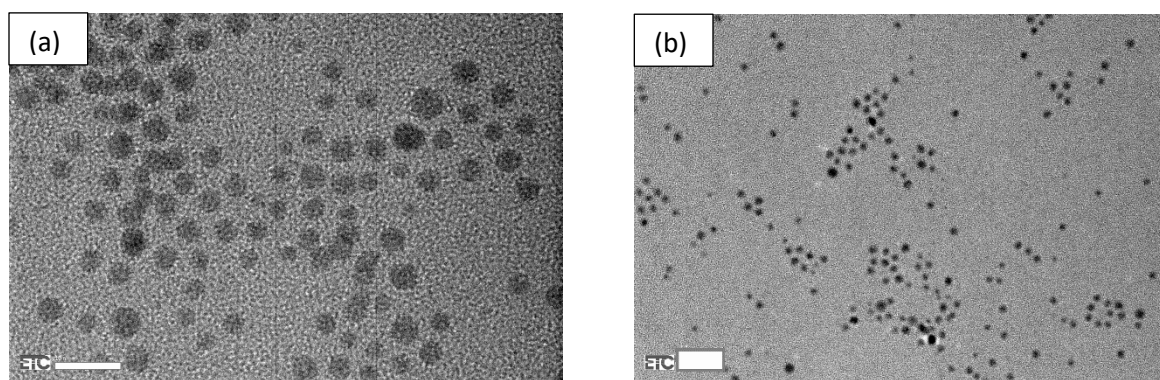


**Figure B1:** Sample 1, Resolution (a) 10nm and (b) 20nm

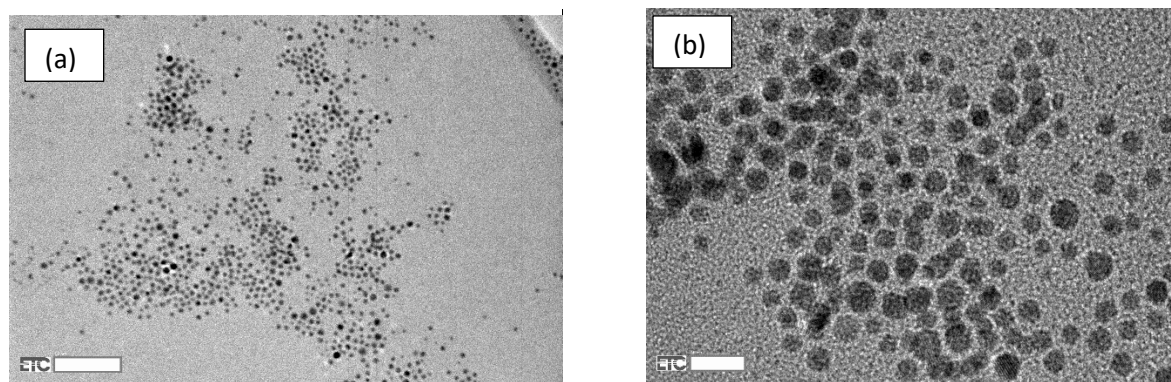


**Figure B2:** Sample 2. Resolution (a) 50nm and (b) 10nm

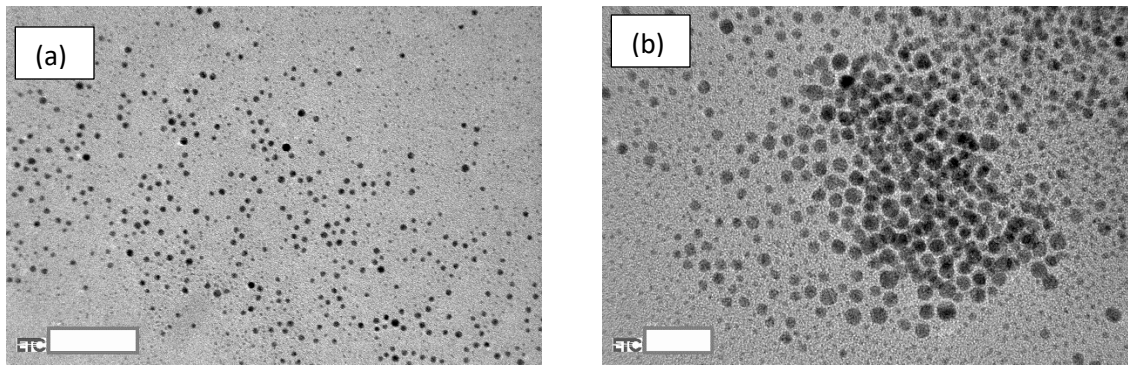


**Figure B3:** Sample 3, Resolution (a) 50nm and (b) 20nm

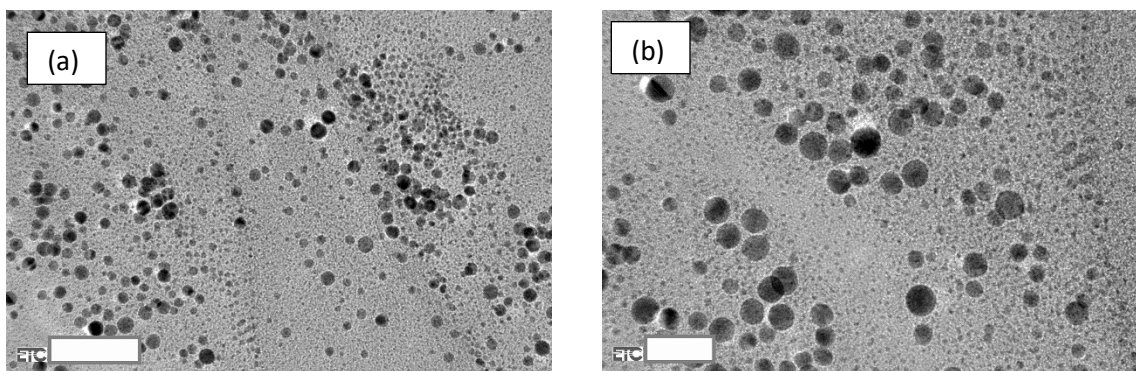


**Figure B4:** Sample 4, Resolution (a) 50nm and (b) 20nm

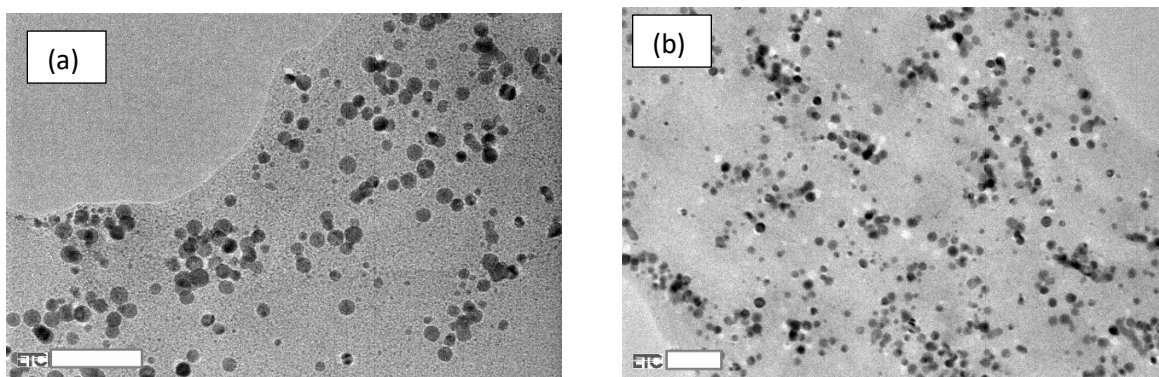


**Figure B5:** Sample 5, Resolution (a) 50nm and (b) 50nm



## Glossary

**SPR:** Surface plasmon resonance (SPR) is a method used to study the interaction between molecules. It is based on a characteristic of surface plasmons, basically, electromagnetic waves that move over the surface of a conductor, like gold or silver (Bakhtiar, 2013).

**Green synthesis:** Green synthesis is a technique for creating substances, compounds, or chemicals without the use of harmful or toxic chemicals and using environmentally friendly techniques. It uses natural resources and biological processes to produce a process that is sustainable and eco-friendly (Shreyash et al., 2021).

**Zwitterion:** A zwitterion is a form of molecule that includes both positive and negative charges inside the same molecule, resulting in a neutral overall charge. These substances are also referred to as "dipolar ions" or "inner salts." The building blocks of proteins, amino acids, frequently contain zwitterions. An amine group (-NH<sub>2</sub>) and a carboxyl group (-COOH) are both present in the amino acid molecule, and they are capable of reacting with one another to create an intermediary molecule known as a zwitterion (Ichikawa, 2017).

**Joback method:** Empirical technique for determining the physical and thermodynamic characteristics of organic molecules is the Joback method. It is based on the concept of group contribution, which states that a molecule's attributes may be calculated by adding the contributions made by each of its chemical groups. The Joback technique may be used to estimate a wide range of parameters such as boiling point, critical temperature, heat capacity, and viscosity for pure liquids and liquid mixes. It entails locating the functional groups or molecular pieces that are present in a molecule and giving each one of them a preset set of group characteristics (Kleiber and Joh, 2010).

# Bibliography

Ahmed, S., A., Ikram, S., and Yudha, S. S. (2016). Biosynthesis of gold nanoparticles: A green approach. *Journal of Photochemistry and Photobiology B-Biology*, 161, 141–153. <https://doi.org/10.1016/j.jphotobiol.2016.04.034>

Ajitha, B., Kumar Reddy, Y. A., Reddy, P. S., Jeon, H. J., and Ahn, C. W. (2016). Role of capping agents in controlling silver nanoparticles size, antibacterial activity and potential application as optical hydrogen peroxide sensor. *RSC Advances*, 6(42), 36171–36179. <https://doi.org/10.1039/c6ra03766f>.

Ali, M. R. K., Wu, Y., Tang, Y., and Xiao, H. (2018). Copper-based metal-organic frameworks for the synthesis of gold nanoparticles and their catalytic applications. *Materials Chemistry Frontiers*, 2(1), 191-198. doi: 10.1039/C7QM00327D

Aljabali, A. a. A., Akkam, Y., Zoubi, M. S. A., Al-Batayneh, K. M., Al-Trad, B., Alrob, O. A., Alkilany, A. M., Benamara, M., and Evans, D. M. (2018). Synthesis of Gold Nanoparticles Using Leaf Extract of *Ziziphus zizyphus* and their Antimicrobial Activity. *Nanomaterials*, 8(3), 174. <https://doi.org/10.3390/nano8030174>.

Al-Malah K.I M. (2017) *Introducing Aspen Plus*. Hoboken, New Jersey: John Wiley and Sons, Inc.

Alsaiari, N. S., Alzahrani, F. M., Amari, A., Osman, H., Harharah, H. N., Elboughdiri, N., and Tahoona, M. A. (2023). Plant and Microbial Approaches as Green Methods for the Synthesis of Nanomaterials: Synthesis, Applications, and Future Perspectives. *Molecules*, 28(1), 463. <https://doi.org/10.3390/molecules28010463>

Altunbek, M., Kuku, G., and Culha, M. (2016). Gold Nanoparticles in Single-Cell Analysis for Surface Enhanced Raman Scattering. *Molecules*, 21(12), 1617. <https://doi.org/10.3390/molecules21121617>.

Amendola, V., Pilot, R., Frascioni, M., Maragò, O. M., and Iatì, M. A. (2017). Surface plasmon resonance in gold nanoparticles: a review. *Journal of Physics: Condensed Matter*, 29(20), 203002. <https://doi.org/10.1088/1361-648x/aa60f3>.

Amina, S. J., and Guo, B. (2020). A Review on the Synthesis and Functionalization of Gold Nanoparticles as a Drug Delivery Vehicle *International Journal of Nanomedicine*, Volume 15, 9823–9857. <https://doi.org/10.2147/ijn.s279094>.

Ananikov, V. P. (2010, March 19). Using nanosized, homogeneous, and heterogeneous catalytic systems in organic synthesis: changing the structure of active center in chemical reactions in solution. SpringerLink. <https://link.springer.com/article/10.1134/S1995078010010015>.

Bakhtiar, R. (2013). Surface Plasmon Resonance Spectroscopy: A Versatile Technique in a Biochemist's Toolbox. *Journal of Chemical Education*, 90(2), 203–209. <https://doi.org/10.1021/ed200549g>.

Barrow, R. (2013). *Inorganic chemistry* (5th ed.). New York, NY: W.H. Freeman and Company.

Bastús, N. G., Comenge, J., and Puntès, V. F. (2011). Kinetically Controlled Seeded Growth Synthesis of Citrate-Stabilized Gold Nanoparticles of up to 200 nm: Size Focusing versus Ostwald Ripening. *Langmuir*, 27(17), 11098–11105. <https://doi.org/10.1021/la201938u>.

Bayda, S., Adeel, M., Tuccinardi, T., Cordani, M., and Rizzolio, F. (2019). The History of Nanoscience and Nanotechnology: From Chemical–Physical Applications to Nanomedicine. *Molecules*, 25(1), 112. <https://doi.org/10.3390/molecules25010112>.

Beamson, G. and Briggs, D. (1992) High resolution monochromated X-ray photoelectron spectroscopy of organic polymers: A comparison between solid state data for organic polymers and gas phase data for small molecules. *Mol. Phys.* 76, 919-936.

Bhaskaran, S., Sharma, N., Tiwari, P., Singh, S. R., and Sahi, S. V. (2019). Fabrication of innocuous gold nanoparticles using plant cells in culture. *Scientific Reports*, 9(1). <https://doi.org/10.1038/s41598-019-48475-9>.

Bigioni, T. (2000). Near-Infrared Luminescence from Small Gold Nanocrystals | Semantic Scholar.

Bloise, N., Strada, S., Dacarro, G., and Visai, L. (2022). Gold Nanoparticles Contact with Cancer Cell: A Brief Update. *International Journal of Molecular Sciences*, 23(14), 7683. <https://doi.org/10.3390/ijms23147683>

Boles, M., and Cengel, Y. (2014). *An Engineering Approach*. New York: McGraw-Hill Education.

Bondarchuk, I., Gurin, V., Dmitruk, I., and Kotko, A. (2013). Temperature dependence of the surface plasmon resonance in gold nanoparticles. *Surface Science*. 608. 275.

Buffat, P., and Borel, J. P. (1976). Size effect on the melting temperature of gold particles. *Physical Review A*, 13(6), 2287–2298. <https://doi.org/10.1103/physreva.13.2287>

Chang, R. (2019). *Chemistry*. New York, NY: McGraw-Hill.

Chari, C. S., Taylor, Z. W., Bezur, A., Xie, S., and Faber, K. T. (2022). Nanoscale engineering of gold particles in 18th century Böttger lusters and glazes. *Proceedings of the National Academy of Sciences*, 119(18). <https://doi.org/10.1073/pnas.2120753119>.

Chaudhary, R., Nawaz, K., Khan, A., Hano, C., Abbasi, B. H., and Anjum, S. (2020). An Overview of the Algae-Mediated Biosynthesis of Nanoparticles and Their Biomedical Applications. *Biomolecules*, 10(11), 1498. <https://doi.org/10.3390/biom10111498>

CheCalc (n.d.). *Properties Estimation Joback Method*. Retrieved November 23, 2022, from [https://checalc.com/solved/property\\_joback.html](https://checalc.com/solved/property_joback.html).

CheGuide (n.d.). *Property Estimation Joback Method*. Retrieved November 25, 2022, from [https://cheguide.com/property\\_estimation.html](https://cheguide.com/property_estimation.html)

Chen, X. R., Li, Q. J., and Wang, X. F. (2014). Gold nanostructures for bioimaging, drug delivery and therapeutics. Elsevier eBooks, 163–176. <https://doi.org/10.1533/9780857099051.2.163>.

Chen, Y., Hung, Y. C., Lin, L., Liao, I., Hong, M., and Huang, G. (2010). Size-dependent impairment of cognition in mice caused by the injection of gold nanoparticles. *Nanotechnology*, 21(48), 485102. <https://doi.org/10.1088/0957-4484/21/48/485102>.

Cortés, H., Hernández-Parra, H., Bernal-Chávez, S. A., Del Prado-Audelo, M. L., Caballero-Florán, I. H., Borbolla-Jiménez, F. V., González-Torres, M., Magaña, J. J., and Leyva-Gómez, G. (2021). Non-Ionic Surfactants for Stabilization of Polymeric Nanoparticles for Biomedical Uses. *Materials*, 14(12), 3197. <https://doi.org/10.3390/ma14123197>.

Csemány, D., Gujás, I., Chong, C. T., and Józsa, V. (2021, May 21). Evaluation of material property estimating methods for n-alkanes, 1-alcohols, and methyl esters for droplet evaporation calculations. *Heat and Mass Transfer*, 57(12), 1965–1979. <https://doi.org/10.1007/s00231-021-03059-0>.

Daniel, MC. and Astruc, D. (2004) Gold Nanoparticles: Assembly, Supramolecular Chemistry, Quantum-Size-Related Properties, and Applications toward Biology, Catalysis, and Nanotechnology. *Chemical Reviews*, 104, 293-346. <http://dx.doi.org/10.1002/chin.200416213>.

De Freitas, L.F., Varca, G.H.C., Batista, J.G.D.S., and Luga, A.B. (2018) An Overview of the Synthesis of Gold Nanoparticles Using Radiation Technologies. *Nanomaterials* 8, 939.

De Jong, W. H., and Borm, P. J. A. (2008). Drug delivery and nanoparticles: Applications and hazards. *International Journal of Nanomedicine*, 133. <https://doi.org/10.2147/ijn.s596>

Deb, S., Ghosh, K., and Shetty, S. (2015). Nanoimaging in cardiovascular diseases: Current state of the art. *Indian Journal of Medical Research*, 141(3), 285. <https://doi.org/10.4103/0971-5916.156557>

Dong, J., Carpinone, P. L., Pyrgiotakis, G., Demokritou, P., and Moudgil, B. M. (2020). Synthesis of Precision Gold Nanoparticles Using Turkevich Method. *Kona Powder and Particle Journal*, 37(0), 224–232. <https://doi.org/10.14356/kona.2020011>.

Doria, G., Conde, J., Veigas, B., Giestas, L., Almeida, C., Assunção, M., Rosa, J., and Baptista, P. V. (2012). Noble Metal Nanoparticles for Biosensing Applications. *Sensors*, 12(2), 1657–1687. <https://doi.org/10.3390/s120201657>.

Dreaden, E. C., Alkilany, A. M., Huang, X., Murphy, C. J., and El-Sayed, M. A. (2012). The golden age: gold nanoparticles for biomedicine. *Chemical Society Reviews*, 41(7), 2740–2779. doi: 10.1039/c1cs15237h.

Dubertret, B., Calame, M., and Libchaber, A. J. (2001). Single-mismatch detection using gold-quenched fluorescent oligonucleotides. *Nature Biotechnology*, 19(4), 365–370. <https://doi.org/10.1038/86762>

Elgie, K. (2022, November 15). What is a Rotary Evaporator? Asynt. <https://www.asynt.com/blog/what-is-a-rotary-evaporator/>

Eustis, S., and El-Sayed, M. A. (2006). Why gold nanoparticles are more precious than pretty gold: Noble metal surface plasmon resonance and its enhancement of the radiative and nonradiative properties of nanocrystals of different shapes. *Chemical Society Reviews*, 35(3), 209–217. <https://doi.org/10.1039/b514191e>

Fairley, N. (2014) CasaXPS, 2.3.17 ed. ed. Casa Software Ltd.

Faraday, M. (1857) X. The Bakerian Lecture. —Experimental relations of gold (and other metals) to light. (1857). *Philosophical Transactions of the Royal Society of London*, 147, 145–181. <https://doi.org/10.1098/rstl.1857.0011>.

Farjadian, F., Ghasemi, A., Gohari, O., Karimi, M., and Hamblin, M. R. (2019). Nanopharmaceuticals and nanomedicines currently on the market: challenges and opportunities. *Nanomedicine*, 14(1), 93–126. <https://doi.org/10.2217/nmm-2018-0120>

Fealy, R. J., Ackerman, S. R., and Ferguson, G. S. (2011). Mechanism of Spontaneous Formation of Monolayers on Gold from Alkyl Thiosulfates. *Langmuir*, 27(9), 5371–5376. <https://doi.org/10.1021/la200143b>

Fernández, L., Ortega, J., Domínguez, L., Lorenzo, D., Santos, A., and Romero, A. (2022). Using Two Group-Contribution Methods to Calculate Properties of Liquid Compounds Involved in the Cyclohexanone Production Operations. *Liquids*, 2(4), 413–431. <https://doi.org/10.3390/liquids2040024>.

Frens, G. (1973). Controlled Nucleation for the Regulation of the Particle Size in Monodisperse Gold Suspensions. *Nature Physical Science*, 241(105), 20–22. <https://doi.org/10.1038/physci241020a0>.

Ghosh, S., Patil, S., Ahire, M., Kitture, R., Kale, S., Pardesi, K., and Bellare, J. (2015). Gnidia glauca flower extract mediated synthesis of gold nanoparticles and evaluation of its chemocatalytic potential. *Journal of Nanoscience and Nanotechnology*, 15(1), 136-143.

Gobbo, P., Biesinger, M.C. and Workentin, M.S. (2013) Facile synthesis of gold nanoparticle (AuNP)–carbon nanotube (CNT) hybrids through an interfacial Michael addition reaction. *Chem. Commun.* 49, 2831-2833.

Hammami, I., Alabdallah, N. M., Jomaa, A. A., and Kamoun, M. (2021). Gold nanoparticles: Synthesis properties and applications. *Journal of King Saud University - Science*, 33(7), 101560. <https://doi.org/10.1016/j.jksus.2021.101560>

Han, G., You, C. C., Kim, B. J., Turingan, R. S., Forbes, N. S., Martin, C. T., and Rotello, V. M. (2006). Light-Regulated Release of DNA and Its Delivery to Nuclei by Means of Photolabile Gold Nanoparticles. *Angewandte Chemie International Edition*, 45(19), 3165–3169. <https://doi.org/10.1002/anie.200600214>.

Haruta, M. (2005). Gold rush. *Nature*, 437(7062), 1098–1099. <https://doi.org/10.1038/4371098a>.

Hassan, H., Sharma, P., Hasan, M., Singh, S., Thakur, D., and Narang, J. (2022). Gold nanomaterials – The golden approach from synthesis to applications. *Materials Science for Energy Technologies*. <https://doi.org/10.1016/j.mset.2022.09.004>

Haydary, J. (2019) *Chemical Process Design and Simulation: Aspen Plus and Aspen Hysys Applications*. Hoboken, New Jersey: American Institute of Chemical Engineers and John Wiley

and Sons, Inc. <https://www.sigmaaldrich.com/GB/en/technical-documents/technical-article/analytical-chemistry/photometry-and-reflectometry/ir-spectrum-table>.

He, Y. J., Liu, S., Kong, L. B., and Liu, Z. (2005). A study on the sizes and concentrations of gold nanoparticles by spectra of absorption, resonance Rayleigh scattering and resonance non-linear scattering. *Spectrochimica Acta Part A: Molecular and Biomolecular Spectroscopy*, 61(13–14), 2861–2866. <https://doi.org/10.1016/j.saa.2004.10.035>.

Hong, R., Han, G., Fernández, J. M., Kim, B. J., Forbes, N. S., and Rotello, V. M. (2006). Glutathione-Mediated Delivery and Release Using Monolayer Protected Nanoparticle Carriers. *Journal of the American Chemical Society*, 128(4), 1078–1079. <https://doi.org/10.1021/ja056726i>

Hu, X., Zhang, Y., Ding, T., Liu, J., and Zhao, H. (2020). Multifunctional Gold Nanoparticles: A Novel Nanomaterial for Various Medical Applications and Biological Activities. *Frontiers in Bioengineering and Biotechnology*, 8. <https://doi.org/10.3389/fbioe.2020.00990>

Huang, X., Jain, P. K., El-Sayed, I. H., and El-Sayed, M. A. (2007). Gold nanoparticles: interesting optical properties and recent applications in cancer diagnostics and therapy. *Nanomedicine*, 2(5), 681–693. <https://doi.org/10.2217/17435889.2.5.681>

Huang, X., Kang, B., Qian, W., Mackey, M. A., Chen, P. C., Oyelere, A. K., El-Sayed, I. H., and El-Sayed, M. A. (2010). Comparative study of photothermolysis of cancer cells with nuclear-targeted or cytoplasm-targeted gold nanospheres: continuous wave or pulsed lasers. *Journal of Biomedical Optics*, 15(5), 058002. <https://doi.org/10.1117/1.3486538>.

Ichikawa, T. (2017). Zwitterions as building blocks for functional liquid crystals and block copolymers. *Polymer Journal*, 49(5), 413–421. <https://doi.org/10.1038/pj.2017.6>.

Imbraguglio, Dario and Giovannozzi, Andrea and Rossi, Andrea. (2013). *Nanometrology*. 185. 193-220. 10.3254/978-1-61499-326-1-193.

Iravani, S. (2011). Green synthesis of metal nanoparticles using plants. *Green Chemistry*, 13(10), 2638-2650. doi: 10.1039/c1gc15386b



Ismail, A. A., Van De Voort, F. R., and Sedman, J. (1997). Chapter 4 Fourier transform infrared spectroscopy: Principles and applications. *Techniques and Instrumentation in Analytical Chemistry*, 93–139. [https://doi.org/10.1016/s0167-9244\(97\)80013-3](https://doi.org/10.1016/s0167-9244(97)80013-3).

Jain, P. K., Huang, X., El-Sayed, I. H., El-Sayed, M. A., and El-Sayed, A. M. (2013). Plasmonic photothermal therapy (PPTT) using gold nanoparticles. *Laser & Photonics Reviews*, 7(1), 46-63.

Jana, N. R., Gearheart, L., and Murphy, C. J. (2001a). Wet Chemical Synthesis of High Aspect Ratio Cylindrical Gold Nanorods. *The Journal of Physical Chemistry B*, 105(19), 4065–4067. <https://doi.org/10.1021/jp0107964>.

Jana, N. R., Gearheart, L., and Murphy, C. J. (2001b). Seeding Growth for Size Control of 5–40 nm Diameter Gold Nanoparticles. *Langmuir*, 17(22), 6782–6786. <https://doi.org/10.1021/la0104323>

Jara, N., Milán, N. S., Rahman, M. A., Mouheb, L., Boffito, D. C., Jeffryes, C., and Dahoumane, S. A. (2021). Photochemical Synthesis of Gold and Silver Nanoparticles—A Review. *Molecules*, 26(15), 4585. <https://doi.org/10.3390/molecules26154585>.

Javed, R., Usman, M., Tabassum, S., and Zia, M. (2016). Effect of capping agents: Structural, optical and biological properties of ZnO nanoparticles. *Applied Surface Science*, 386, 319–326. <https://doi.org/10.1016/j.apsusc.2016.06.042>

Javed, R., Zia, M., Naz, S., Aisida, S. O., Ain, N. U., and Ao, Q. (2020). Role of capping agents in the application of nanoparticles in biomedicine and environmental remediation: recent trends and future prospects. *Journal of Nanobiotechnology*, 18(1). <https://doi.org/10.1186/s12951-020-00704-4>

Jha, D., Haider, M. B., Kumar, R., & B. (2016). Extractive desulfurization of dibenzothiophene using phosphonium-based ionic liquid: Modeling of batch extraction experimental data and simulation of continuous extraction process. *Chemical Engineering Research & Design*, 111, 218–222. <https://doi.org/10.1016/j.cherd.2016.05.006>.

Ji, X., Song, X., Li, J., Bai, Y., Yang, W., and Peng, X. (2007). Size Control of Gold Nanocrystals in Citrate Reduction: The Third Role of Citrate. *Journal of the American Chemical Society*, 129(45), 13939–13948. <https://doi.org/10.1021/ja074447k>.

Ju-Nam, Y., Abdussalam-Mohammed, W., and Ojeda Ledo, J. (2016). Highly stable noble metal nanoparticles dispersible in biocompatible solvents: synthesis of cationic phosphonium gold nanoparticles in water and DMSO. *Faraday Discussions*, 186, 77-93.

Ju-Nam, Y., Bricklebank, N., Allen, D. T., Gardiner, P., Light, M. E., and Hursthouse, M. B. (2006). Phosphonioalkylthiosulfate zwitterions—new masked thiol ligands for the formation of cationic functionalised gold nanoparticles. *Organic and Biomolecular Chemistry*, 4(23), 4345–4351. <https://doi.org/10.1039/b610480k>.

Ju-Nam, Y., Chen, Y.-S., Ojeda, J.J., Allen, D.W., Cross, N.A., Gardiner, P.H.E., and Bricklebank, N. (2012). Water-soluble gold nanoparticles stabilized with cationic phosphonium thiolate ligands. *RSC Advances*, 2 (27), 10345-10351. <http://doi.org/10.1039/C2RA21421K>.

Kalmodia, S., Parameswaran, S., Yang, W., Barrow, C. J., and Krishnakumar, S. (2015). Attenuated Total Reflectance Fourier Transform Infrared Spectroscopy: An analytical technique to understand therapeutic responses at the molecular level. *Scientific Reports*, 5(1). <https://doi.org/10.1038/srep16649>

Kamalakaran, S., Prakash, M., Chambaud, G., and Hochlaf, M. (2018). Adsorption of Hydrophobic and Hydrophilic Ionic Liquids at the Au(111) Surface. *ACS Omega*, 3(12), 18039–18051. <https://doi.org/10.1021/acsomega.8b02163>.

Khan, N., Mir, M. C., Ngowi, E. E., Zafar, U., Khakwani, M. M. a. K., Khattak, S., Zhai, Y., Jiang, E., Zheng, M., Duan, S., Wei, J., Wu, D., and Ji, X. (2021). Nanomedicine: A Promising Way to Manage Alzheimer's Disease. *Frontiers in Bioengineering and Biotechnology*, 9. <https://doi.org/10.3389/fbioe.2021.630055>

Khlebtsov, N. (2011, February 22). Biodistribution and toxicity of engineered gold nanoparticles: a review of in vitro and in vivo studies. *Chemical Society Reviews* (RSC Publishing). <https://pubs.rsc.org/en/content/articlelanding/2011/CS/C0CS00018C>.

- Khlebtsov, N. G., and Dykman, L. A. (2010). Optical properties and biomedical applications of plasmonic nanoparticles. *Journal of Quantitative Spectroscopy and Radiative Transfer*, 111(1), 1–35. <https://doi.org/10.1016/j.jqsrt.2009.07.012>
- Kim, B. J., Bang, J., Hawker, C. J., and Kramer, E. J. (2006). Effect of Areal Chain Density on the Location of Polymer-Modified Gold Nanoparticles in a Block Copolymer Template. *Macromolecules*, 39(12), 4108–4114. <https://doi.org/10.1021/ma060308w>.
- Kitching, M., Ramani, M., and Marsili, E. (2015). Fungal biosynthesis of gold nanoparticles: mechanism and scale up. *Microbial Biotechnology*, 8(6), 904–917. <https://doi.org/10.1111/1751-7915.12151>
- Kleiber, M., and Joh, R. (2010). D1 Calculation Methods for Thermophysical Properties. *Springer EBooks*, 119–152. [https://doi.org/10.1007/978-3-540-77877-6\\_10](https://doi.org/10.1007/978-3-540-77877-6_10).
- Kong, F., Zhang, J., Li, R., Wang, Z., and Wang, W. (2017). Unique Roles of Gold Nanoparticles in Drug Delivery, Targeting and Imaging Applications. *Molecules*, 22(9), 1445. <https://doi.org/10.3390/molecules22091445>.
- Kumar, S. S., Kwak, K., and Lee, D. (2011). Electrochemical Sensing Using Quantum-Sized Gold Nanoparticles. *Analytical Chemistry*, 83(9), 3244–3247. <https://doi.org/10.1021/ac200384w>.
- Kumar, S., Kumar, S., Mishra, S. K., Srivastava, A., and Pandey, A. K. (2019). Recent advances in the synthesis and biomedical applications of gold nanoparticles: a comprehensive review. *ChemistrySelect*, 4(35), 10528-10544. doi: 10.1002/slct.201901563.
- Laidler, K. J., Meiser, J. H., and Sanctuary, B. C. (2019). *Physical chemistry*. Hachette UK.
- Landvik, N. E., Skaug, V., Mohr, B., Verbeek, J., and Zienolddiny, S. (2018). Criteria for grouping of manufactured nanomaterials to facilitate hazard and risk assessment, a systematic review of expert opinions. *Regul. Toxicol. Pharmacol.* 95, 270–279. doi:10.1016/j.yrtph.2018.03.027
- Latha, C. K., Raghasudha, M., Aparna, Y., M, R., Ravinder, D., K, J., Veerasomaiah, P., and Shridhar, D. (2017). Effect of Capping Agent on the Morphology, Size and Optical Properties of

In2O3 Nanoparticles. *Materials Research*, 20(1), 256–263. <https://doi.org/10.1590/1980-5373-mr-2016-0292>.

Lee, J., Mahendra, S., and Alvarez, P. J. J. (2010). Nanomaterials in the Construction Industry: A Review of Their Applications and Environmental Health and Safety Considerations. *ACS Nano*, 4(7), 3580–3590. <https://doi.org/10.1021/nn100866w>

Lee, K. X., Shameli, K., Yew, Y. P., Teow, S., Jahangirian, H., Rafiee-Moghaddam, R., and Webster, T. J. (2020). Recent Developments in the Facile Bio-Synthesis of Gold Nanoparticles (AuNPs) and Their Biomedical Applications. *International Journal of Nanomedicine*, Volume 15, 275–300. <https://doi.org/10.2147/ijn.s233789>.

Lee, S., Yoon, S. M., Shin, H. J., Joo, W. J., Yi, D. K., Choi, J. Y., Amarnath, C. A., and Paik, U. (2008). Hierarchical organization of Au nanoparticles in a poly(vinyl carbazole) matrix for hybrid electronic devices. *Nanotechnology*, 19(7), 075606. <https://doi.org/10.1088/0957-4484/19/7/075606>

Leng, W., Pati, P., and Vikesland, P. J. (2015). Room temperature seed mediated growth of gold nanoparticles: mechanistic investigations and life cycle assessment. *Environmental Science. Nano*, 2(5), 440–453. <https://doi.org/10.1039/c5en00026b>

Li, X., Wang, J., Sun, L., and Wang, Z. (2010). Gold nanoparticle-based colorimetric assay for selective detection of aluminium cation on living cellular surfaces. *Chem. Commun.*, 46(6), 988–990. <https://doi.org/10.1039/b920135a>.

Lim, Z. J., Li, J. J., Ong, C. N., Yung, L. L., and Bay, B. (2011). Gold nanoparticles in cancer therapy. *Acta Pharmacologica Sinica*, 32(8), 983–990. <https://doi.org/10.1038/aps.2011.82>

Lindberg, B.J., Hamrin, K., Johansson, G., Gelius, U., Fahlman, A., Nordling, C. and Siegbahn, K. (1970) Molecular Spectroscopy by Means of ESCA II. Sulfur compounds. Correlation of electron binding energy with structure. *Phys. Scr.* 1, 286-298.

Lohse, S. E., Dahl, J. A., and Hutchison, J. E. (2010). Direct Synthesis of Large Water-Soluble Functionalized Gold Nanoparticles Using Bunte Salts as Ligand Precursors. *Langmuir*. <https://doi.org/10.1021/la904306a>.

Lukkari, J., Meretoja, M., Kartio, I., Laajalehto, K., Rajamäki, M., Lindström, M., and Kankare, J. (1999). Organic Thiosulfates (Bunte Salts): Novel Surface-Active Sulfur Compounds for the Preparation of Self-Assembled Monolayers on Gold. *Langmuir*, 15(10), 3529–3537. <https://doi.org/10.1021/la9811719>.

Luo, D. H., Wang, X., Burda, C., and Basilion, J. P. (2021). Recent Development of Gold Nanoparticles as Contrast Agents for Cancer Diagnosis. *Cancers*, 13(8), 1825. <https://doi.org/10.3390/cancers13081825>.

Mansoori, G. A., Mohazzabi, P., McCormack, P., and Jabbari, S. (2007). Nanotechnology in cancer prevention, detection and treatment: bright future lies ahead. *World Review of Science, Technology and Sustainable Development*, 4(2/3), 226. <https://doi.org/10.1504/wrstd.2007.013584>.

Mao, X., Li, Z. P., and Tang, Z. Y. (2010). One pot synthesis of monodispersed L-glutathione stabilized gold nanoparticles for the detection of Pb<sup>2+</sup> ions. *Frontiers of Materials Science*, 5(3), 322–328. <https://doi.org/10.1007/s11706-011-0118-4>.

McNeillie, A., Brown, D.H., Smith, W.E., Gibson, M. and Watson, L. (1980) X-ray photoelectron spectra of some gold compounds. *Journal of the Chemical Society, Dalton Transactions*, 767-770.

Mettler-Toledo International Inc. (n.d.). *Continuous Stirred Tank Reactors (CSTRs)*. Retrieved December 19, 2022, from [https://www.mt.com/gb/en/home/applications/L1\\_AutoChem\\_Applications/L2\\_ReactionAnalyses/continuous-stirred-tank-reactors](https://www.mt.com/gb/en/home/applications/L1_AutoChem_Applications/L2_ReactionAnalyses/continuous-stirred-tank-reactors).

Michael, A., Singh, A. K., Roy, A., and Islam, M. S. (2022). Fungal- and Algal-Derived Synthesis of Various Nanoparticles and Their Applications. *Bioinorganic Chemistry and Applications*, 2022, 1–14. <https://doi.org/10.1155/2022/3142674>.

Milan, J., Niemczyk, K., and Kus-Liśkiewicz, M. (2022). Treasure on the Earth—Gold Nanoparticles and Their Biomedical Applications. *Materials*, 15(9), 3355. <https://doi.org/10.3390/ma15093355>.

Mitchell, M. E., Billingsley, M. M., Haley, R. M., Wechsler, M. E., Peppas, N. A., and Langer, R. (2021). Engineering precision nanoparticles for drug delivery. *Nature Reviews Drug Discovery*, 20(2), 101–124. <https://doi.org/10.1038/s41573-020-0090-8>

Mjalli, F. S., Naser, J., Jibril, B. Y., Alizadeh, V., and Gano, Z. S. (2014). Tetrabutylammonium Chloride Based Ionic Liquid Analogues and Their Physical Properties. *Journal of Chemical & Engineering Data*, 59(7), 2242–2251. <https://doi.org/10.1021/je5002126>.

Mohrhusen, L., and Osmić, M. (2017). Sterical ligand stabilization of nanocrystals versus electrostatic shielding by ionic compounds: a principle model study with TEM and XPS. *RSC Advances*, 7(21), 12897–12907. <https://doi.org/10.1039/c6ra27454d>.

Molnár, Z. (2018, March 2). Green synthesis of gold nanoparticles by thermophilic filamentous fungi. *Nature*. <https://www.nature.com/articles/s41598-018-22112-3>.

Mountrichas, G., Pispas, S., & Kamitsos, E. I. (2014). Effect of Temperature on the Direct Synthesis of Gold Nanoparticles Mediated by Poly(dimethylaminoethyl methacrylate) Homopolymer. *Journal of Physical Chemistry C*, 118(39), 22754–22759. <https://doi.org/10.1021/jp505725v>.

Nagarajan, R. (2008). Nanoparticles: Building Blocks for Nanotechnology. In ACS symposium series (pp. 2–14). American Chemical Society. <https://doi.org/10.1021/bk-2008-0996.ch001>.

Narayanan, R. (2010). Recent Advances in Noble Metal Nanocatalysts for Suzuki and Heck Cross-Coupling Reactions. *Molecules*, 15(4), 2124–2138. <https://doi.org/10.3390/molecules1504212>.

Nikoobakht, B., and El-Sayed, M. A. (2003). Preparation and growth mechanism of gold nanorods (NRs) using seed-mediated growth method. *Chemistry of Materials*, 15(10), 1957-1962. doi: 10.1021/cm020732l.

NIST X-ray Photoelectron Spectroscopy Database, NIST Standard Reference Database No. 20, National Institute of Standards and Technology, Gaithersburg MD, 20899 (2000). doi:10.18434/T4T88K

Niu, Z., and Li, Y. (2013). Removal and Utilization of Capping Agents in Nanocatalysis. *Chemistry of Materials*, 26(1), 72–83. <https://doi.org/10.1021/cm4022479>

Nordlander, P., Oubre, C., Prodan, E., Li, K., and Stockman, M. I. (2004). Plasmon hybridization in metallic nanoparticles. *Nano Letters*, 4(5), 561-566.

Ostwald, W. (1904). Faraday Lecture. Elements and compounds. *Journal of the Chemical Society*, 85, 506. <https://doi.org/10.1039/ct9048500506>.

Park, C., Youn, H., Kim, H., Noh, T., Kook, Y. H., Oh, E. T., Park, H. J., and Kim, C. (2009). Cyclodextrin-covered gold nanoparticles for targeted delivery of an anti-cancer drug. *Journal of Materials Chemistry*, 19(16), 2310. <https://doi.org/10.1039/b816209c>.

Pastoriza-Santos, I., and Liz-Marzán, L. M. (2009). N,N-Dimethylformamide as a Reaction Medium for Metal Nanoparticle Synthesis. *Advanced Functional Materials*, 19(5), 679–688. <https://doi.org/10.1002/adfm.200801566>.

PeakD. (n.d.). *Transmission Electron Microscope: Principle and Working ChemFam*. Retrieved January 31, 2023, from: <https://peakd.com/hive-196387/@splash-of-angs63/transmission-electron-microscope-principle>.

Petersen, N., Girard, M., Riedinger, A., and Valsson, O. (2022). The Crucial Role of Solvation Forces in the Steric Stabilization of Nanoplatelets. *Nano Letters*, 22(24), 9847–9853. <https://doi.org/10.1021/acs.nanolett.2c02848>.

Pillai, R. G., and Freund, M. S. (2011). Self-Assembly of Alkylthiosulfates on Gold: Role of Electrolyte and Trace Water in the Solvent. *Langmuir*, 27(14), 9028–9033. <https://doi.org/10.1021/la200945e>.

Popovtzer, R., Singh, I. P., Kotov, N. A., Popovtzer, A., Balter, J. M., Carey, T. E., and Kopelman, R. (2008). Targeted Gold Nanoparticles Enable Molecular CT Imaging of Cancer. *Nano Letters*, 8(12), 4593–4596. <https://doi.org/10.1021/nl8029114>.

Ramalingam, V. (2019). Multifunctionality of gold nanoparticles: Plausible and convincing properties. *Advances in Colloid and Interface Science*, 271, 101989. <https://doi.org/10.1016/j.cis.2019.101989>.

Reslan, M., and Kayser, V. (2018). Ionic liquids as biocompatible stabilizers of proteins. *Biophysical Reviews*, 10(3), 781–793. <https://doi.org/10.1007/s12551-018-0407-6>.

Santhosh, P. B., Genova, J., and Chamati, H. (2022). Green Synthesis of Gold Nanoparticles: An Eco-Friendly Approach. *Chemistry*, 4(2), 345–369. <https://doi.org/10.3390/chemistry4020026>.

Sathya, S. (2017). Separation of algal pigments by thin layer chromatography (tlc) and high performance liquid chromatography (hplc). <https://www.semanticscholar.org/paper/separation-of-algal-pigments-by-thin-layer-%28TLC%20Sathya/d662d04918cdf8ef9b6eed6ced5c8df01f434c>.

Sengupta, C., Mitra, P., Chatterjee, S., Bhattacharjee, G., Satpati, B., and Basu, S. (2018). Photoinduced electronic interactions between acridine derivatives and small gold nanoparticles: A spectroscopic insight. *Journal of Molecular Liquids*, 272, 198–208. <https://doi.org/10.1016/j.molliq.2018.09.080>.

Shah, M. A., Pirzada, B. M., Price, G. J., LShibiru, A., and Qurashi, A. (2022). Applications of nanotechnology in smart textile industry: A critical review. *Journal of Advanced Research*, 38, 55–75. <https://doi.org/10.1016/j.jare.2022.01.008>.

Shankar, S. S., Akhilesh Rai., Balaprasad Ankamwar., Amit Singh., Absar Ahmad & Murali Sastry Biological synthesis of triangular gold nanoprisms. *Nat. Mater.* 3, 482–488 (2004).

Sharma, C. (2021, November 4). Melting Point Apparatus. <https://studiousguy.com/melting-point-apparatus/>

Sharma, N. (2012, June 20). Exploitation of marine bacteria for production of gold nanoparticles - Microbial Cell Factories. *BioMed Central*. <https://microbialcellfactories.biomedcentral.com/articles/10.1186/1475-2859-11-86>.



Shreyash, N., Bajpai, S., Khan, M. S., Vijay, Y., Tiwary, S., and Sonker, M. (2021). Green Synthesis of Nanoparticles and Their Biomedical Applications: A Review. *ACS Applied Nano Materials*, 4(11), 11428–11457. <https://doi.org/10.1021/acsanm.1c02946>.

Siddiqi, K. S. (2016, February 24). Fabrication of Metal Nanoparticles from Fungi and Metal Salts: Scope and Application - *Nanoscale Research Letters*. SpringerOpen. <https://nanoscalereslett.springeropen.com/articles/10.1186/s11671-016-1311-2>.

Sigma Aldrich ir-spectrum-table. (n.d.). *technical-documents* Retrieved February 25, 2023, from <https://www.sigmaaldrich.com/US/en/technical-documents/technical-article/analytical-chemistry/photometry-and-reflectometry>.

Singh, J., Dutta, T., Kim, K., Rawat, M., Samddar, P., and Kumar, P. (2018). ‘Green’ synthesis of metals and their oxide nanoparticles: applications for environmental remediation. *Journal of Nanobiotechnology*, 16(1). <https://doi.org/10.1186/s12951-018-0408-4>

Singh, R. K., and Prasad, R. (2009). Green synthesis of gold nanoparticles using *Azadirachta indica* leaf extract. *Colloids and Surfaces B: Biointerfaces*, 73(2), 175-180.

Skoog, D. A., Holler, J. F., and Crouch, S. R. (2023). *Principles of Instrumental Analysis*, 6th Edition (6th ed.). CENGAGE INDIA

Slepička, P., Kasálková, N. S., Siegel, J., Kolská, Z., and Švorčík, V. (2019). Methods of Gold and Silver Nanoparticles Preparation. *Materials*, 13(1), 1. <https://doi.org/10.3390/ma13010001>.

Sokolova, V., Mekky, G., Van Der Meer, S. B., Seeds, M. C., Atala, A., and Epple, M. (2020). Transport of ultrasmall gold nanoparticles (2 nm) across the blood–brain barrier in a six-cell brain spheroid model. *Scientific Reports*, 10(1). <https://doi.org/10.1038/s41598-020-75125-2>.

Soroush, M., and Kravaris, C. (1993). Optimal design and operation of batch reactors. 2. A case study. *Industrial & Engineering Chemistry Research*, 32(5), 882–893. <https://doi.org/10.1021/ie00017a016>.

Starnes, D. L., Jain, A. and Sahi, S. V. *In planta* engineering of gold nanoparticles of desirable geometries by modulating growth conditions: an environment-friendly approach. *Environ. Sci. Technol.* 44, 7110–7115 (2010).

Sun, K., Qiu, J., Liu, J., and Miao, Y. (2009). Preparation and characterization of gold nanoparticles using ascorbic acid as reducing agent in reverse micelles. *Journal of Materials Science*, 44(3), 754–758. <https://doi.org/10.1007/s10853-008-3162-4>

Swierczewska, M., Lee, S., and Chen, X. (2011). The design and application of fluorophore–gold nanoparticle activatable probes. *Physical Chemistry Chemical Physics*, 13(21), 9929. <https://doi.org/10.1039/c0cp02967j>.

Thuy, N. T. B., Yokogawa, R., Yoshimura, Y., Fujimoto, K., Koyano, M., and Maenosono, S. (2010). Surface-enhanced Raman spectroscopy for facile DNA detection using gold nanoparticle aggregates formed via photoligation. *The Analyst*, 135(3), 595. <https://doi.org/10.1039/b919969a>.

Tiwari, P. M., Vig, K., Dennis, V. A., and Singh, S. R. (2011). Functionalized Gold Nanoparticles and Their Biomedical Applications. *Nanomaterials*, 1(1), 31–63. <https://doi.org/10.3390/nano1010031>.

Tran, H. V., Doan, H. A., Chandler, B. D., and Grabow, L. C. (2016a). Water-assisted oxygen activation during selective oxidation reactions. *Current Opinion in Chemical Engineering*, 13, 100–108. <https://doi.org/10.1016/j.coche.2016.08.010>

Tran, M. T., DePenning, R., Turner, M., and Padalkar, S. (2016b). Effect of citrate ratio and temperature on gold nanoparticle size and morphology. *Materials Research Express*, 3(10), 105027. [doi.org/10.1088/2053-1591/3/10/105027](https://doi.org/10.1088/2053-1591/3/10/105027).

Tripathi, K., and Driskell, J. D. (2018). Quantifying Bound and Active Antibodies Conjugated to Gold Nanoparticles: A Comprehensive and Robust Approach To Evaluate Immobilization Chemistry. *ACS Omega*, 3(7), 8253–8259. <https://doi.org/10.1021/acsomega.8b00591>

Turkevich, J., Stevenson, P. C., and Hillier, J. (1951). A study of the nucleation and growth processes in the synthesis of colloidal gold. *Discussions of the Faraday Society*, 11, 55. <https://doi.org/10.1039/df9511100055>.

Vajtai, R. (2013). Springer Handbook of Nanomaterials (Springer Handbooks) (2013th ed.). Springer.

Valderrama, J. O., and Rojas, R. G. (2009). Critical Properties of Ionic Liquids. Revisited. *Industrial & Engineering Chemistry Research*, 48(14), 6890–6900. <https://doi.org/10.1021/ie900250g>.

Van der Putten, D., Zanoni, R., Coluzza, C. and Schmid, G. (1996) Angle-resolved X-ray photoelectron spectroscopic experiments on the full series of molecular [Au<sub>55</sub>(PR<sub>3</sub>)<sub>12</sub>Cl<sub>6</sub>] clusters. *Journal of the Chemical Society, Dalton Transactions*, 1721-1725.

Vines, J. B., Yoon, J. H., Ryu, N. H., Lim, D., and Park, H. (2019). Gold Nanoparticles for Photothermal Cancer Therapy. *Frontiers in Chemistry*, 7. <https://doi.org/10.3389/fchem.2019.00167>.

Vollmer, C., Redel, E., Abu-Shandi, K., Thomann, R., Manyar, H., Hardacre, C., and Janiak, C. (2010). Microwave Irradiation for the Facile Synthesis of Transition-Metal Nanoparticles (NPs) in Ionic Liquids (ILs) from Metal-Carbonyl Precursors and Ru-, Rh-, and Ir-NP/IL Dispersions as Biphasic Liquid-Liquid Hydrogenation Nanocatalysts for Cyclohexene. *Chemistry - a European Journal*, 16(12), 3849–3858. <https://doi.org/10.1002/chem.200903214>.

Wagner, C., Riggs, W., Davis, L., Moulder, J. and Muilenberg, G. (1979) *Handbook of X-ray photoelectron spectroscopy*, Perkin-Elmer Corp. Eden Prairie, MN, 38.

Wu, Y., Ali, M. R. K., Chen, K., Fang, N., and El-Sayed, M. A. (2019). Gold nanoparticles in biological optical imaging. *Nano Today*, 24, 120–140. <https://doi.org/10.1016/j.nantod.2018.12.006>.

Xia, Y., Gilroy, K. D., Peng, H., and Xia, X. (2017). Seed-Mediated Growth of Colloidal Metal Nanocrystals. *Angewandte Chemie*, 56(1), 60–95. <https://doi.org/10.1002/anie.201604731>

West Campus Materials Characterization Core. (n.d.). *X-ray Photoelectron Spectroscopy (XPS)*. Retrieved February 15, 2023, from: <https://ywcmatsci.yale.edu/xps>.

Yadav, J. K., Jasrotia, P., Bhardwaj, A. K., Kashyap, P. L., Kumar, S., Singh, M., and Singh, G. (2021). Nanopesticides: Current status and scope for their application in agriculture. *Plant Protection Science*, 58(No. 1), 1–17. <https://doi.org/10.17221/102/2020-pps>.

Yafout, M., Ousaid, A., Khayati, Y., and Otmani, I. S. E. (2021). Gold nanoparticles as a drug delivery system for standard chemotherapeutics: A new lead for targeted pharmacological cancer treatments. *Scientific African*, 11, e00685. <https://doi.org/10.1016/j.sciaf.2020.e00685>

Yang, H., Li, M., Li, C., Luo, Q., Zhu, M., Tian, H., and Zhu, W. (2020). Unraveling Dual Aggregation-Induced Emission Behavior in Steric-Hindrance Photochromic System for Super Resolution Imaging. *Angewandte Chemie*, 59(22), 8560–8570. <https://doi.org/10.1002/anie.201909830>.

Yee, C.K., Ulman, A., Ruiz, J.D., Parikh, A., White, H. and Rafailovich, M. (2003) Alkyl Selenide- and Alkyl Thiolate-Functionalized Gold Nanoparticles: Chain Packing and Bond Nature. *Langmuir* 19, 9450-9458. [Original source: <https://studycrumb.com/alphabetizer>]

Yeh, Y. C., Creran, B., and Rotello, V. M. (2012). Gold nanoparticles: preparation, properties, and applications in bionanotechnology. *Nanoscale*, 4(6), 1871–1880. <https://doi.org/10.1039/c1nr11188d>.

Zavaleta, C. L., Smith, B. R., Walton, I., Doering, W., Davis, G., Shojaei, B., Natan, M. J., and Gambhir, S. S. (2009). Multiplexed imaging of surface enhanced Raman scattering nanotags in living mice using noninvasive Raman spectroscopy. *Proceedings of the National Academy of Sciences*, 106(32), 13511–13516. <https://doi.org/10.1073/pnas.0813327106>.

Zawrah, M., Khattab, R., Girgis, L., El Daidamony, H., and Abdel Aziz, R. E. (2016). Stability and electrical conductivity of water-base Al<sub>2</sub>O<sub>3</sub> nanofluids for different applications. *HBRC Journal*, 12(3), 227–234. <https://doi.org/10.1016/j.hbrcj.2014.12.001>.

Zhang, G., Yang, Z., Lu, W., Zhang, R., Huang, Q., Tian, M., Li, L., Liang, D., and Li, C. (2009). Influence of anchoring ligands and particle size on the colloidal stability and in vivo biodistribution of polyethylene glycol-coated gold nanoparticles in tumor-xenografted mice. *Biomaterials*, 30(10), 1928–1936. <https://doi.org/10.1016/j.biomaterials.2008.12.038>

Zhao, P., Li, N., and Astruc, D. (2013). State of the art in gold nanoparticle synthesis. *Coordination Chemistry Reviews*, 257(3–4), 638–665. <https://doi.org/10.1016/j.ccr.2012.09.002>

Zheng, X. X., and Tan, Y. N. (2020). Recent development of nucleic acid nanosensors to detect sequence-specific binding interactions: From metal ions, small molecules to proteins and pathogens. *Sensors International*, 1, 100034. <https://doi.org/10.1016/j.sintl.2020.100034>.

Zsigmondy, R. (1909). Colloids and the Ultra Microscope. *Journal of the American Chemical Society*, 31(8), 951–952. <https://doi.org/10.1021/ja01938a017>.

Zuber, A., Purdey, M. S., Schartner, E. P., Forbes, C. J., Van Der Hoek, B., Giles, D. E. A., Abell, A. D., Monro, T. M., and Ebendorff-Heidepriem, H. (2016). Detection of gold nanoparticles with different sizes using absorption and fluorescence based method. *Sensors and Actuators B-chemical*, 227, 117–127. <https://doi.org/10.1016/j.snb.2015.12.044>.

Zuo, J. M., and Spence, J. C. H. (2016). *Advanced Transmission Electron Microscopy: Imaging and Diffraction in Nanoscience*. Springer Publishing.